Upper Extremity Interaction with a Helicopter Side Airbag: Injury Criteria for Dynamic Hyperextension of the Female Elbow Joint

Gail Ann Hansen

Thesis submitted to the Faculty of the
Virginia Polytechnic Institute and State University
in partial fulfillment of the requirements for the degree of

Master of Science
In
Mechanical Engineering

Dr. Stefan M. Duma, Chair
Dr. Joel D. Stitzel
Dr. Michael L. Madigan

April 22, 2004
Blacksburg, Virginia

Keywords: Upper Extremity, Elbow, Hyperextension, Side Airbag, Injury

Upper Extremity Interaction with a Helicopter Side Airbag: Injury Criteria for Dynamic Hyperextension of the Female Elbow Joint

Gail Ann Hansen

ABSTRACT

This paper describes a three part analysis to characterize the interaction between the female upper extremity and a helicopter cockpit side airbag system and to develop dynamic hyperextension injury criteria for the female elbow joint. Part I involved a series of 10 experiments with an original Army Black Hawk helicopter side airbag. A 5th percentile female Hybrid III instrumented upper extremity was used to demonstrate side airbag upper extremity loading. Two out of the 10 tests resulted in high elbow bending moments of 128 Nm and 144 Nm. Part II included dynamic hyperextension tests on 24 female cadaver elbow joints. The energy source was a drop tower utilizing a three-point bending configuration to apply elbow bending moments matching the previously conducted side airbag tests. Post-test necropsy showed that 16 of the 24 elbow joint tests resulted in injuries. Injury severity ranged from minor cartilage damage to more severe joint dislocations and transverse fractures of the distal humerus. Peak elbow bending moments ranged from 42.4 Nm to 146.3 Nm. Peak bending moment proved to be a significant indicator of any elbow injury ($p=0.02$) as well as elbow joint dislocation ($p=0.01$). Logistic regression analyses were used to develop single and multivariate injury risk functions. Using peak moment data for the entire test population, a 50% risk of obtaining any elbow injury was found at 56 Nm while a 50% risk of sustaining an elbow joint dislocation was found at 93 Nm for the female population. These results

indicate that the peak elbow bending moments achieved in Part I are associated with a greater than 90% risk for elbow injury. Subsequently, the airbag was re-designed in an effort to mitigate this as well as the other upper extremity injury risks. Part III assessed the enhanced side airbag module to ensure injury risks had been reduced prior to implementing the new system. To facilitate this, 12 enhanced side airbag deployments were conducted using the same procedures as Part I. Results indicate that the re-designed side airbag has effectively mitigated elbow injury risks induced by the original side airbag design. It is anticipated that this study will provide researchers with additional injury criteria for assessing upper extremity injury risk caused by both military and automotive side airbag deployments.

Acknowledgements

This research, along with my other accomplishments at Virginia Tech, would not have been possible without the guidance of my advisor, the help of my lab mates, the support of my family and friends, and my faith in God.

I would like to thank my advisor, Stefan Duma, for the valuable opportunities to learn, experience, and achieve in the field of biomechanics, for the benefit of his laboratory.

My experience, first as a member of the Impact Biomechanics Laboratory and then as a member of the Center for Injury Biomechanics, would not have been enjoyable without my fellow lab mates. In particular, I want to thank Eric for being my closest friend, big brother, and constant source of laughter at Virginia Tech; who was there for me and believed in me through good times and bad. I also want to thank Joel for the great deal of advice, time, and patience he has provided me while teaching me about biomechanics and life.

I want to thank my Dad, Mom, and big sister, Diane, for their constant support and encouragement throughout my life, especially during the past 6 years of my challenging education. Their words of wisdom and experience have helped me through some of my most difficult challenges. They are my greatest role models and their happiness is my truest source of motivation.

Finally, and most importantly, I want to thank Rich for his continual love and inspiration throughout the many ups and downs of life. May God always be with us to guide us through wherever our lives might take us together.

Table of Contents

List of Figures

List of Tables

1 Introduction

While modern Army helicopters incorporate crashworthiness features such as energy-absorbing landing gear and seats, self-sealing fuel systems, and harness restraints, helicopter aviators continue to be at high risk of injury during survivable mishaps. A study performed by Shanahan (1989) demonstrated that approximately 80% of helicopter crash injuries are caused by impacts between the aviators and the aircraft structure. To reduce the incidence of these impact injuries, the United States Army investigated incorporating airbags as a supplemental restraint system in its helicopter fleet. Shanahan (1993) projected a 23% reduction of injuries and 50% reduction in fatalities during survivable helicopter mishaps through the use of airbags. Based upon these studies, development of a Cockpit Airbag System (CABS) for retrofit into existing aircraft was begun in the mid-1990s. The US Army chose the UH-60A/L Black Hawk helicopter as the first aircraft for which a cockpit airbag system was designed. Side airbags were mounted outboard of each crewstation, affixed to a rigid side armor panel, providing aviator flail strike protection during impacts with roll or yaw components. Following preliminary tests, concerns arose over the risk of unnecessary deployments of the CABS and the subsequent threat of side airbag-induced upper extremity injury to aviators (McEntire, 2003). In particular, women have been considered the most vulnerable aviators to helicopter airbag loading due to their smaller stature, bone structure, and loss of bone mineral density, along with their increasing role in the military (Duma, 1999, 2003).

The interaction between a deploying side airbag and the upper extremity has been shown by several studies to result in a range of upper extremity injuries. Kallieris (1997),

who used the Hybrid III 50th percentile male dummy and male cadavers, found one humerus fracture out of five cadaver tests. Jaffredo (1998) found a wrist injury in a cadaver test that was the result of the hand becoming entrapped in the handgrip as the side airbag forced the upper extremity forward. In tests with small female cadavers, Duma (1998) found chondral and osteochondral fractures in the elbow joint for seven out of the 12 cadaver tests that had been subjected to upper extremity loading from a deploying seat-mounted side airbag. A follow up study by Duma (2001) evaluated the same seat-mounted side airbag and the effect of a door mounted handgrip with six small female cadavers. The tests resulted in chondral and osteochondral fractures of the elbow in four of the six upper extremities, humerus fractures in two of the tests, and wrist injuries in two of the tests. Overall, the upper extremity region with the highest incidence of observed injuries as a result of a side airbag deployment was the elbow.

Furthermore, recent studies have produced injury risk functions for forearm and humerus fracture based on mid-shaft bending loads (Duma, 1999, 2003a) and wrist injury as a function of axial loads acting through the wrist (Duma, 2003b). Another study, purposed to develop a fracture tolerance for the elbow joint relative to the fracture risk attributed to side airbag loading, produced a multivariate risk function based upon the 5th percentile female that predicts a 50% risk of elbow fracture at a compressive elbow load of 1780 N and load angle of 30° superior to the longitudinal axis of the forearm ($p < 0.01$) (Duma, 2002). Other studies have also produced dose-response models for elbow injury during airbag loading (Duma, 1998, 2000). These models predict the risk of elbow injury based upon axial loading of the elbow, as this condition was the primary mechanism of injury encountered during these studies. However, side airbag contact

with the upper extremity can also impart large bending loads to the elbow joint, particularly during hyperextension of the elbow. Injury criteria are not currently available for use in evaluating the risk of elbow injury associated with side airbag induced rotational bending moments produced by hyperextension.

This paper describes a three part analysis to characterize the interaction between the female upper extremity and a helicopter cockpit side airbag system as well as develop injury criteria for the upper extremity elbow joint. The purpose of Part I is to characterize side airbag-related upper extremity loading to the pilot and copilot occupants when exposed to the original UH-60 CABS side airbag, specifically during a non-crash deployment. The goal of Part II is to investigate injury resulting from rotational loading of the elbow joint in hyperextension under dynamic loading conditions similar to a cockpit side airbag deployment and to develop elbow injury criterion to assess upper extremity injury risk. The purpose of Part III is to assess a re-designed, enhanced UH-60 CABS side airbag to characterize side airbag-related upper extremity loading to ensure risks obtained from the original design have been reduced prior to implementing the new system.

2 Background Anatomy

The upper extremity is composed of six morphologically distinct regions: the shoulder, upper arm or humerus, elbow, lower arm or forearm, wrist, and hand. This paper focuses on the humerus, elbow, forearm, and wrist regions (Figure 1). The distal head of the humerus and the proximal ends of the radius and ulna comprise the elbow joint. The elbow joint allows flexion of the forearm toward the humerus, extension of the

forearm away from the humerus, and one half of the forearm pronation and supination rotations. Closer examination of the elbow joint reveals that flexion and extension is guided by the trochlear notch of the ulna, which rotates along the trochlea of the humerus. Flexion can range from the anatomically neutral position, which is full extension, to 145° in full flexion. As the forearm reaches full extension, the proximal trochlear notch reaches the joint stop and compresses into the olecranon fossa located on the posterior side of the distal humerus. This motion is guided primarily by four ligaments: the anterior, posterior, and ulnar collateral ligaments between the distal humerus and ulna, as well as the radial collateral ligament between the distal humerus and the radius.

Upper extremity injuries can be characterized using the Abbreviated Injury Scale (AIS). Injuries for the upper limb can range from AIS 1 level tissue contusions to AIS 3 level comminuted fractures of the long bones. In particular, the elbow joint has a range of AIS injury codes from AIS 1 to AIS 3. The minor elbow joint injuries are AIS 1 values for contusions, sprains, single ligament dislocations, and minor damage to the articular cartilage surfaces. More severe AIS 2 elbow injuries include lacerations into the joint with ligament or nerve damage, joint dislocations as well as fractures through the cartilage surfaces into the underlying bone. The most severe injury possible for the elbow joint is an AIS 3 injury that is characterized by massive destruction of bone and cartilage. It should be noted that the AIS is a threat to life coding system and has limited application to characterizing elbow joint injuries that are not life threatening but may result in long term pain and loss of function. For this study an elbow joint dislocation

(AIS 2) is defined to include anterior joint capsule disruptions, although capsule disruption could occur without joint dislocation.

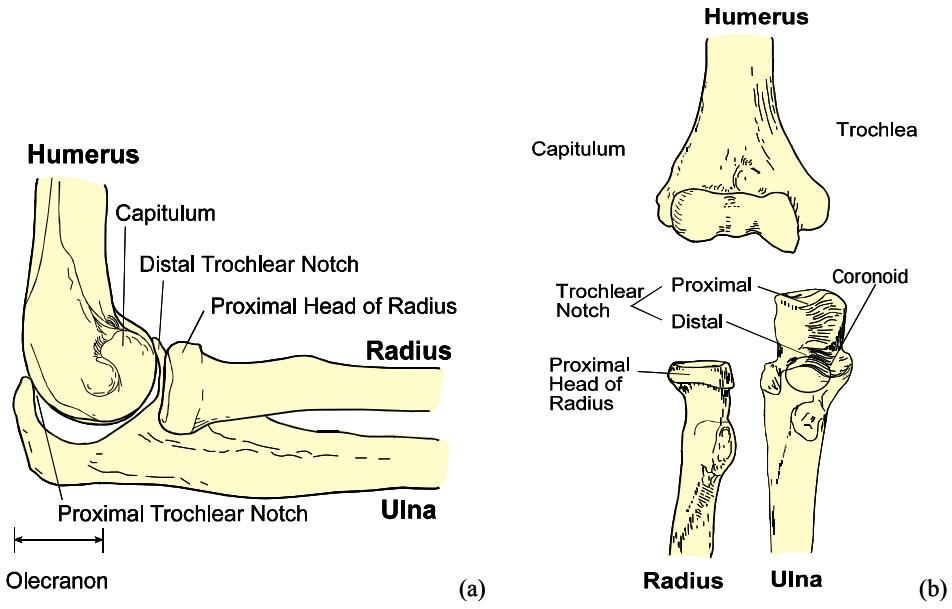

Figure 1: Anatomy of the elbow joint: a) Lateral view, b) Anterior view.

3 Methods

In Part I, 10 original UH-60 CABS side airbag tests were conducted in a Black Hawk helicopter using a 5th percentile female Hybrid III dummy and instrumented upper extremity. For Part II, a single dynamic hyperextension impact test was performed on 24 matched pair human cadaver upper extremities utilizing a three-point bending configuration to initiate dynamic hyperextension of the cadaver elbow joint. Part III followed the same basic methodology as Part I with 12 enhanced UH-60 CABS side airbag modules tested.

3.1 Part I: Original Side Airbag Dummy Upper Extremity Tests

This study was conducted to determine the interaction between an original CABS side airbag deployment and the outboard upper extremity of helicopter aviators. Ten tests

were conducted in a UH-60 Black Hawk helicopter (Figure 2). External electrical power was supplied to operate the aircraft hydraulic systems allowing the flight controls to move as naturally as possible, in the absence of aerodynamic forces, should an airbag or flight control interaction occur. The tests used a 5th percentile female Hybrid III-type anthropomorphic test device (ATD) (First Technology Safety Systems, Plymouth, MI) seated in the cockpit of the aircraft. A SAE 5th percentile female instrumented upper extremity (Denton, Inc., Model 4380, Rochester Hills, MI) was used to record loads produced during upper extremity interactions with the deploying side airbag. A total of 10 side airbags, 5 pilot and 5 copilot modules, were utilized for these tests. These airbags were production-representative versions of the original CABS side airbag, which was a tethered design with a 60 L inflation capacity.

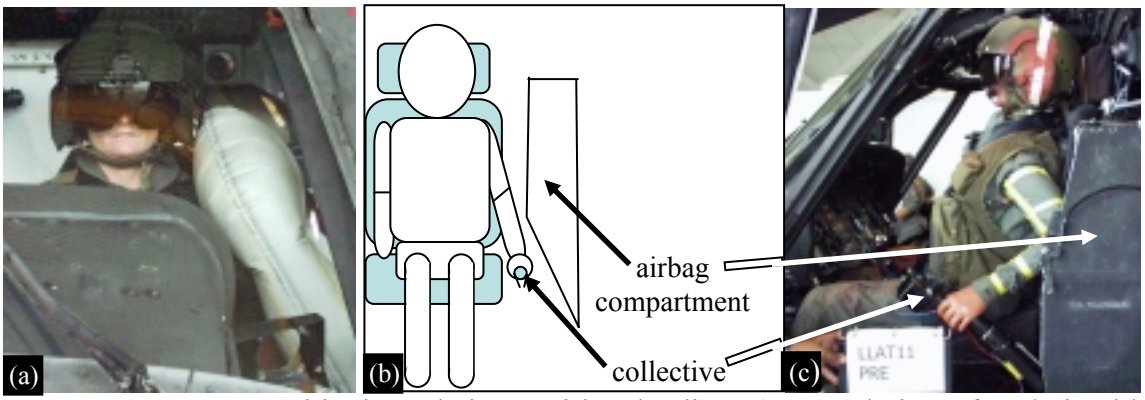

Figure 2: Dummy positioning relative to airbag loading: a) Frontal view of cockpit with side airbag deployed, b) Frontal view of positioning with relevant interior components, c) Lateral view of cockpit with relevant interior components.

The instrumented upper extremity provided 24 channels of data including upper (Denton 3780, Rochester Hills, MI) and lower (Denton, 4461) extremity six-axis load cells, an elbow joint two-axis load cell (Denton, 3781) and rotary potentiometer (Denton, 4005), an upper arm two-axis angular rate sensor, and lower arm axis angular rate sensor.

Load cell data were recorded at a sampling frequency of 10,000 Hz and filtered to CFC 600. The data from the instrumented upper extremity were compared to accepted small female upper extremity injury criteria developed for assessing the risk of airbag induced injury (Duma, 1999, 2003a). Moments recorded in the upper arm were analyzed to assess the risk of humerus fracture, and lower arm moments were examined to determine the risk of radius or ulnar fracture. An Ektapro (Kodak, Rochester, NY) high-speed video system, recording at 1000 fps, was used to document the airbag deployments. The video analysis was used to assess side airbag interaction with the upper extremity and upper extremity interaction with the cyclic in the right crewseat or pilot tests, and the collective in the left crewseat or copilot tests.

During each test, the positions of the crewseat and dummy were selected to place the dummy in positions characteristic of actual flight perceived to be potentially hazardous (Figure 2). The intent of these tests was to place the instrumented upper extremity in the deployment path of the side airbag, and thus at a risk of airbag induced injury. The helicopter pilot and copilot crewseats were adjusted to five aviator positions with respect to fore and aft and up and down seat placement (Table 1). The dummy was dressed in representative aircrew attire consisting of a one-piece Nomex® flight suit, SRU-21/P survival vest, and SPH-4 flight helmet. The aviator's restraint system was fastened and adjusted to a light tension with the inertia reel unlocked. The dummy was positioned such that its left hand gripped the collective and its right hand grasped the cyclic. In both the pilot and copilot positions, the initial location of the right extremity is more medial than the left since the right extremity grasps the cyclic centrally positioned in front of the pilot. For both crewseat positions, the right upper extremity crosses the

right femur, while the left upper extremity is at the pilot's side and parallel to the femur, gripping the collective. The initial configuration of the dummies in the pilot and copilot positions resulted in different potential loading scenarios. The right upper extremity of the dummy in the pilot position grasped the cyclic and the left upper extremity of the dummy in the copilot position grasped the collective. These two extremities were in the path of the deploying side airbags. The left extremity of the copilot dummy was closer to a side airbag than the right extremity of the pilot dummy.

Table 1: Crewseat position matrix.

Test ID	Aspect	Seat Position	
		Fore/Aft	Up/Down
1.01	Left	Full Aft	Down
1.02	Left	Midpoint	Midpoint
1.03	Left	Full Fore	Midpoint
1.04	Left	Full Aft	Midpoint
1.05	Left	Midpoint	Midpoint
1.06	Right	Full Aft	Midpoint
1.07	Right	Full Aft	Above Midpoint
1.08	Right	Full Aft	Above Midpoint
1.09	Right	Midpoint	Midpoint
1.10	Right	Full Fore	Midpoint

3.2 Part II: Upper Extremity Injury Criteria Development

The purpose of Part II was to investigate injury resulting from rotational loading of the elbow joint in hyperextension under dynamic loading conditions similar to a cockpit side airbag deployment and to develop elbow injury criterion to assess upper extremity injury risk. A single dynamic hyperextension impact test was performed on 24 matched pair human cadaver upper extremities (12 cadavers). The energy source was a drop tower utilizing a three-point bending configuration to provide dynamic hyperextension of the elbow joint with bending moments matching the onset rate, peak

moment, and momentum transfer of the previously conducted original CABS side airbag tests.

3.3 Subject Information

All cadaver upper extremities were obtained from females 29 to 85 years old. Pre-test OsteoGrams were obtained for each upper extremity (Compumed, Inc., Los Angeles, CA). These OsteoGrams were used to examine the Bone Mineral Density (BMD) of the test subjects to identify if any specimen possessed a pre-existing osteoporotic condition (Table 2, Appendix A). BMD is the measured amount of calcium in regions of the bones. The BMD index is the readout from the x-ray in arbitrary units and results are reported with respect to the normal population. A t-score can be used to compare the subject's bone mineral density with that of the general population whereas a z-score can be used to compare the bone mineral density of a subject with the average score for their age. The t-score is generally low for elderly subjects. A t-score of -1 corresponds to one standard deviation below the mean for a 30-year old subject, meaning the individual is at the 37th percentile for bone mineral density, or close to normal. T-scores of 2 and 3 correspond to 97^{th} and 99^{th} percentiles, respectively.

Table 2: Cadaver upper extremity data and test matrix.

Test ID	Subject Number	Aspect (Left/Right)	Age (years)	Mass (kg)	BMD Index	T-Score	Z-Score
2.01	1	Left	61	53.98	77.9	-3.0	-1.2
2.02	1	Right	61	53.98	77.9	-3.0	-1.2
2.03	2	Left	67	63.41	75.2	-3.3	-1.0
2.04	2	Right	67	63.41	75.2	-3.3	-1.0
2.05	3	Left	73	45.36	73.7	-3.4	-0.7
2.06	3	Right	73	45.36	73.7	-3.4	-0.7
2.07	4	Left	64	56.70	89.2	-2.0	0.0
2.08	4	Right	64	56.70	89.2	-2.0	0.0
2.09	9	Right	63	44.90	109.6	-0.1	1.6
2.10	8	Right	29	85.30	126.5	1.4	1.4
2.11	5	Right	59	79.40	124.4	1.3	2.3
2.12	6	Right	54	49.90	90.0	-1.9	-0.9
2.13	9	Left	63	44.90	109.6	-0.1	1.6
2.14	8	Left	29	85.30	126.5	1.4	1.4
2.15	5	Left	59	79.40	124.4	1.3	2.3
2.16	6	Left	54	49.90	90.0	-1.9	-0.9
2.17	7	Right	58	97.50	120.3	0.9	1.8
2.18	10	Right	65	60.30	88.9	-2.0	0.0
2.19	11	Right	85	52.20	74.3	-3.4	-0.4
2.20	12	Right	42	54.40	96.4	-1.3	-1.3
2.21	7	Left	58	97.50	120.3	0.9	1.8
2.22	10	Left	65	60.30	88.9	-2.0	0.0
2.23	11	Left	85	52.20	74.3	-3.4	-0.4
2.24	12	Left	42	54.40	96.4	-1.3	-1.3

3.4 Experimental Configuration

To stabilize the upper extremity in the test configuration, the proximal two thirds of tissue was removed from the humerus and inserted into a rigid square aluminum potting cup with polymer filler (Bondo Corporation, Atlanta, GA) (Figure 3). The head of the humerus was removed using a bone saw to ensure a proper fit into the potting cup. Each upper extremity was preconditioned manually by flexing and extending it 10 times prior to testing. To maintain bending in the sagittal plane, a semicircular roller support was attached to the wrist and the aluminum pot connected to the proximal humerus. The rollers at the ends of the specimen were then placed on greased horizontal reaction plates.

The distance between the reaction plates was adjustable to accommodate the various lengths of the upper extremities used for the tests. The upper extremity was positioned on top of the reaction plates with the distal end to the right such that the impactor head would contact the humerus pot upon impact. The forearm was positioned in full supination with the elbow entirely extended over the supports.

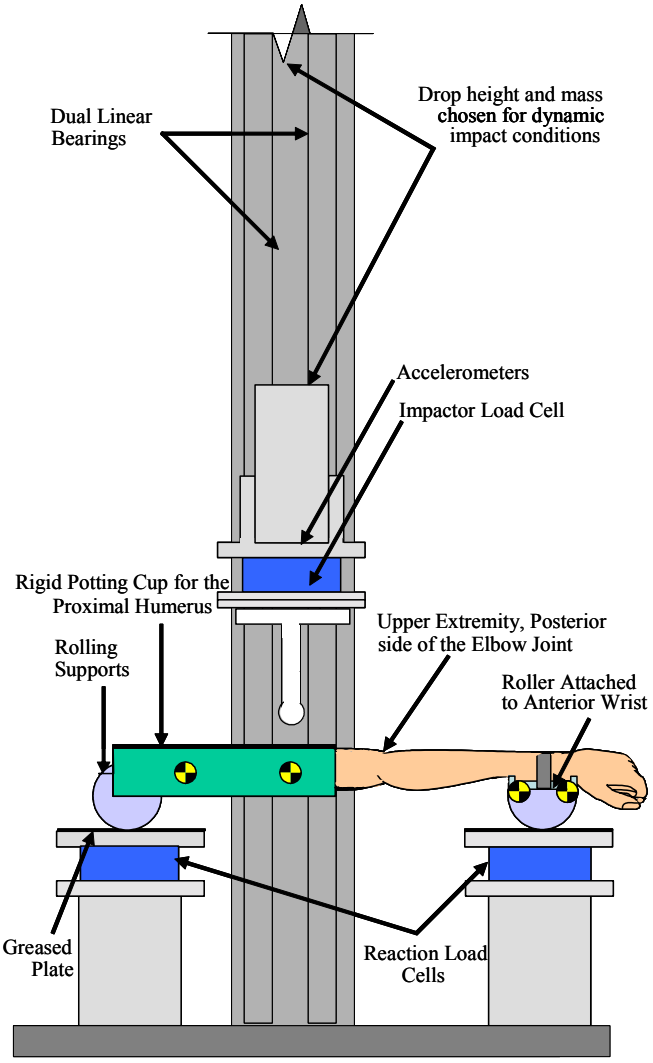

Figure 3: Drop test configuration for dynamic hyperextension of the cadaver elbow joint.

The upper extremities were randomly divided into two equal groups. Each group was subjected to one of the following impact scenarios: 9.75 kg impactor mass at a high

energy drop height of 0.910 m, or the same impactor mass at a low energy drop height of 0.303 m. The impactor assembly traveled on four reciprocating roller bearings connected to two linear shafts to reduce lateral flexibility. Instrumentation included six-axis load cells placed on the impactor and two supports, as well as accelerometers used for inertial compensation. The impactor load cell (Denton 1968, 22,240 N, Rochester Hills, MI) was used to measure loads exerted onto the specimen by the impactor. Each reaction plate was supported by a single reaction load cell (Denton 5768, 11,120 N, Rochester Hills, MI) that measured the loads exerted by each end of the upper extremity. An accelerometer (Endevco 7264B, 2000 G, San Juan Capistrano, CA) was attached to the impactor head to allow for inertial compensation of the mass between the upper extremity and active axis of the load cell. During the loading, the impactor head contacted a trigger strip positioned on top of the humerus pot to initiate the data acquisition for each test. Data from the load cells and accelerometers were recorded at a sampling frequency of 30,000 Hz with 16-bit Analog-to-Digital conversion resolution (Iotech WBK16, Cleveland, OH). Test kinematics were captured by high-speed video at 2,000 fps (Vision Research, Phantom IV, Wayne, NJ). All channels were filtered to CFC 600.

3.5 Post-Test Analysis

Post-test detailed necropsies and cartilage ink staining analyses were conducted. Necropsies were performed to reveal the presence of bony fractures of the humerus, ulna, or radius, or large chondral and osteochondral fractures of the elbow joint as well as ligament damage and joint capsule disruption. Ink staining was used to highlight small fissures on the cartilage surface.

A free-body diagram illustrates the three-point bending configuration of the upper extremity with the layout of the left, F_{LR}, and right, F_{RR}, reaction forces and the inertially compensated impactor force, F_{IMP}, recorded from the three load cells. Using D'Alembert's method, a generalized inertial term, *ma*, and disregarding rotational inertia, the dynamic equilibrium equation is developed (Equation 1, Figure 4). In this study, the generalized inertial term was the difference between the impactor force and the sum of the reaction forces, representing the inertia from the linear acceleration of the effective mass of the upper extremity during the impact event. The moment about the elbow joint was determined using the reaction force measured by the right load cell. The right support was used to calculate the bending moment about the elbow as it does not include the inertial effects of the upper extremity. For each upper extremity, the right support force was multiplied by the individual forearm length, as measured from the right wrist roller to the center of rotation of the elbow joint, x, resulting in the value of the moment about the elbow joint (Equation 2).

$$\text{Impactor Force } (F_{IMP}) = F_{LR} + F_{RR} + ma \quad (1)$$

$$\text{Elbow Moment } (m) = (F_{RR})(x) \quad (2)$$

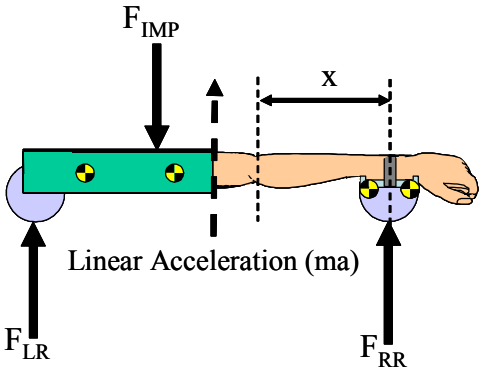

Figure 4: Free-body diagram of impactor and reaction forces during impact with cadaver upper extremity.

3.6 Statistical Analysis

A statistical analysis was performed to characterize the forces acting on the cadaver specimens and correlate them to the anatomic injury assessments of necropsy and ink staining. As a part of this analysis, a logistic regression analysis was performed to develop injury risk functions based upon experimental results. The binary subject variables were injury or no injury and specific injury outcome values, while the anthropometric and test data, such as mass and peak moment, were the independent test variables in this analysis. The specific input variables analyzed were age, specimen mass, BMD, pre-existing hyperextension, energy, and peak moment while the binary, injury output variables analyzed were injury, severe injury, fracture, dislocation/disruption, ligament damage, and cartilage damage. The statistical analysis comprised three parts.

First, the Pearson correlation coefficients, or R values, were computed with statistical software (SAS Institute, Inc., Cary, NC) to measure the strength of linear relationships between the input and output variables. An R-value found to be greater than 0.5 demonstrated a strong correlation between variables.

Second, a logistic model, using a standard logistic regression from the same SAS procedure described above, was used to perform a single variate analysis for the determination of p-values. This method tested if the correlations were zero, assuming a normal distribution. However, since no adjustment was made for the matched pairs, the relationships obtained by these p-values could only be considered preliminary. P-values near or below 0.05 were considered to be significant.

Third, a logistic model using a paired GENMOD logistic regression analysis was used to perform a single variate analysis for the determination of p-values. This model

was preferred over the previous logistic model due to its ability to use a binomial distribution, which was more appropriate for analyzing the binary injury or no injury variables existing in this analysis. Also, this method could account for two samples or a matched pair from each subject, providing more accurate estimates of variability and tests of significance. P-values near or below 0.05 were considered to be significant. In addition, risk function curves were developed. For certain combinations of risk factors, additional GENMOD models were investigated. Again logistic models were fit to the data and risk functions derived to investigate the combined effect of these variables on injury. The goodness of fit to the model was evaluated for each risk function using a likelihood ratio test to output chi square values ($\acute{\alpha} = 0.1$). The test was calculated as -2 multiplied by the difference between the likelihood for the intercept only model and the likelihood for the model containing the variables. For models with one, two, or three degrees of freedom, a chi square value greater than 2.7, 4.6, and 6.25 were considered to be good, respectively.

Finally, a Consistent Threshold (CT) non-parametric model, chosen for its capability of being a maximum likelihood estimate, was used to quantitatively assess the goodness of fit of the previous logistic regression parametric model (Nusholtz, 1999). A study performed by Domenico and Nusholtz (2003) stated that it is incorrect to assume the shape of the injury risk curve for impact experiments and that non-parametric data analysis is better suited for biomechanical data since it is not constrained by a prior specified risk form. However, a more recent analysis performed by Kent (2004) found that differences between the parametric and non-parametric were only found to be most notable at the tails of the parametric curve. This study also found that when choosing a

parametric distribution, no one parametric distribution studied was consistently more appropriate than any other when compared to a non-parametric distribution.

3.7 Part III: Enhanced Side Airbag Dummy Upper Extremity Tests

The purpose of Part III was to assess a re-designed, enhanced UH-60 CABS side airbag to characterize side airbag-related upper extremity axial and rotational loading to ensure risks obtained from the original design were reduced prior to implementing the new system. To facilitate this, 12 enhanced side airbag deployments were conducted using 6 pilot and 6 copilot modules. The airbag modules used were production-representative versions of the enhanced UH-60 CABS side airbag, which was also a tethered design with a minimized 45 L inflation capacity.

The basic methodology of this study followed the same configuration, instrumentation, video analysis, and data acquisition procedures as Part I. However, additional accelerometers were used on the upper and lower segments of the instrumented upper extremity to measure wrist and elbow axial loading in light of recently developed injury criteria (Duma 1998, 2000, 2002, 2003b). Axial loads recorded in the wrist were analyzed to assess the risk for any type of wrist injury, whereas axial loads measured in the elbow were used to assess the risk of distal trochlear notch injuries based on a load angle 30˚ vertical of the long axis of the forearm. Also, the elbow bending moment injury risk function created for the female upper extremity in Part II was used to determine injury risk from the enhanced side airbag.

All 12 tests were conducted with the dummy seated in similar aviator positions as Part I except for test 3.06, which was added to the present test series as a worst-case position, meant to produce the maximum interaction between the left upper extremity and

the enhanced side airbag. In this test, the seat was positioned at the full extent of its forward and upward travel. This position is extreme, but not unreasonable, particularly for aviators of short stature or sitting height.

4 Results

4.1 Part I: Original Side Airbag Dummy Upper Extremity Tests

Video analysis revealed considerable contact between the deploying side airbag and the dummy's outboard upper extremity in the pilot and copilot crewstations. The deploying side airbag often made initial contact with the shoulder. The initial deployment trajectory was dependent upon the initial position of the dummy such that the side airbag appeared to seek unoccupied areas. The side airbag placed the left upper extremity in hyperextension in three out of the five tests when the left hand did not freely release from the collective (Figure 5).

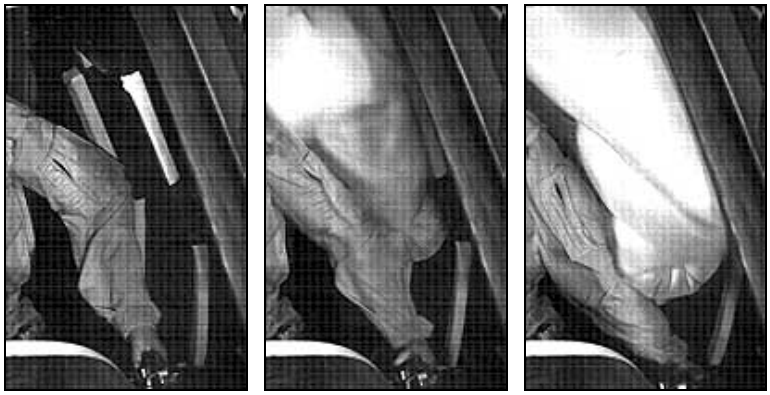

Figure 5: Dummy upper extremity hyperextension when collective restrains the hand.

The peak force and moment values of all tests were compared against injury risk curves proposed for the instrumented upper extremity with respect to the forearm and humerus (Duma, 1999, 2003a) (Table 3). No injury criteria were available at the time for

use in evaluating the risk of elbow injury associated with the rotational loads produced by hyperextension. Therefore, the risk caused by the determined elbow bending moments was unknown. High risks of forearm fracture were observed during three out of the five left side airbag tests. These risks exceeded a 90% chance of fracture to the radius or ulna. Also, high risks of humerus fracture were observed during two out of the five left side airbag tests with risks that exceeded an 80% chance of fracture. Higher moment values and injury risks were obtained for the left extremity of the dummy in the copilot position.

Table 3: Summary of Part I results: Peak values due to original side airbag loading of the dummy upper extremity.

Test ID	Aspect	Humerus Bending Moment (Nm) (% Risk)	Humerus Axial Load (N)		Forearm Bending Moment (Nm) (% Risk)	Forearm Axial Load (N)		Elbow Bending Moment (Nm)
			Compression	Tension		Compression	Tension	
1.01	Left	65.8 (0.3)	482.5	1103.7	24.9 (5.0)	244.3	388.0	10.0
1.02	Left	143.2 (81.0)	1285.1	1282.7	108.3 (94.5)	547.1	860.2	128.0
1.03	Left	20.5 (0.0)	223.2	465.9	33.9 (10.0)	331.7	742.6	22.8
1.04	Left	74.0 (0.6)	430.4	615.6	329.5 (99.0)	227.6	612.2	35.6
1.05	Left	191.1 (99.7)	1047.0	1461.0	125.1 (99.0)	2677.6	1028.2	143.6
1.06	Right	49.9 (0.1)	179.9	335.2	11.5 (1.5)	49.1	426.0	14.2
1.07	Right	96.1 (4.5)	99.8	755.6	32.3 (9.0)	408.5	442.7	12.7
1.08	Right	59.0 (0.1)	199.4	760.4	10.4 (1.4)	334.2	372.5	13.5
1.09	Right	9.8 (0.0)	75.5	65.7	**	**	**	**
1.10	Right	14.0 (0.0)	152.0	75.8	5.8 (1.0)	27.8	237.3	5.7

** Data acquisition system failure.

4.2 Part II: Upper Extremity Injury Criteria Development

The onset rate, peak bending moment, and momentum transfer values attributed to the side airbag and drop tower energy sources from Parts I and II, respectively, were

found to be similar. This similarity was determined by comparing instrumented upper extremity tests to cadaver dynamic hyperextension tests (Figure 6).

The peak elbow bending moments ranged from 42.4 Nm to 146.3 Nm (Table 4, Appendix B). By comparing the moment versus time plots of two matched pair specimens, while subject 7 and subject 12 were both exposed to the same amount of energy, subject 7 obtained an elbow joint dislocation with medial and lateral ligaments almost completely torn, whereas subject 12 had only an elbow joint dislocation (Figure 7).

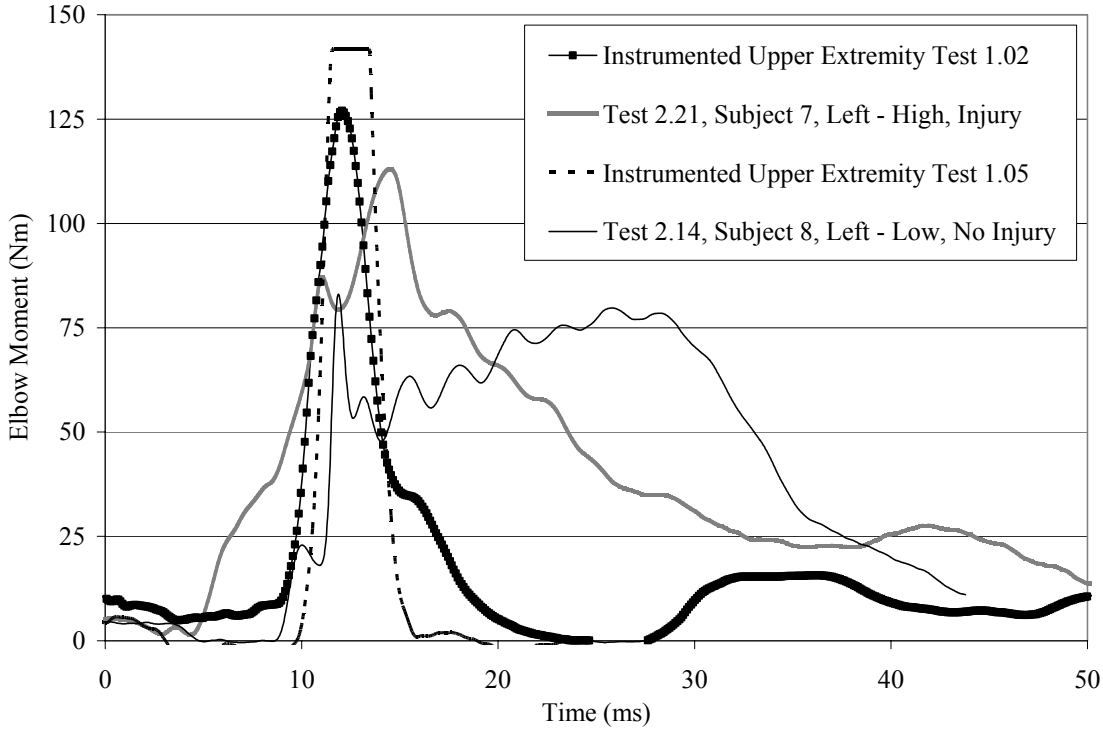

Figure 6: Comparison of bending moment between cadaver dynamic hyperextension tests and dummy side airbag tests.

Post-test necropsies showed that 16 of the 24 elbow joint tests resulted in injury. The types of injuries observed, either singularly or in combination, were fractures, joint dislocations, ligament damage, cartilage damage, or anterior capsule disruption (Table 5).

The types of chondral and osteochondral fractures that occurred were to the humerus, coronoid, radial head, trochlea, trochlear notch, and olecranon (Figures 8 and 9). Injuries ranged in severity from minor cartilage lesions and ligament dislocations (AIS 1), to anterior capsule tears, chondral fractures to the radial head, and coronoid and joint dislocations (AIS 2), to the most severe transverse fractures of the distal humerus (Appendix C, D).

All 12 high energy tests resulted in injuries totaling 5 joint dislocations, 9 fractured limbs, 3 ligament injured limbs, 1 cartilage injury, and 1 anterior capsule disruption. Eight of the 12 low energy tests sustained no injuries, whereas the other 4 specimens obtained 3 fractured limbs, 1 ligament injury, and 1 anterior capsule disruption. Note that the small number of capsule disruptions reported here occurred without a joint dislocation and were not investigated statistically. None of the low injury tests sustained joint dislocations or cartilage injury.

Table 4: Cadaver test data and summary binary injury outputs.

Test ID	Subject Number	Aspect (Left/Right)	Drop Height (m)	Peak Elbow Moment (Nm)	Summary Binary Injury Outputs		
					Any Injury (Y/N)	Any Severe Injury (Y/N)	Fracture (Y/N)
2.01	1	Left	0.910	86.1	Yes	Yes	Yes
2.02	1	Right	0.303	58.3	No	No	No
2.03	2	Left	0.303	42.4	Yes	Yes	Yes
2.04	2	Right	0.910	68.9	Yes	Yes	Yes
2.05	3	Left	0.910	77.8	Yes	Yes	Yes
2.06	3	Right	0.303	45.3	No	No	No
2.07	4	Left	0.303	49.6	Yes	No	No
2.08	4	Right	0.910	92.7	Yes	Yes	Yes
2.09	9	Right	0.303	60.9	No	No	No
2.10	8	Right	0.910	141.7	Yes	No	No
2.11	5	Right	0.303	55.0	Yes	Yes	Yes
2.12	6	Right	0.910	52.6	Yes	Yes	Yes
2.13	9	Left	0.910	146.3	Yes	Yes	Yes
2.14	8	Left	0.303	83.0	No	No	No
2.15	5	Left	0.910	90.1	Yes	Yes	Yes
2.16	6	Left	0.303	55.9	No	No	No
2.17	7	Right	0.303	71.6	No	No	No
2.18	10	Right	0.910	89.1	Yes	Yes	Yes
2.19	11	Right	0.303	49.8	No	No	No
2.20	12	Right	0.910	102.1	Yes	Yes	No
2.21	7	Left	0.910	113.0	Yes	Yes	No
2.22	10	Left	0.303	60.2	Yes	Yes	Yes
2.23	11	Left	0.910	75.8	Yes	Yes	Yes
2.24	12	Left	0.303	47.9	No	No	No

Table 5: Cadaver test binary injury outputs.

Test ID	Subject Number	Specific Binary Injury Outputs				
		Humerus Fracture (Y/N)	Coronoid Fracture (Y/N)	Dislocation/ Disruption (Y/N)	Ligament Damage (Y/N)	Cartilage Damage (Y/N)
2.01	1	Yes	Yes	No	No	No
2.02	1	No	No	No	No	No
2.03	2	No	Yes	No	No	No
2.04	2	No	No	No	Yes	No
2.05	3	Yes	No	No	No	No
2.06	3	No	No	No	No	No
2.07	4	No	No	Yes	No	Yes
2.08	4	No	No	Yes	No	No
2.09	9	No	No	No	No	No
2.10	8	No	No	Yes	No	No
2.11	5	No	Yes	No	Yes	No
2.12	6	Yes	No	No	No	No
2.13	9	No	Yes	Yes	No	No
2.14	8	No	No	No	No	No
2.15	5	Yes	No	No	No	Yes
2.16	6	No	No	No	No	No
2.17	7	No	No	No	No	No
2.18	10	Yes	No	No	No	Yes
2.19	11	No	No	No	No	No
2.20	12	No	No	Yes	No	No
2.21	7	No	No	Yes	Yes	No
2.22	10	Yes	No	No	No	No
2.23	11	No	Yes	Yes	Yes	No
2.24	12	No	No	No	No	No

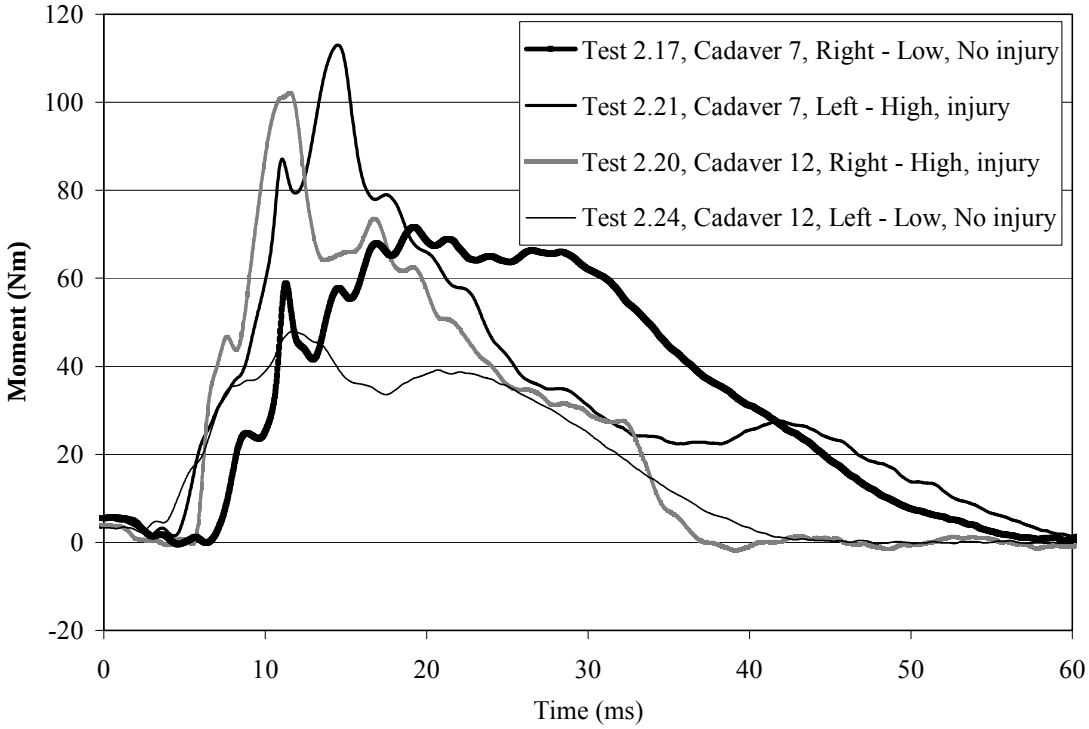

Figure 7: Elbow moment versus time plot for two cadaver matched pair specimen.

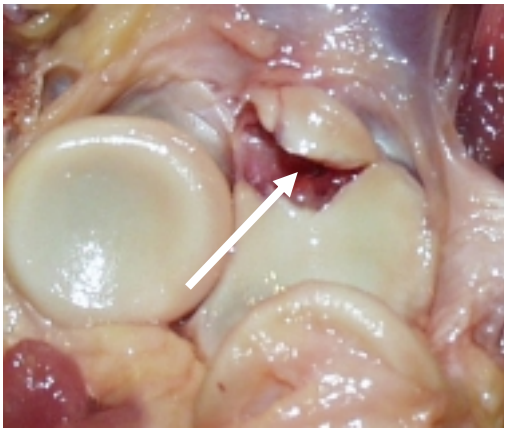

Figure 8: Test 2.03 - Avulsion, osteochondal fracture of the coronoid.

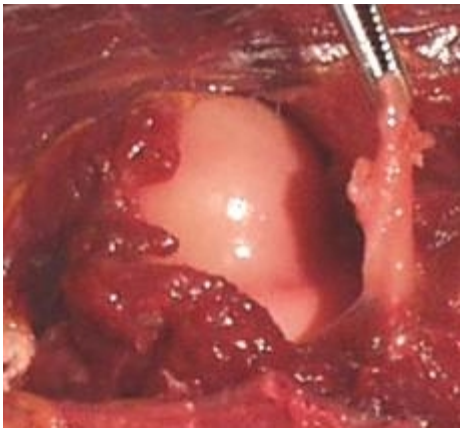

Figure 9: Test 2.10 - Disruption of the anterior capsule.

4.3 Statistical Correlations for Cadaver Tests

Strong statistical correlations were found between peak elbow bending moment and the risk for any elbow injury as well as between peak elbow bending moment and the risk for elbow joint dislocation (R=0.421, R=0.630). Impact energy correlated well with every output variable except ligament and cartilage damage (Table 6).

Table 6: Correlation coefficients (R-values) for cadaver tests.

	Test Variables					
Subject Variables	Age	Specimen Mass	BMD	Pre-existing Hyperextension	Energy	Peak Moment
Any Injury	0.097	0.066	-0.021	0.125	**0.707**	**0.421**
Severe Injury	0.261	-0.032	-0.129	0.060	**0.676**	0.281
Dislocation	-0.101	0.081	0.177	0.130	**0.458**	**0.630**
Fracture	0.380	-0.178	-0.239	0.000	**0.500**	0.086
Ligament Damage	0.238	0.313	0.071	-0.079	0.224	0.040
Cartilage Damage	0.077	-0.021	-0.072	-0.147	0.209	0.101

Peak elbow bending moment proved to be a significant indicator of the risk of any elbow injury and the risk of elbow joint dislocation based upon the single variate logistic model using a standard logistic regression assuming a normal distribution (p=0.041, p=0.001). Again, all relationships between energy and the output variables, minus ligament and cartilage damage, were significant (Table 7).

Table 7: Logistic regression single variate p-value data for cadaver tests.

	Test Variables					
Subject Variables	Age	Specimen Mass	BMD	Pre-existing Hyperextension	Energy	Peak Moment
Any Injury	0.650	0.758	0.924	0.561	**0.000**	**0.041**
Severe Injury	0.218	0.882	0.549	0.781	**0.000**	0.183
Dislocation	0.638	0.708	0.409	0.546	**0.024**	**0.001**
Fracture	0.067	0.407	0.261	1.000	**0.013**	0.688
Ligament Damage	0.262	0.137	0.743	0.713	0.294	0.852
Cartilage Damage	0.722	0.921	0.736	0.492	0.328	0.640

Peak elbow bending moment proved to be a significant indicator of the risk of any elbow injury and the risk of elbow joint dislocation based upon the single variate logistic model using a GENMOD paired logistic regression analysis assuming a binomial distribution (p=0.019, p=0.009). Again, all relationships between energy and the output variables, minus ligament and cartilage damage, were found to be significant as could be expected. Also, a significant relationship was found between age and ligament damage as well as specimen mass and ligament damage (p= 0.026, p=0.030) (Table 8).

Table 8: GENMOD logistic regression single variate p-value data for cadaver tests.

	Test Variables					
Subject Variables	Age	Specimen Mass	BMD	Pre-existing Hyperextension	Energy	Peak Moment
Any Injury	0.364	0.632	0.885	0.428	0.999	**0.019**
Severe Injury	0.145	0.843	0.525	0.681	**0.002**	0.380
Dislocation	0.469	0.556	0.299	0.558	**0.020**	**0.009**
Fracture	0.059	0.382	0.318	1.000	**0.004**	0.686
Ligament Damage	**0.026**	**0.030**	0.728	0.673	0.330	0.805
Cartilage Damage	0.244	0.707	0.197	0.999	0.999	0.064

4.4 Injury Risk Functions

All 24 dynamic hyperextension impact tests were included in the analysis that produced single variate risk functions for any elbow injury or joint dislocation with respect to the peak elbow bending moment applied during the test. This analysis yielded single variate risk curves as a function of applied peak elbow bending moment alone with the ***x*** variable as the applied peak bending moment through the elbow joint (Equation 3, Table 9 and 10). These curves can be used to determine the risk of any elbow injury or joint dislocation for any bending moment value. For example, for the entire test population, this function predicts a 50% risk of any elbow injury at 56 Nm with a 100% probability of any elbow injury at 186 Nm. At 93 Nm and 194 Nm this risk function

calculates a 50% and 100% risk of elbow joint dislocation, respectively (Figure 10). This function, applied to the elbow bending moment data taken from the original CABS side airbag tests, revealed aviator elbow injury risks that ranged from 6.2% - 99.1% with two peak bending moments of 128 Nm and 144 Nm that achieved a greater than 95% risk. A 4.7% risk for any elbow injury was found at 0 Nm as a function of the parametric logistic regression curve. However, this risk is eliminated when applying the Consistent Threshold Method.

$$\text{Probability of Any Elbow Injury or Dislocation } (x) = \frac{1}{1+e^{(a-b\cdot x)}} \qquad (3)$$

However, more complete multivariate risk functions were determined by individually combining specimen mass and age with the applied peak elbow bending moment (Appendix E). This risk function included the ***y*** variable as either the specimen mass in kilograms or age in years in addition to the ***x*** variable as the applied peak bending moment through the elbow joint (Equation 4). The combination of specimen mass and peak bending moment produced a risk function that was a near significant indicator of any elbow injury (p=0.061), and a good significant indicator of elbow joint dislocation (p=0.001). This risk function can be used to determine the risk of any elbow injury or dislocation for any bending moment value in combination with any specimen mass or age. For example, this function predicts a 50% risk of any elbow injury at 53 Nm for a 48 kg, 5th percentile female, 63 Nm for a 78 kg, 50th percentile male, and 69 Nm for a 98 kg, 95th percentile male. Furthermore, this function predicts a 50% risk of elbow joint dislocation at 85 Nm, 97 Nm, and 105 Nm for the same respective weight classes. This risk function also calculates a 50% risk for any elbow injury at 54 Nm for a 65 year

old, 72 Nm for a 45 year old, and 90 Nm for a 25 year old. At 89 Nm, 100 Nm, and 111 Nm, this risk function calculates a 50% risk of dislocation of the elbow joint at the ages of 65, 45, and 25 years old, respectively.

$$\text{Probability of Any Elbow Injury or Dislocation } (x,y) = \frac{1}{1+e^{(a-b\cdot x-c\cdot y)}} \quad (4)$$

Next, multiple variate analyses were investigated (Appendix E). These terms involved the combination of both specimen mass and age with the applied peak elbow bending moment. This risk function included the ***z*** variable as specimen age in years, the ***y*** variable as specimen mass in kilograms, and the ***x*** variable as the applied peak bending moment through the elbow joint (Equation 5). It can be used to determine the risk of any elbow injury or dislocation for any bending moment value in combination with any specimen mass and age. For example, adjusting for a 48 kg, 40 year old, 5th percentile female, a 50% risk of obtaining any elbow injury was determined at 76 Nm while a 50% risk of obtaining a dislocation was found at 98 Nm.

$$\text{Probability of Any Elbow Injury or Dislocation } (x,y,z) = \frac{1}{1+e^{(a-b\cdot x-c\cdot y-d\cdot z)}} \quad (5)$$

Table 9: Risk function data for any elbow injury using GENMOD logistic regression.

Risk Factors to Any injury	**Risk Function Coefficients**				**chi square value**	**p-value**
	a	**b**	**c**	**d**		
Moment	-3.0195	0.0540			5.620	**0.019**
Moment + Mass	-2.0880	0.0605	-0.0203		5.592	**0.061**
Moment + Age	-7.6087	0.0676	0.0608		7.741	**0.021**
Moment + Mass + Age	-7.3547	0.0684	-0.0036	0.0594	7.750	**0.051**

Table 10: Risk function data for elbow joint dislocation using GENMOD logistic regression.

Risk Factors to Dislocation	Risk Function Coefficients				chi square value	p-value
	a	b	c	d		
Moment	-6.4258	0.0691			10.377	**0.009**
Moment + Mass	-5.2840	0.0796	-0.0315		10.993	**0.001**
Moment + Age	-10.238	0.0817	0.0456		11.266	**0.001**
Moment + Mass + Age	-8.7735	0.0863	-0.0218	0.0379	11.513	**0.001**

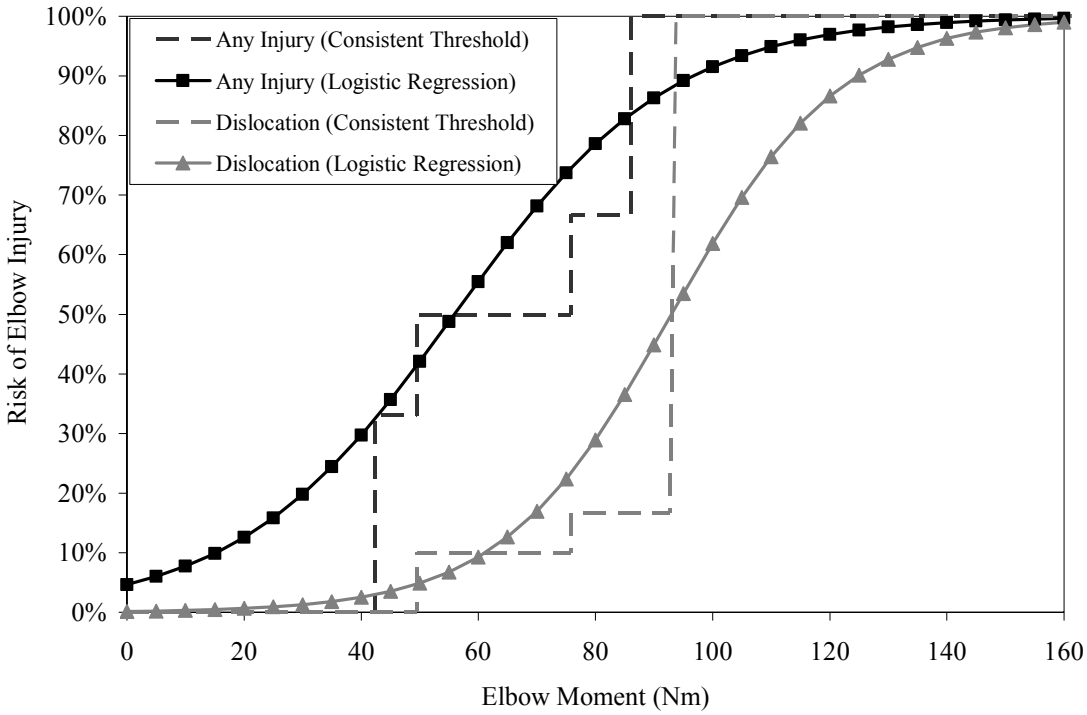

Figure 10: Risk of any elbow injury (p=0.019) or elbow joint dislocation (p=0.009) based upon peak elbow bending moment for female cadaver specimen.

4.5 Part III: Enhanced Side Airbag Dummy Upper Extremity Tests

High-speed video revealed considerable contact between the deploying side airbag and the dummy's outboard upper extremity and shoulder in the pilot and copilot crewstation. In two tests of the original side airbag design, high probabilities of left humerus fracture were recorded at 81% and 99.7%. Comparable tests of the enhanced bag showed a 0% chance of humerus fracture (Table 11). In two of the four right upper

extremity comparable test pairs, the risk of right humerus fracture was marginally increased with the enhanced side airbag design. The highest probability of right humerus fracture due to the enhanced side bag with typical dummy seat placement was only 3.6%. With the dummy seated in the worst case position, a 28.6% risk of left humerus fracture was found.

When comparing the results of the enhanced side airbag test to the results of the original side airbag tests, in all five comparable test pairs of the left forearm, the probability of forearm fracture was reduced. In these test pairs, the highest probability of fracture was only 1.1%, not including the worst case. The highest probability of fracture due to the enhanced side airbag in any test was the worst case test recorded at 2.5%. When considering the right forearm, the highest probability of fracture due to the enhanced side bag was 1.1%.

Table 11: Summary of Part III results: Peak values due to enhanced side airbag loading of the dummy upper extremity.

Test ID	Aspect	Humerus Bending Moment (Nm) (% Risk)	Humerus Axial Load (N)		Forearm Bending Moment (Nm) (% Risk)	Forearm Axial Load (N)		Elbow Bending Moment (Nm) (% Risk)	Elbow Axial Load (N) (% Risk)	Wrist Axial Load (N) (% Risk)
			Compression	Tension		Compression	Tension			
3.01	Left	19.9 (0.0)	114.2	152.9	3.2 (<1.0)	87.9	44.2	3.7 (5.6)	199.6 (0.2)	55.9 (1.4)
3.02	Left	21.7 (0.0)	110.5	167.3	2.6 (<1.0)	45.7	29.9	2.8 (5.4)	156.2 (0.2)	-39.0 (1.1)
3.03	Left	28.3 (0.0)	451.9	219.0	7.3 (1.0)	222.3	76.5	4.6 (5.9)	567.0 (0.9)	103.8 (1.6)
3.04	Left	32.2 (0.0)	381.5	242.7	8.1 (1.1)	224.7	29.9	4.5 (5.9)	491.0 (0.7)	207.8 (2.1)
3.05	Left	59.9 (0.1)	403.2	215.4	4.5 (<1.0)	447.1	32.9	14.1 (9.5)	920.9 (3.3)	114.9 (1.6)
3.06	Left	118.4 (28.6)	371.8	276.5	17.0 (2.5)	653.8	30.4	23.9 (15.1)	1220.6 (9.3)	353.8 (3.0)
3.07	Right	9.3 (0.0)	398.5	150.6	3.0 (<1.0)	148.8	35.4	2.1 (5.2)	240.4 (0.3)	101.0 (1.6)
3.08	Right	93.1 (3.6)	889.7	399.5	7.5 (1.0)	625.2	50.5	19.3 (12.2)	977.1 (4.0)	401.5 (3.4)
3.09	Right	16.4 (0.0)	215.6	112.4	4.7 (<1.0)	142.8	93.5	2.4 (5.3)	252.1 (0.3)	-123.2 (0.9)
3.10	Right	80.0 (1.0)	668.6	320.6	7.4 (1.0)	489.2	148.5	21.2 (13.3)	757.0 (1.8)	282.4 (2.5)
3.11	Right	85.6 (1.7)	629.3	281.5	9.5 (1.1)	528.9	133.1	20.2 (12.7)	781.5 (2.0)	462.8 (3.9)
3.12	Right	9.8 (0.0)	773.0	104.3	3.3 (<1.0)	68.8	19.1	2.8 (5.4)	171.7 (0.2)	46.8 (1.4)

Based upon the elbow bending moment injury risk function developed in Part II, a maximum probability of elbow injury was found to be 9.5% and 13.3% for left and right elbow joints, respectively, when exposed to an enhanced side airbag deployment. These values exclude the worst case test, which was found to have a 15.1% risk. However, these risk values, including the worst case, are greatly reduced in comparison to the peak elbow bending moment risk values found in Part I that exceeded 95% risk due to the original CABS design. Also, the peak axial force values were compared against new injury risk curves proposed for the instrumented upper extremity with respect to the elbow joint (Duma, 1998, 2002). All axial elbow joint loads obtained by the enhanced

airbag showed to have an overall minimal risk of causing injury, with a maximum risk occurring at 9.3 % for the left elbow joint and 4.0% for the right elbow joint.

5 Discussion

The newly developed elbow injury risk functions predict a 50% risk of any elbow injury at 56 Nm with a 100% probability of any elbow injury at 186 Nm. Also, at 93 Nm and 194 Nm, this risk function calculates a 50% and 100% risk of elbow joint dislocation, respectively. These results indicate that a higher moment is required to cause an elbow joint dislocation than to cause any combination of injuries. This could be caused by the fact that a brittle bone fracture may require less force than the dislocation of a strong elbow joint. Taking into account the broad range of human specimen age and BMD data presented in this current study further strengthens this argument. Therefore, if a bone fracture does not initially occur, the force is able to continue to heighten to a point at which it is able to dislocate the joint. Also, less force is required to incur minor injuries, such as minor cartilage lesions and ligament dislocations, which are included in the risk for any injury. Furthermore, it is noted that all joint dislocations (AIS 2) occurred during only high energy tests while more severe injuries such as fractures (AIS 3) occurred in both energy levels. Although extra-articular fractures may be considered severe on a threat to life scale, they are medically simpler to repair with less long term pain. In contrast, elbow joint dislocation can lead to long term pain and even loss of functionality if the condition becomes arthritic.

The decrease in humerus and forearm axial compression and tension in the left upper extremity is a positive effect of the enhanced airbag system, but the reason for an

increase in right upper extremity loads in axial compression is unclear. Differences in outboard upper extremity position between the right and left seats may account for these findings. Manipulation of the collective lever by the left upper extremity requires flexion and extension of the elbow while the forearm remains generally parallel to the long axis of the aircraft. Operation of the cyclic by the right upper extremity is more complex, requiring movement of the cyclic head forward, backward, left, and right, with the forearm generally deviating medially to allow grasping of the centrally mounted cyclic handgrip. It is not immediately apparent why the measured axial compressive forces should decrease in the left upper extremity but increase in the right upper extremity with the introduction of the enhanced side airbag. Side airbag trajectory may play a part in generating axial loads. The deployment trajectory of the enhanced side airbag is different from the original design as are the unfolding and inflation patterns (Figure 11). The initial deployment trajectory of the enhanced airbag appeared to be upward, toward the upper shoulder area, as opposed to forward toward the upper extremity as in the original design. Loads generated by this interaction could be transferred through the elbow into the forearm resulting in elevated forearm axial compressive loads. The deploying airbag also appears to be less inflated, allowing the bag to go around the aviator's upper extremity and shoulder. In the previous side airbag design, the deploying bag appeared to be more fully inflated as it deployed from the module, and thus more likely to contact the body regions as it deployed forward. The aggressivity of an airbag is representative of the deploying airbag's energy in the form of geometry, velocity, mass, deployment trajectory, and pressure, and can be interpreted as the airbag system's potential to do harm. The aggressivity of the enhanced side airbag may have increased over the original

design, as the gas generator is the same while the bag size and volume have been reduced. This potential increase in bag aggressivity due to bag volume reduction may be mitigated by altering its deployment trajectory and pattern to areas less likely to be occupied by an aviator.

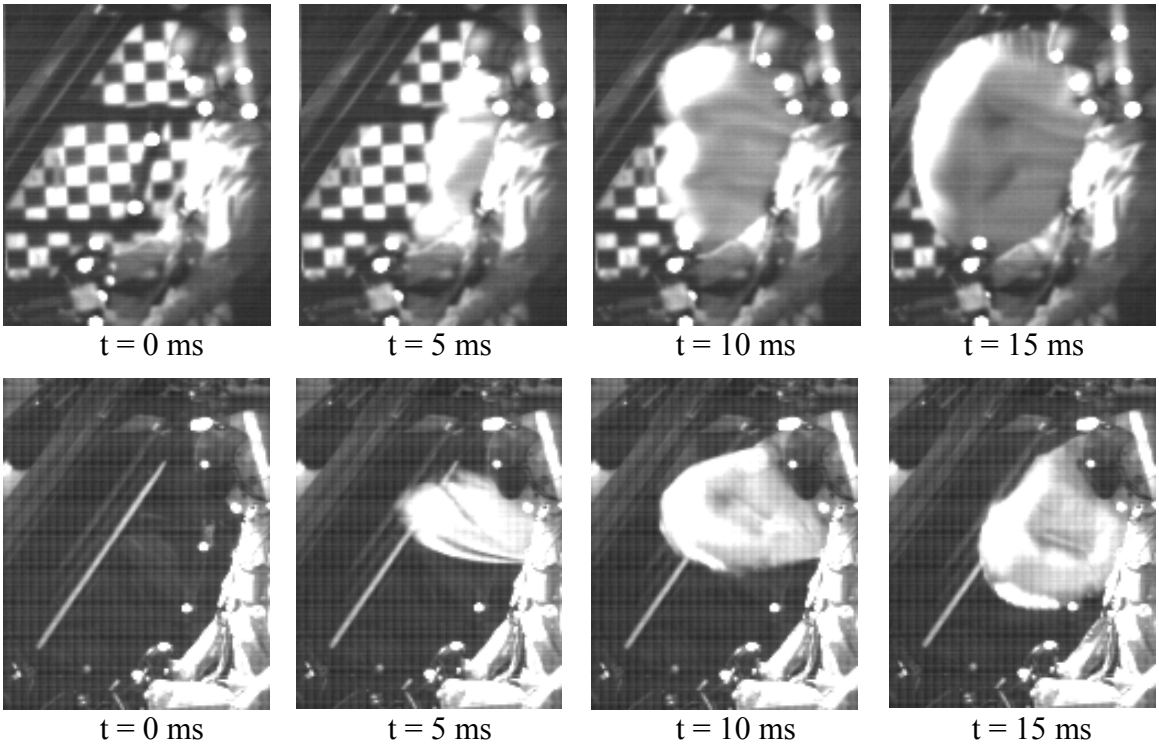

Figure 11: Comparison of original and enhanced side airbag deployment trajectories. Upper photographic series: original side airbag; lower photographic series: enhanced side airbag.

There are numerous variables affecting the airbag system performance and injury potential. Anthropometric measures influencing side airbag injury potential could include sitting shoulder height, shoulder breadth, hip width, upper arm length, and lower arm length. Flight control and aviator position at the time of airbag deployment further complicates injury risk estimation. Using all available upper extremity injury criteria, the

enhanced CABS side airbag was found to have reduced the risk of injury to the upper extremity compared to the original CABS side airbag system.

The SAE 5th percentile female instrumented upper extremity has been shown to be capable of characterizing the upper extremity response under airbag loading (Bass, 1997; Duma, 1998; Brozoski, 2003). The instrumentation package of the device was designed to quantify the kinematics and kinetics of the upper extremity while being loaded by a deploying airbag. Humerus moments recorded in the subject and dummy have been found to have similar responses such that the dynamic injury tolerance for the 5th percentile female humerus of 128 Nm was recommended for use with the dummy (Duma, 1998). The elbow of the SAE 5th percentile female instrumented upper extremity is a single degree of freedom joint allowing flexion and extension but not pronation and supination rotations observed in the human upper extremity. This loss of rotation is not significant to the current application given the symmetry of the upper extremity shaft. On the distal end of the dummy upper extremity, two strain gages can measure bending moments along the X and Y axis. The elbow bending moment in hyperextension, MY, can be evaluated directly by these strain gages. Based upon the determination of this study that peak elbow bending moment is a significant indicator of any elbow injury ($p=0.02$) and of elbow joint dislocation ($p=0.01$), various risk functions were developed to define elbow injury criteria based upon specimen age, specimen mass, and moment values similar to those applied by an airbag. Consequently, these risk functions can be applied directly to the elbow bending moment, MY, of the instrumented dummy upper extremity for future side airbag loading analyses. While there may be some biofidelity limitations, this is the best available data at this time.

6 Conclusions

Airbag contact with the upper extremity can impart large bending loads to the elbow joint, particularly during hyperextension of the elbow. This three part analysis characterized the interaction between the female upper extremity and a helicopter cockpit side airbag system as well as developed injury criteria for the upper extremity elbow joint. First, through a series of 10 side airbag deployments with a 5th percentile female Hybrid III instrumented upper extremity, it was determined that the original CABS Black Hawk helicopter side airbag system caused high loads and moments in the upper extremity resulting in high injury risk to the aviator. Large bending moments in the forearm and humerus were associated with high risk for fracture. Two out of the ten tests resulted in high elbow bending moments of 128 Nm and 144 Nm.

Second, dynamic hyperextension tests were performed on 24 female cadaver elbow joints to apply elbow bending moments matching the previously conducted side airbag tests. Post-test necropsies showed that 16 of the 24 elbow joint tests resulted in injuries. Injury severity ranged from minor AIS 1 injuries, such as ligament and cartilage damage to more severe AIS 2 injuries like joint dislocations and AIS 3 injuries like transverse fractures of the distal humerus. Peak elbow bending moments ranged from 42.4 Nm to 146.3 Nm. Peak bending moment proved to be a significant indicator of any elbow injury ($p=0.02$) as well as elbow joint dislocation ($p=0.01$). Logistic regression analyses were used to develop single and multiple variate injury risk functions. Using peak elbow bending moment data for the entire test population, a 50% risk of obtaining any elbow injury was found at 56 Nm while a 50% risk of sustaining an elbow joint dislocation was found at 93 Nm for the female specimen. These results indicate that the

peak elbow bending moments achieved in Part I are associated with a greater than 90% risk for elbow injury. This risk assessment revealed a high risk of injury to the upper extremities in the event of an inadvertent deployment of the original helicopter side airbag system. Subsequently, the airbag was re-designed in an effort to mitigate upper extremity injury risks.

Third, 12 upper extremity tests, performed with a methodology similar to Part I, determined that the enhanced side airbag design mitigated injury risk by reducing high probabilities of elbow joint injury to 13% or less. The discovery that injury could result from deployment of the enhanced CABS side airbag should not detract from other evidence that, when fielded, it will save aviator lives and reduce injury. In summary, using all available upper extremity injury criteria, the enhanced CABS side airbag greatly reduced the risk of injury to the upper extremity compared to the original CABS side airbag system. This study provides researchers with a comprehensive set of injury criteria for assessing upper extremity injury risk caused by side airbag deployments. This research can also be applied to the design improvement of other helicopter side airbag systems to prevent and reduce injuries to the aviators. It is anticipated that this study will provide researchers with a comprehensive set of injury criteria for assessing upper extremity injury risk caused by both military and automotive side airbag deployments.

References

Association for the Advancement of Automotive Medicine, The Abbreviated Injury Scale, 1998 Revision, Des Plains, IL, 1998.

Bass, C.R., Duma, S.M., Crandall, J.R., Morris, R., Martin, P., Pilkey, W.D., Hurwitz, S.R., Khaewpong, N., Eppinger, R., Sun, E. (1997) The Interaction of Airbags With Upper Extremities. Proc. 41st Stapp Car Crash Conference, pp. 101-110. Society of Automotive Engineers, Warrendale, PA.

Brozoski, F.T., McEntire, B.J., Crowley, J.S., Alem, N.M., Lewis, A., Dillard, R. (2003) Upper Extremity Injury Risk During Deployment of the Enhanced UH-60 Lateral Airbag. Fort Rucker, AL: United States Army Aeromedical Research Laboratory, USAARL Report #2003-21.

Denton, Inc. (2001) User's Guide for the Enhanced Airbag Interaction Arm (Model 4380), Rochester Hills, MI 48309.

Di Domenico, L., Nusholtz, G. (2003) Comparison of Parametric and Non-Parametric Methods for Determining Injury Risk. SAE Paper No. 011362. Society of Automotive Engineers, Warrendale, PA.

Diggle, P.J., Liang, K.Y., Zeger, S.L. (1994) Analysis of Longitudinal Data, Oxford: Clarendon Press.

Duma, S.M. (2000) Injury Criteria for the Small Female Upper Extremity. Ph. D. Dissertation, University of Virginia, Charlottesville, VA.

Duma, S.M., Boggess, B.M., Bass, C.R., Crandall, J.R. (2003a) Injury Risk Functions for the 5th Percentile Female Upper Extremity. SAE Paper No. 010166. Society of Automotive Engineers, Warrendale, PA.

Duma, S.M., Boggess, B.M., Crandall, J.R., Hurwitz, S.R. (2001) Upper Extremity Interaction with a Side Airbag: The Effect of a Door Handgrip. Proc. of the 17th International Technical Conference on the Enhanced Safety of Vehicles. National Highway Traffic Safety Administration, Washington, DC.

Duma, S.M., Boggess, B.M., Crandall, J.R., Mac Mahon, C.B. (2002) Fracture Tolerance of the Small Female Elbow Joint in Compression: The Effect of Load Angle Relative to the Long Axis of the Forearm. Proc. 46th Stapp Car Crash Conference, pp. 195-210. Society of Automotive Engineers, Warrendale, PA.

Duma, S.M., Boggess, B.M., Crandall, J.R., Mac Mahon, C.B. (2003b) Injury Risk Function for the Small Female Wrist in Axial Loading. Accident Analysis and Prevention 35:869-875.

Duma, S.M., Crandall, J.R., Hurwitz, S.R., Pilkey, W.D. (1998) Small Female Upper Extremity Interaction with a Deploying Side Airbag. Proc. 42nd Stapp Car Crash Conference, pp. 47-63. Society of Automotive Engineers, Warrendale, PA.

Duma, S.M., Schrieber, P.H., McMaster, J.D., Crandall, J.R., Bass, C.R., Pilkey, W.D. (1999) Dynamic Injury Tolerances for Long Bones of the Female Upper Extremity. Journal of Anatomy 194:463-471.

First Technology Safety Systems. (1997) Hybrid III 5th Female Dummy (Model 880105-000-XH) Plymouth, MI 48170.

Hosmer, D.J., Lemeshow S. (1989) Applied Logistic Regression, John Wiley and Sons, Inc., New York.

Jaffredo, A.S., Potier, P., Robin, S., Jean-Yves, L.C., Lassau, J.P. (1998) Upper Extremity Interaction with Side Impact Bags. International Research Council on the Biomechanics of Impact, Goteborg, Sweden.

Kallieris, D., Rizzetti, A., Mattern, R., Jost, S., Priemer, P., Unger, M. (1997) Response and Vulnerability of the Upper Arm through Side Airbag Deployment. SAE Paper No. 973323. Society of Automotive Engineers, Warrendale, PA.

Kent, R., Funk, J. (2004) Data Censoring and Parametric Distribution Assignment in the Development of Injury Risk Functions from Biomechanical Data. SAE Paper No. 010317. Society of Automotive Engineers, Warrendale, PA.

Longford, N.T. (1993) Random Coefficient Models, Clarendon Press, Oxford.

McEntire, B.J., Brozoski, F.T., Alem, N.M. (2003) Predicting Airbag-Related Injury using Anthropometric Test Devices. Fort Rucker, AL: United States Army Aeromedical Research Laboratory, USAARL Report #2004-01.

Nusholtz, G., Mosier, R. (1999) Consistent Threshold Estimate for Doubly Censored Biomechanical Data. SAE Paper No. 010714. Society of Automotive Engineers, Warrendale, PA.

Pintar, F.A., Yoganandan, N., Eppinger, R.H. (1998) Response and Tolerance of the Human Forearm to Impact Loading. SAE Paper No. 983149. Society of Automotive Engineers, Warrendale, PA.

SAS Institute, Inc. (1999) SAS/STAT User's Guide, version 8, volume 2. SAS Institute, Inc., Cary, NC.

Shanahan, D. F., Shanahan, M.O. (1989) Injury in U.S. Army Helicopter Crashes Fiscal Years October 1979-September 1985. Journal of Trauma 29(4):415-423.

Shanahan, D.F., Shannon, S.G., Bruckart, J.E. (1993) Projected Effectiveness of Air Bag Supplemental Restraint Systems in U.S. Army Helicopter Crashes, Oct. 79 – Sept. 85. Fort Rucker, AL: United States Army Aeromedical Research Laboratory, USAARL Report #93-31.

Appendix A: Cadaver Upper Extremity Preparation Worksheet

Table A1: Upper extremity pre-test measurements.

Test Number	Length of Pot to left roller (mm)	Olecranon to hand roller (mm)	Olecranon to impactor blade (mm)	Distance between rollers (mm)	Distance from joint to right hand roller (mm)	Angle and Direction of Pot to horizontal (˚)		Angle and Direction of Ulna to horizontal (˚)	
2.01	284	220	138	515	205	8.0	up	4.0	up
2.02	275	225	135	550	210	9.0	up	6.0	up
2.03	280	185	130	525	170	2.0	up	5.0	down
2.04	285	225	150	575	210	4.0	up	3.0	down
2.05	270	220	140	525	205	2.0	down	5.0	down
2.06	265	240	130	555	225	1.4	down	2.0	down
2.07	267	225	125	527	210	7.7	down	8.6	down
2.08	273	240	145	558	225	6.2	down	8.5	down
2.09	272	237	120	523	222	4.0	up	6.0	up
2.10	255	250	120	562	235	6.4	up	6.0	up
2.11	255	235	155	543	220	11.5	up	12.2	up
2.12	260	220	140	520	205	7.0	up	9.5	up
2.13	255	225	115	510	210	6.2	up	6.5	up
2.14	255	245	115	535	230	7.0	up	6.0	up
2.15	255	230	135	532	215	5.7	up	7.0	up
2.16	253	220	135	507	205	5.5	up	7.3	up
2.17	265	230	160	555	215	5.0	up	3.0	up
2.18	260	225	140	533	210	3.0	up	2.0	up
2.19	256	205	145	520	190	5.7	up	6.4	up
2.20	268	240	150	565	225	3.0	down	5.6	down
2.21	260	210	145	535	195	2.8	up	2.4	up
2.22	262	225	140	534	210	0.0	------	1.5	up
2.23	257	195	125	500	180	5.6	up	8.0	up
2.24	260	225	130	520	210	10.0	down	10.5	down

Appendix B: Cadaver Upper Extremity Test Data

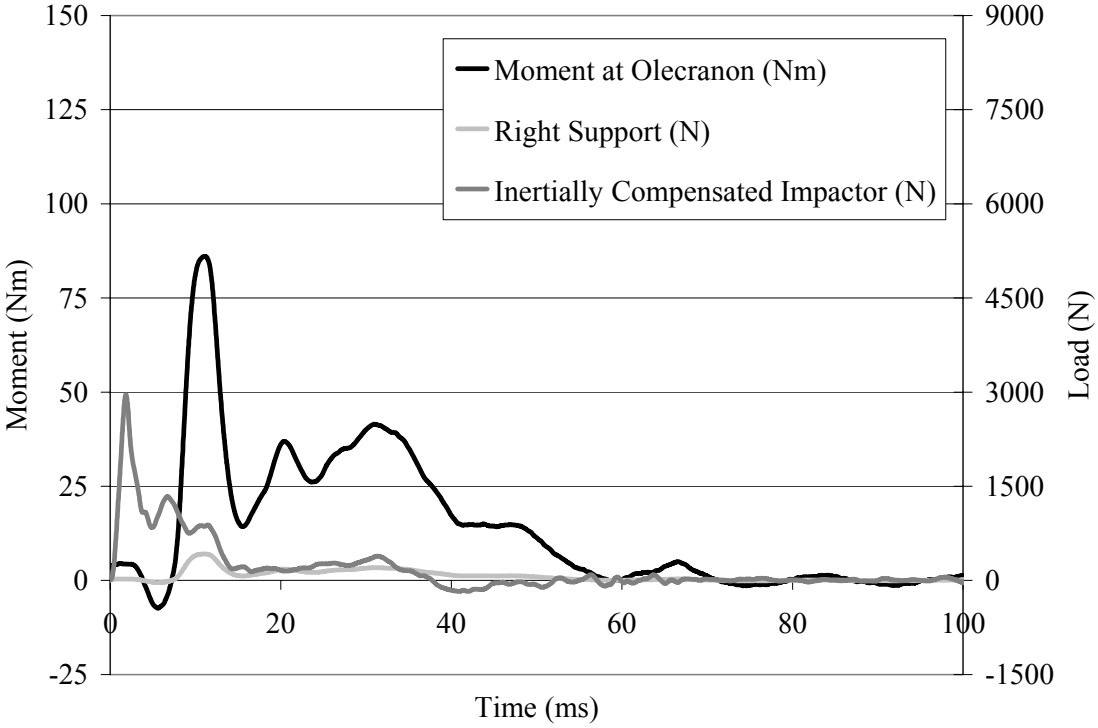

Figure B1: Moment vs. time plot for test 2.01 – high energy.

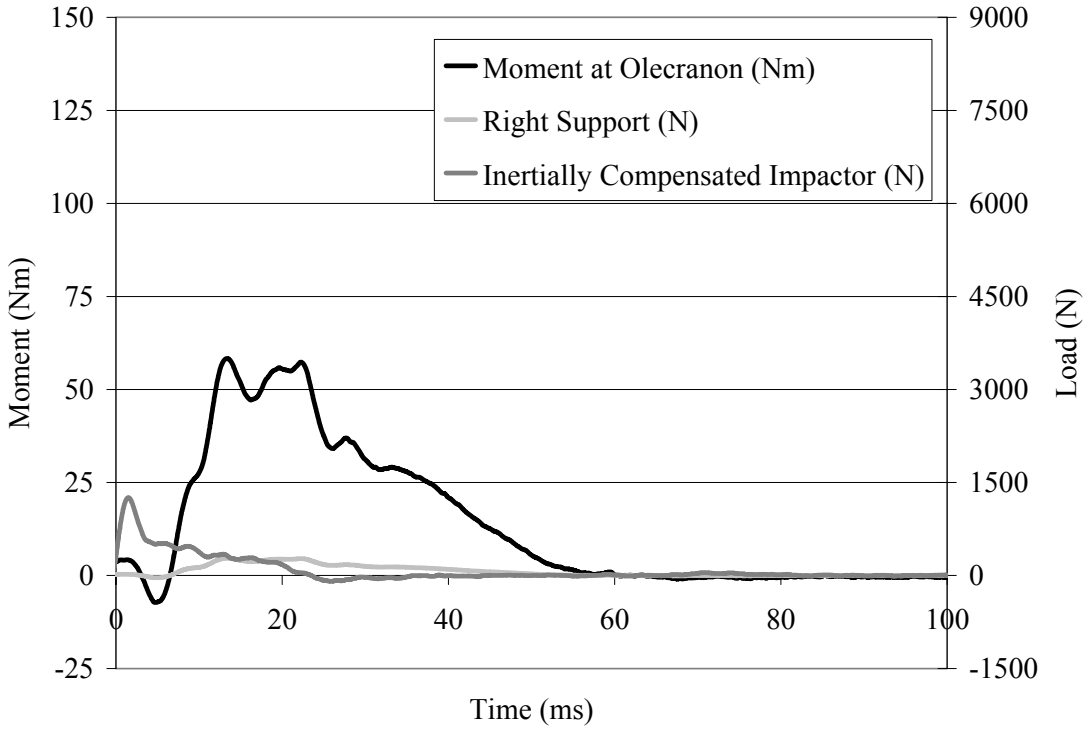

Figure B2: Moment vs. time plot for test 2.02 – low energy.

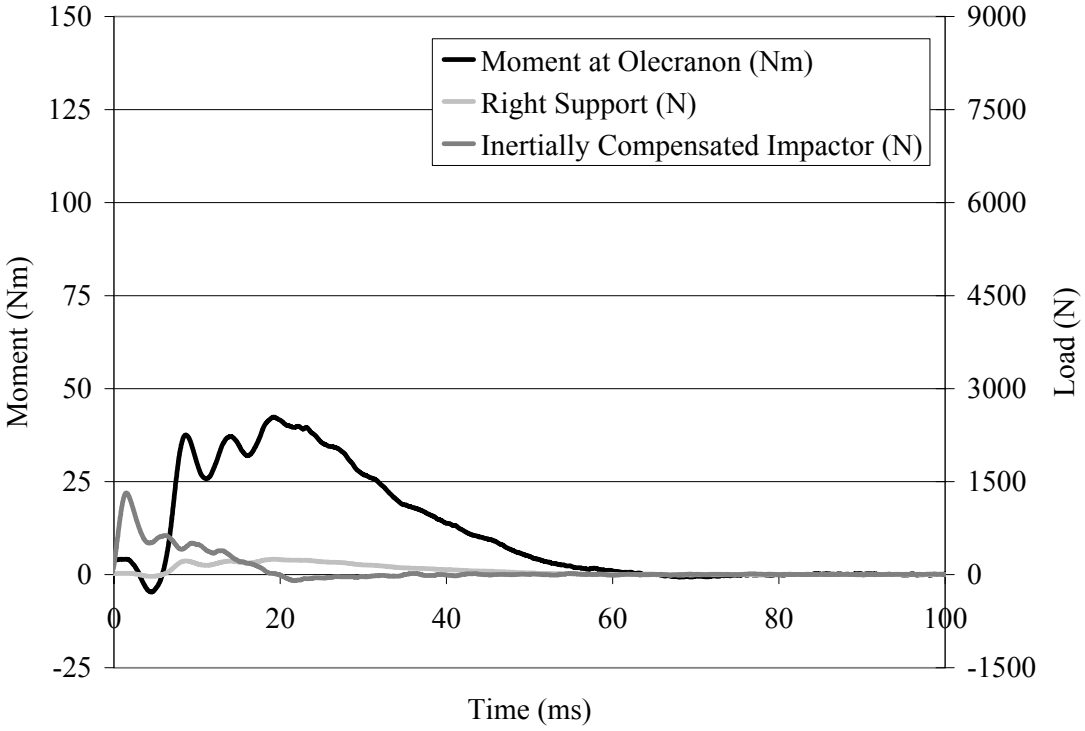

Figure B3: Moment vs. time plot for test 2.03 – low energy.

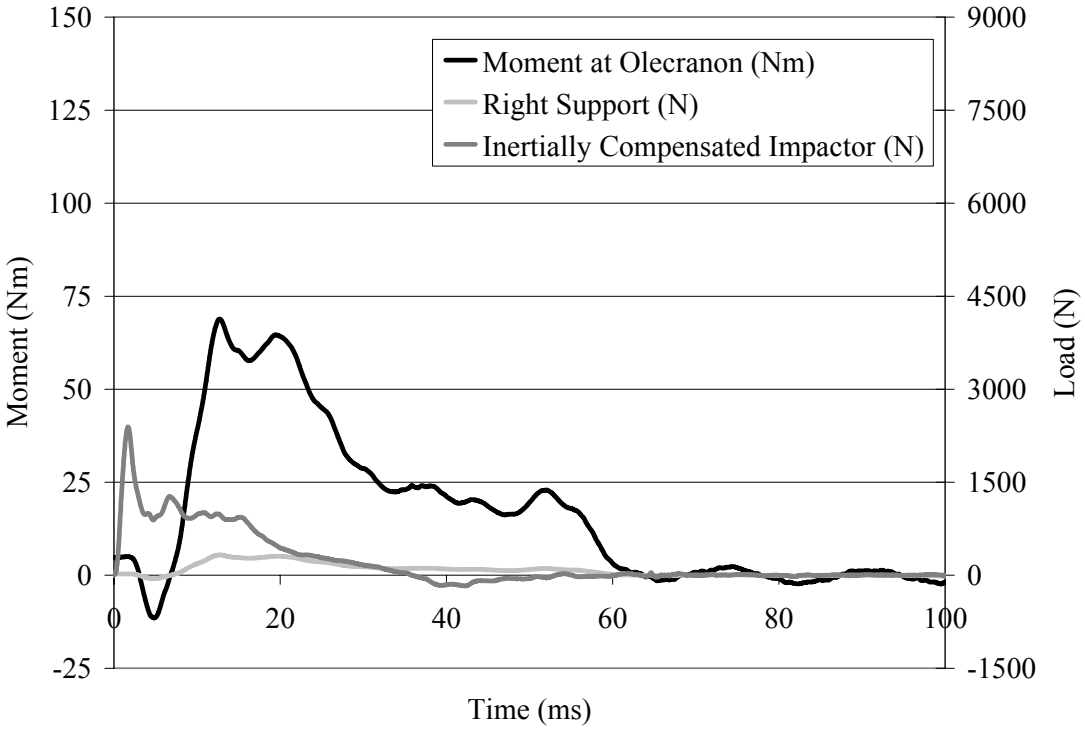

Figure B4: Moment vs. time plot for test 2.04 – high energy.

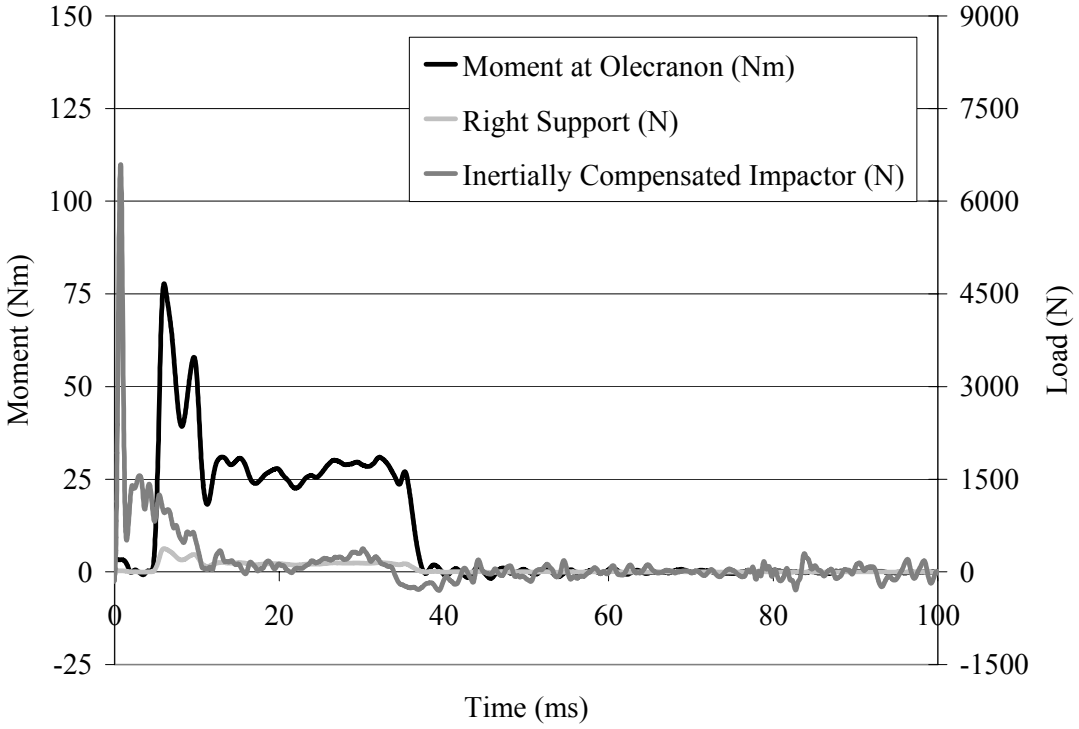

Figure B5: Moment vs. time plot for test 2.05 – high energy.

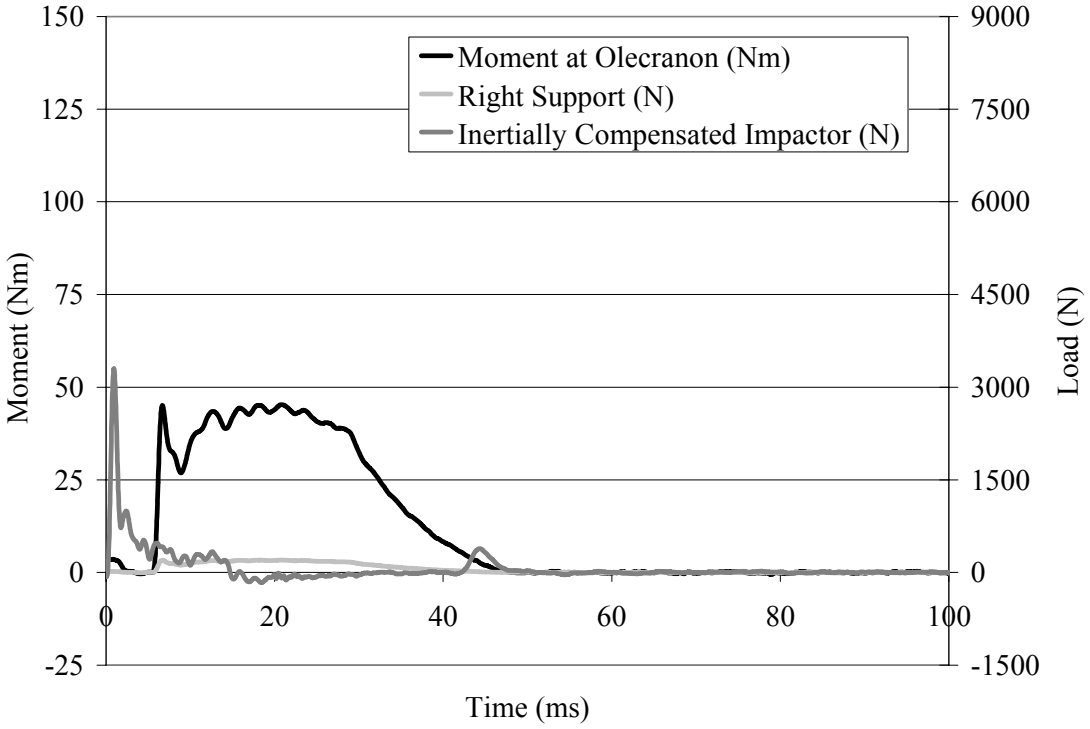

Figure B6: Moment vs. time plot for test 2.06 – low energy.

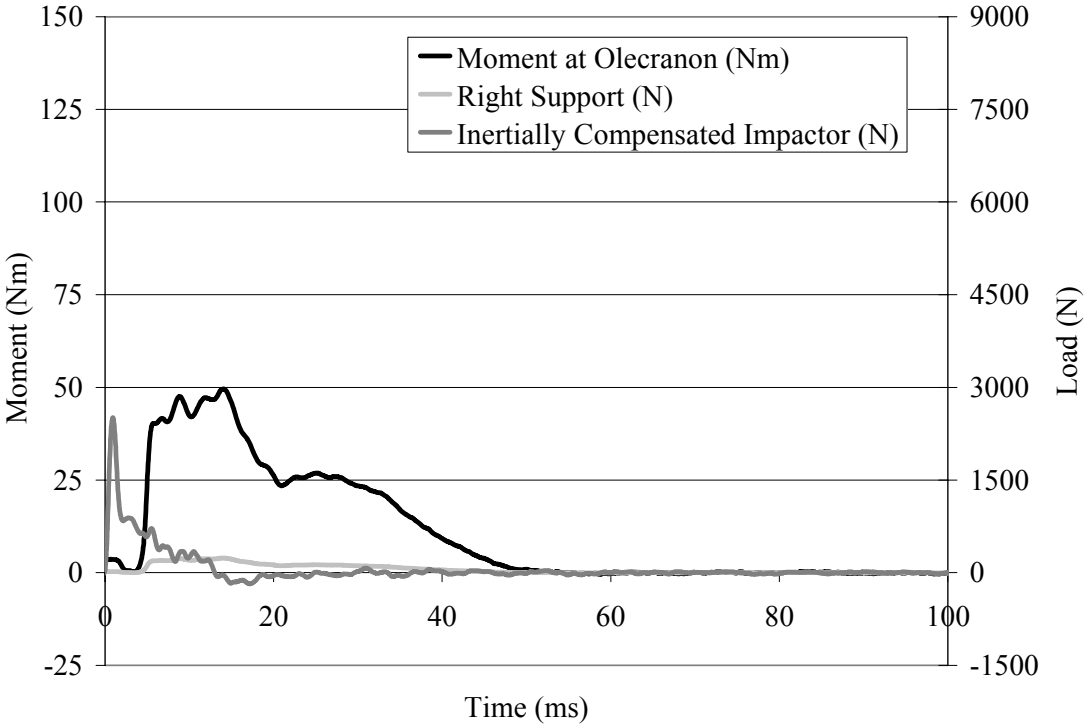

Figure B7: Moment vs. time plot for test 2.07 – low energy.

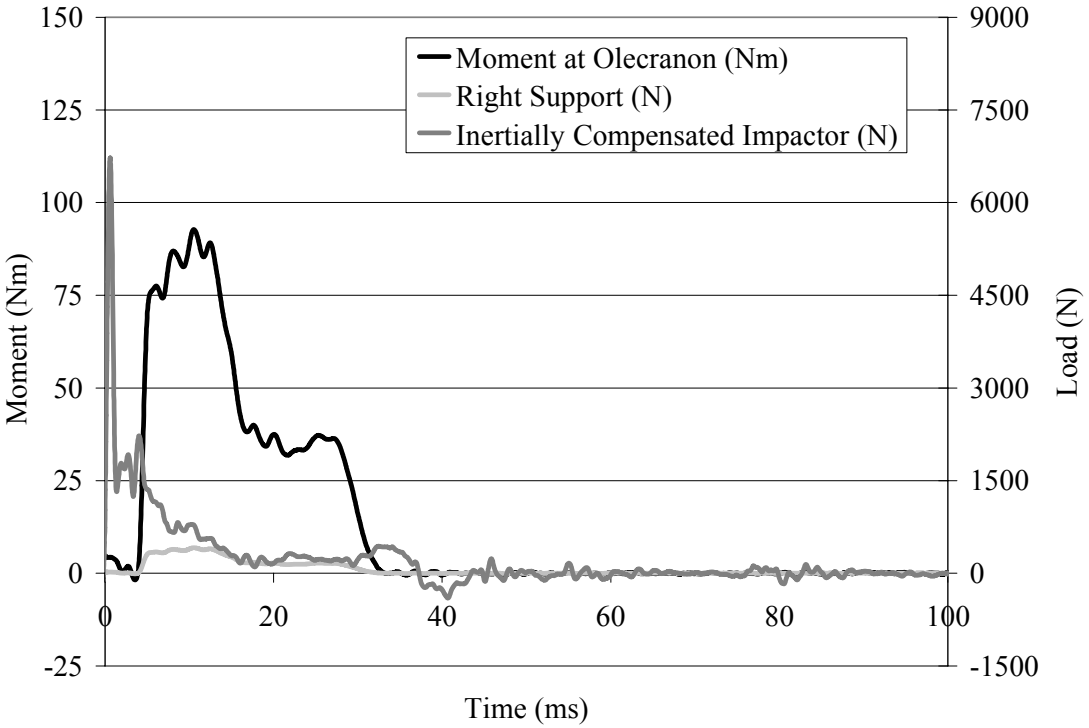

Figure B8: Moment vs. time plot for test 2.08 – high energy.

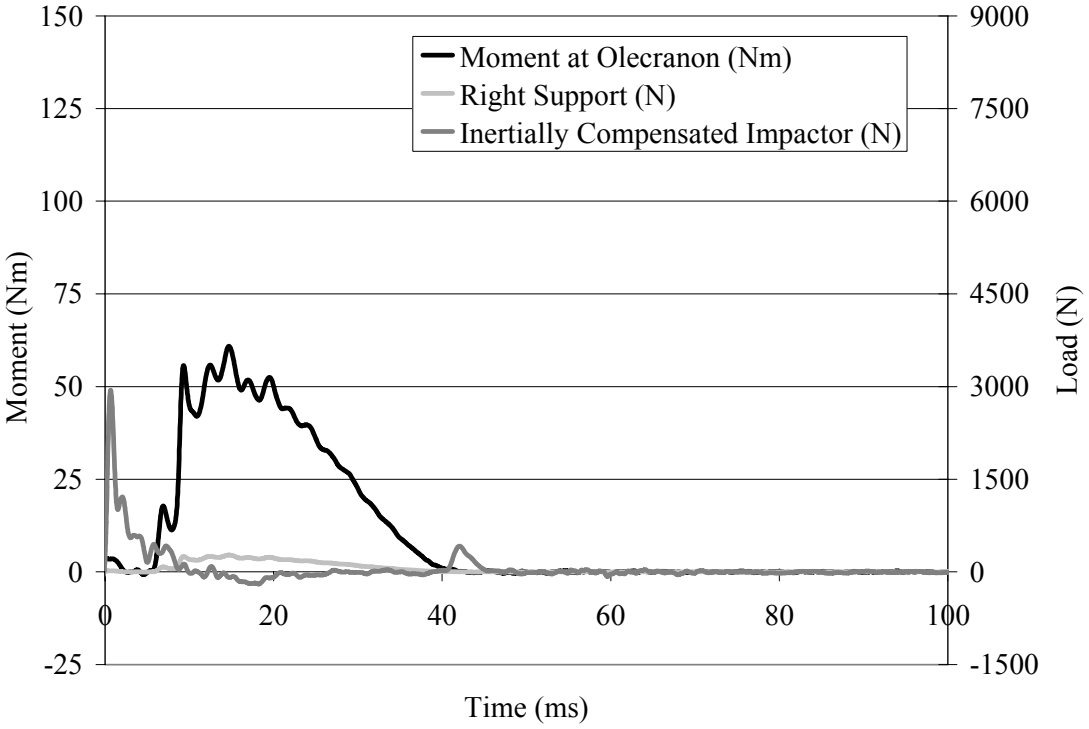

Figure B9: Moment vs. time plot for test 2.09 – low energy.

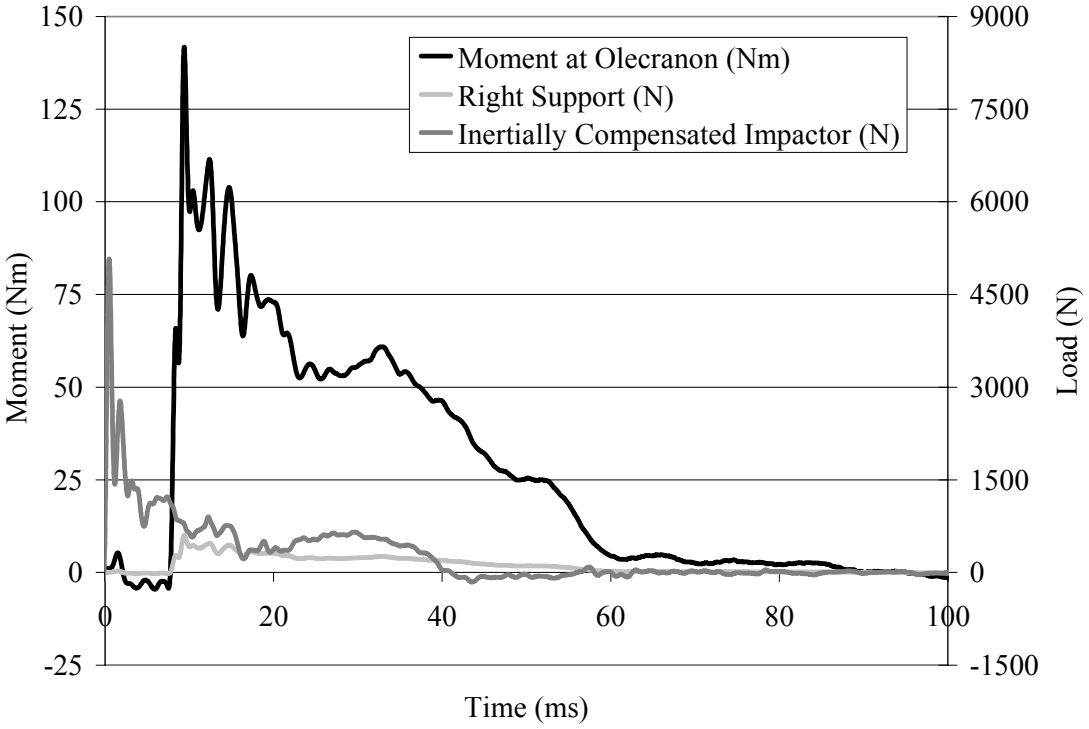

Figure B10: Moment vs. time plot for test 2.10 – high energy.

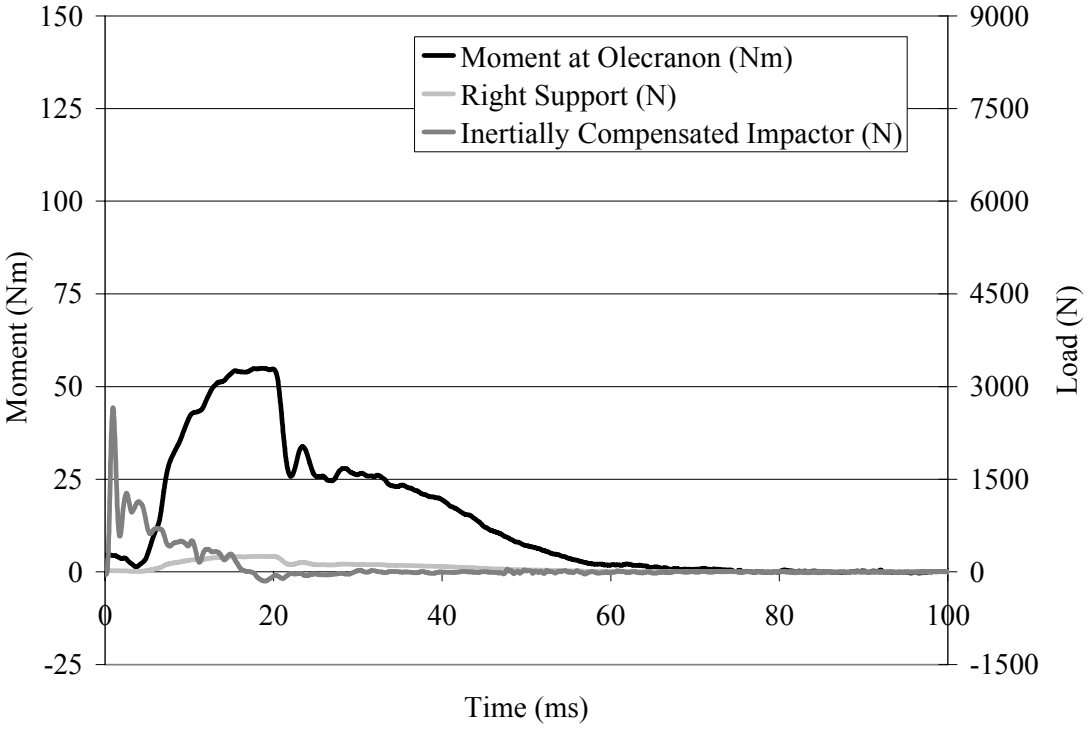

Figure B11: Moment vs. time plot for test 2.11 – low energy.

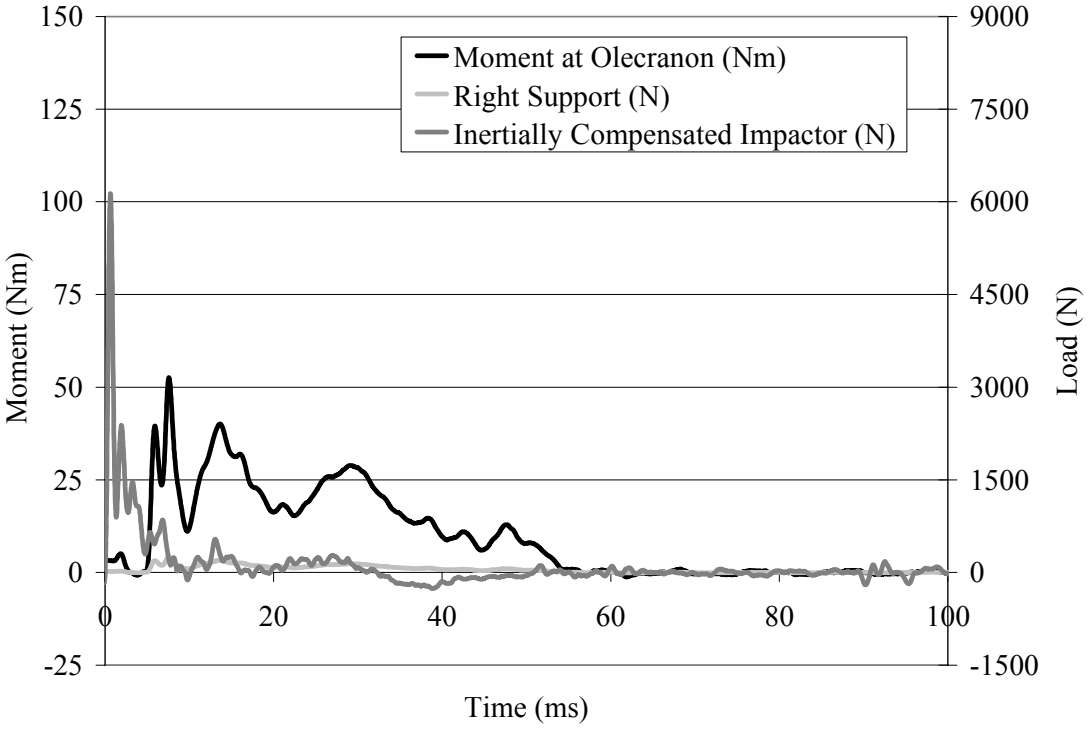

Figure B12: Moment vs. time plot for test 2.12 – high energy.

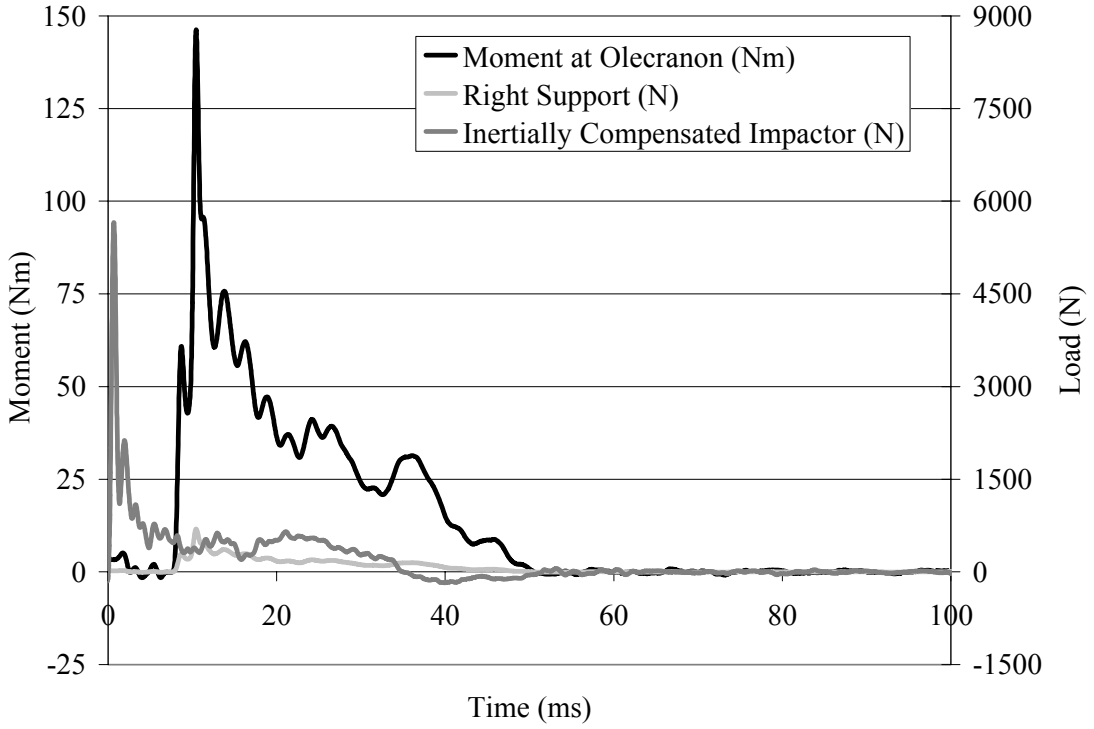

Figure B13: Moment vs. time plot for test 2.13 – high energy.

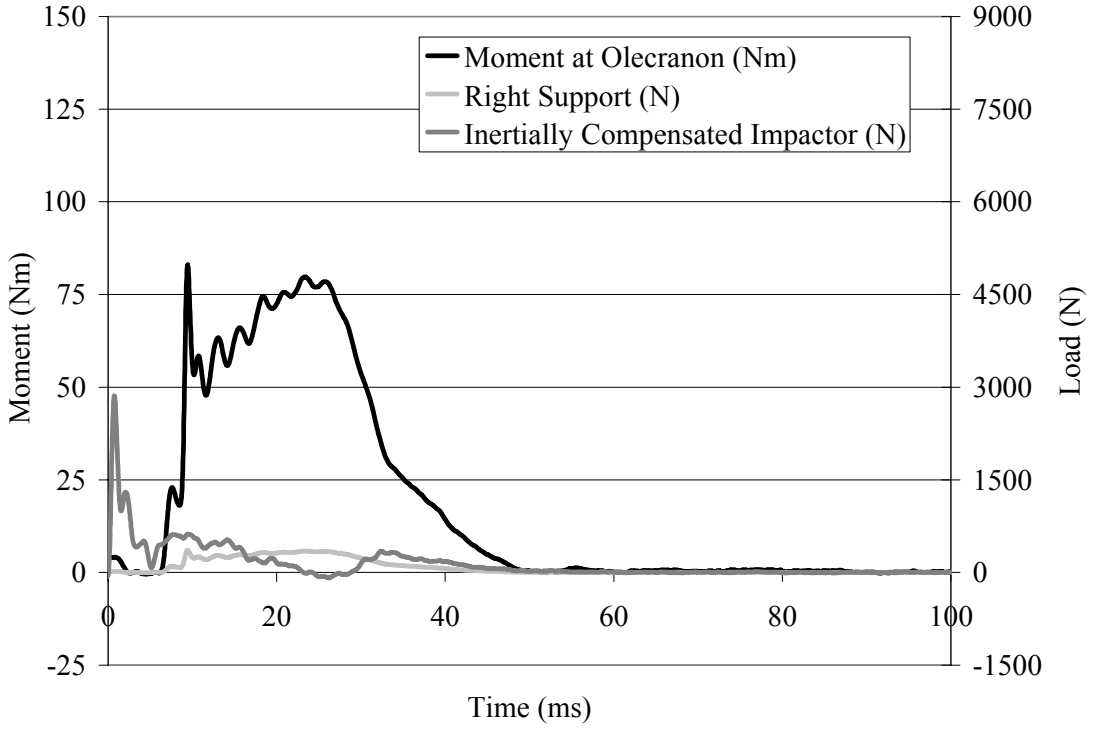

Figure B14: Moment vs. time plot for test 2.14 – low energy.

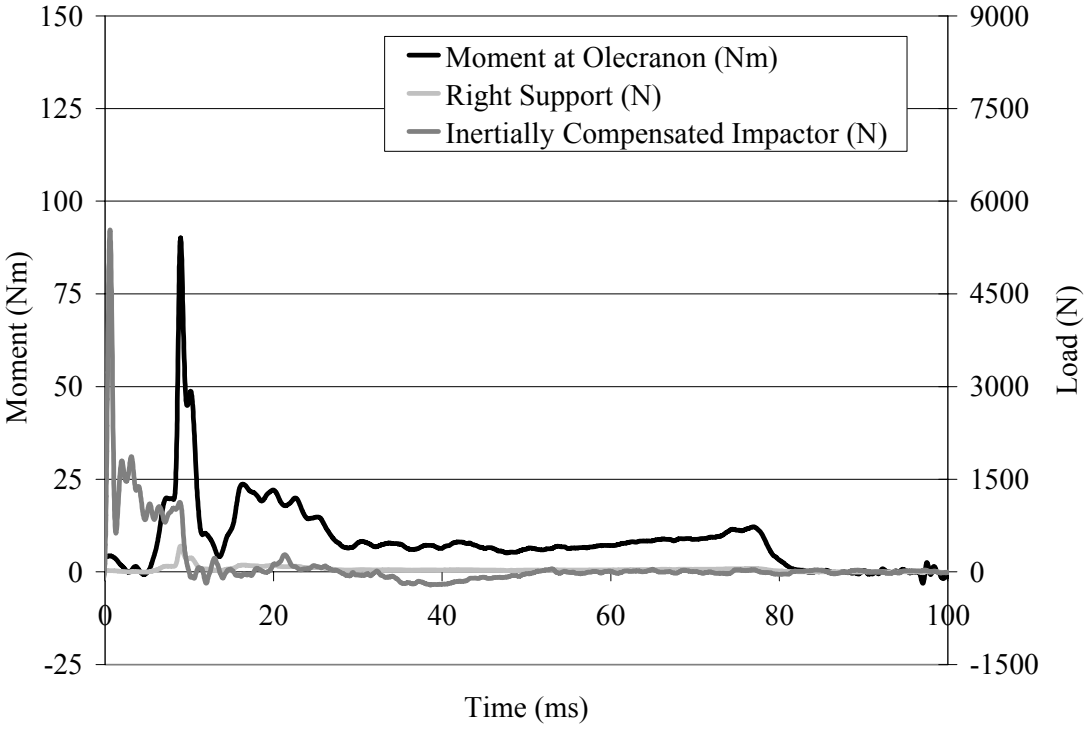

Figure B15: Moment vs. time plot for test 2.15 – high energy.

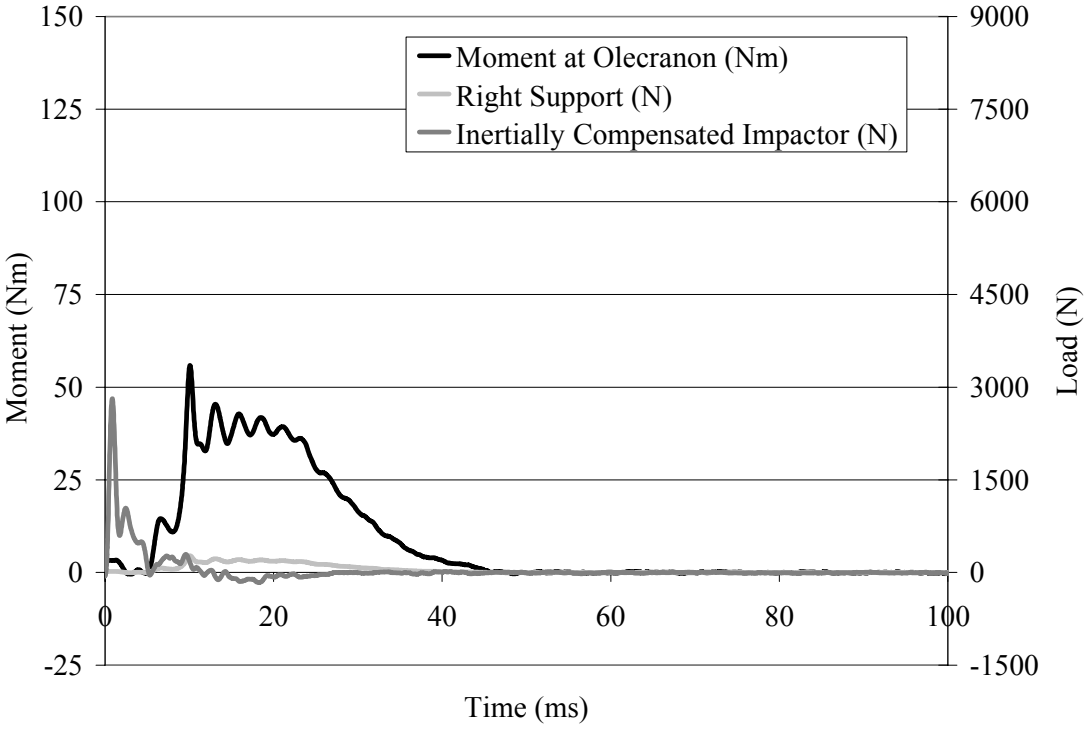

Figure B16: Moment vs. time plot for test 2.16 – low energy.

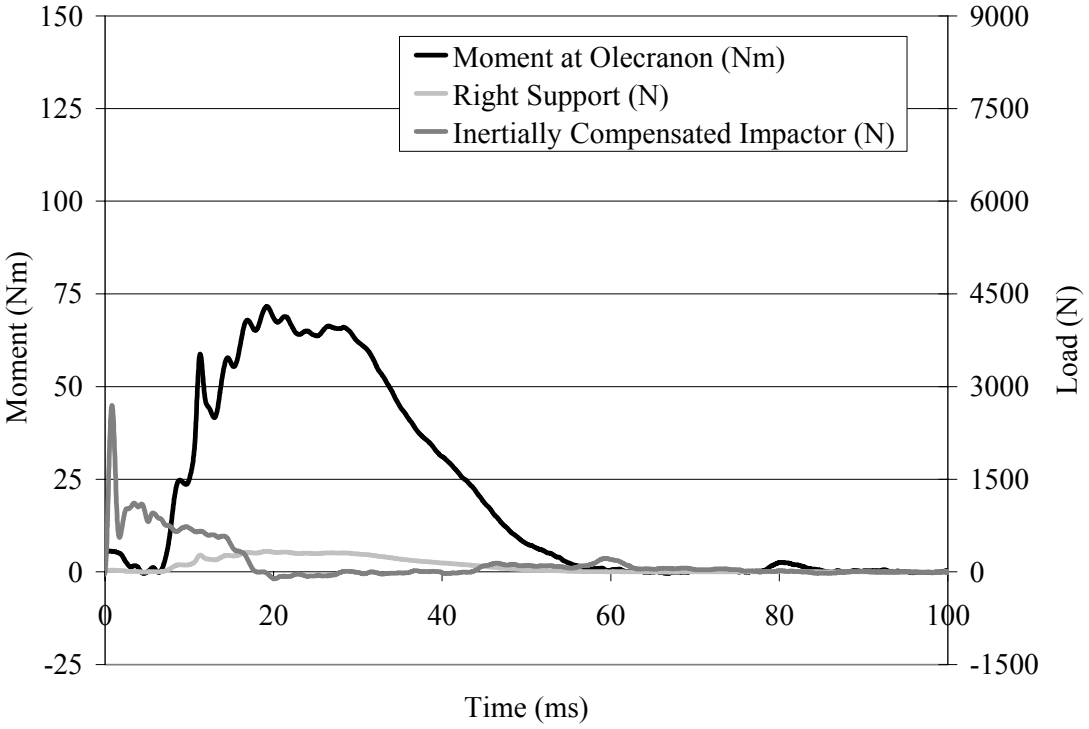

Figure B17: Moment vs. time plot for test 2.17 – low energy.

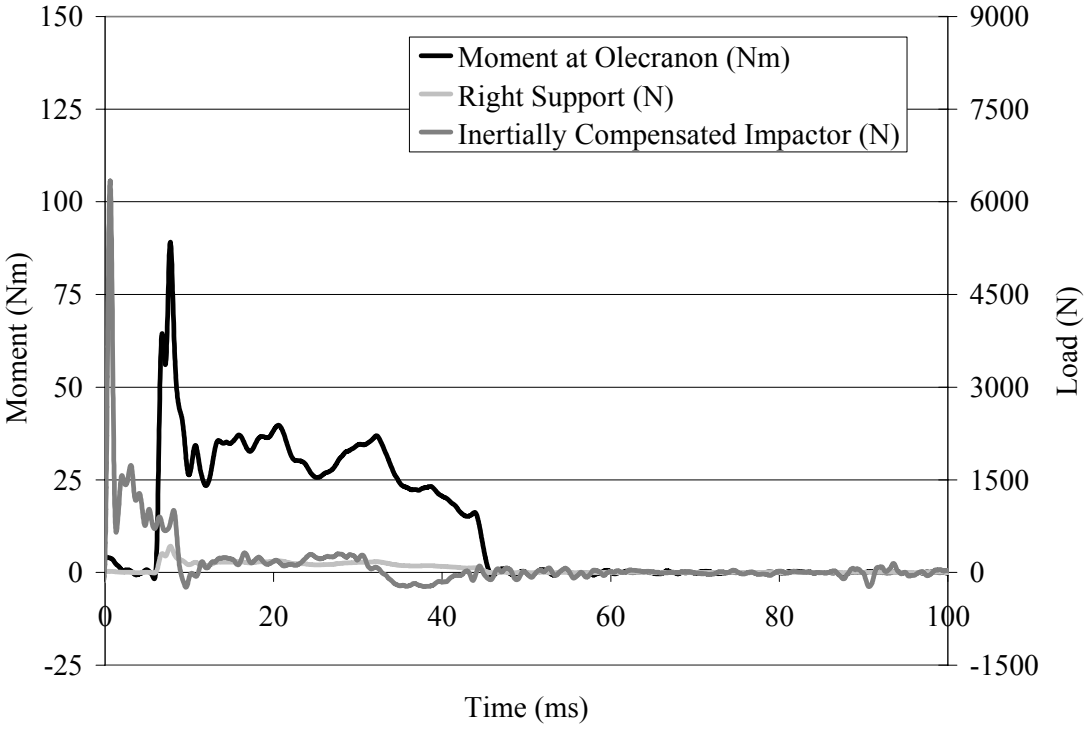

Figure B18: Moment vs. time plot for test 2.18 – high energy.

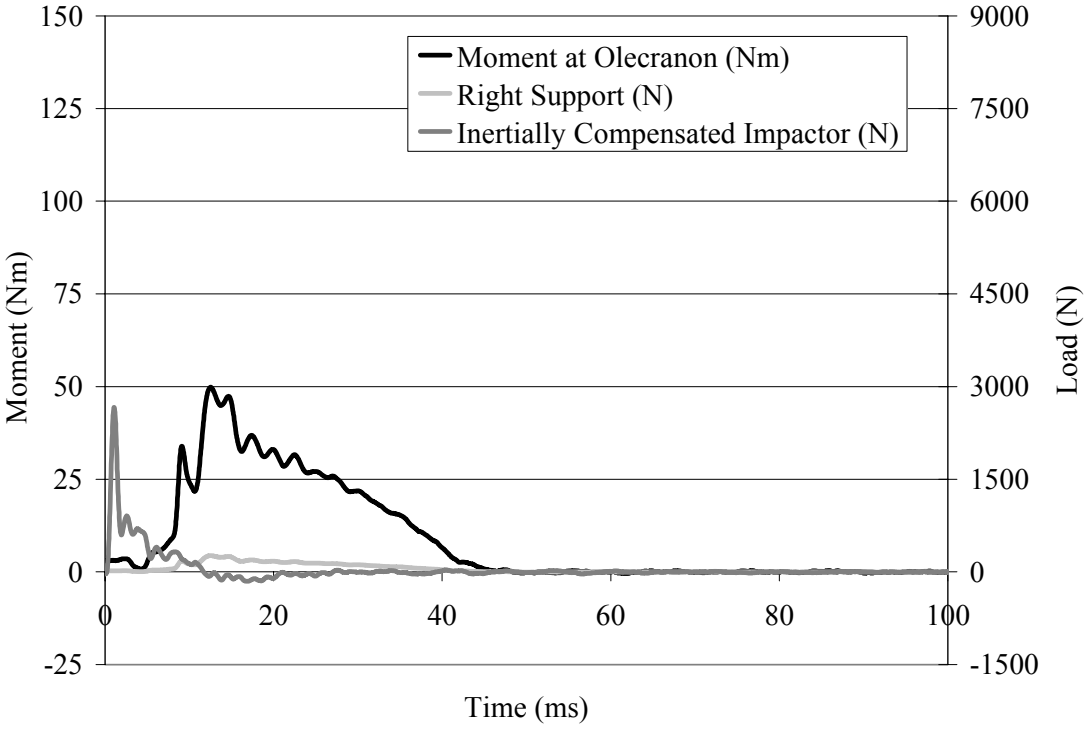

Figure B19: Moment vs. time plot for test 2.19 – low energy.

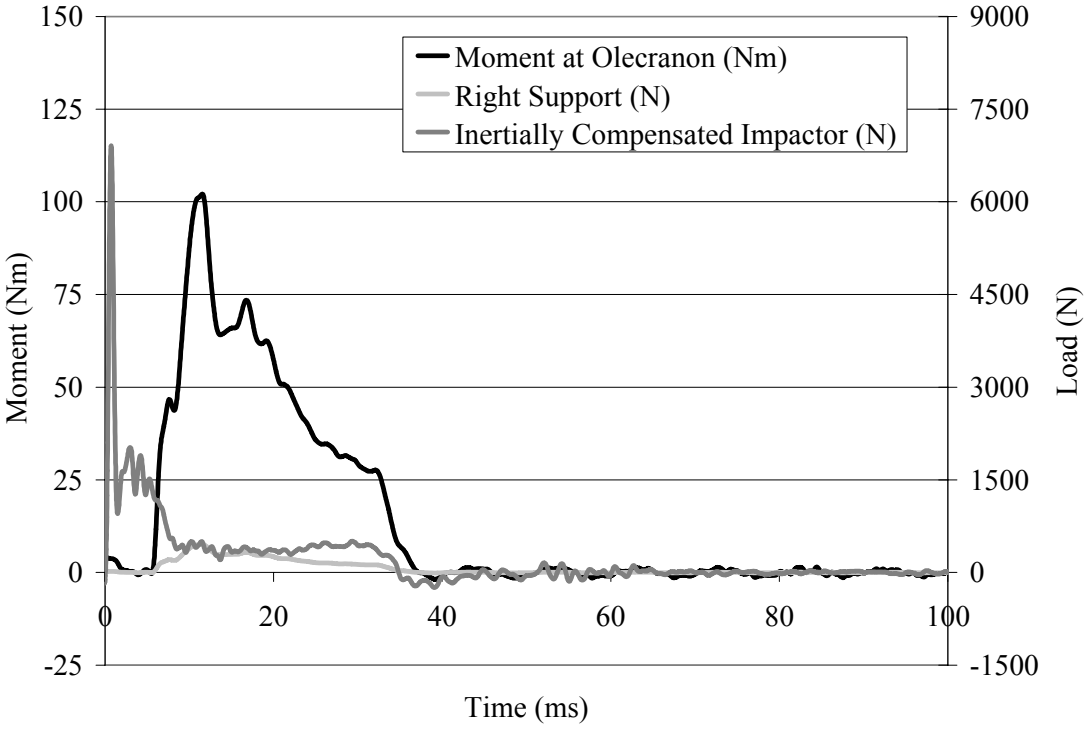

Figure B20: Moment vs. time plot for test 2.20 – high energy.

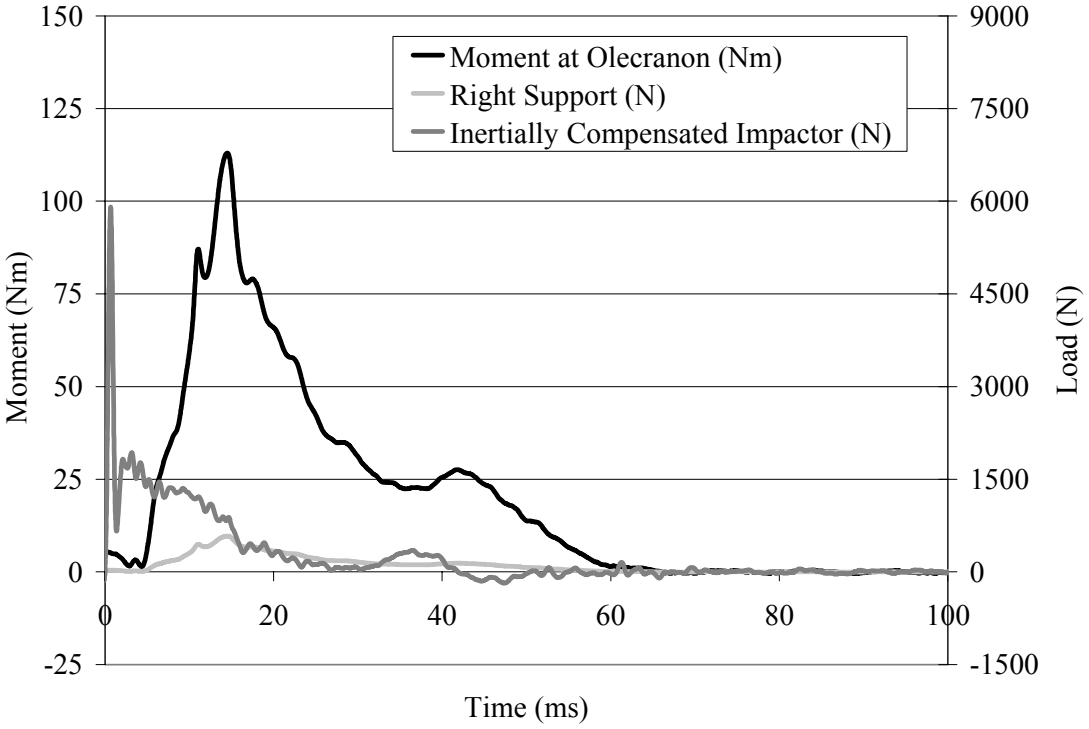

Figure B21: Moment vs. time plot for test 2.21 – high energy.

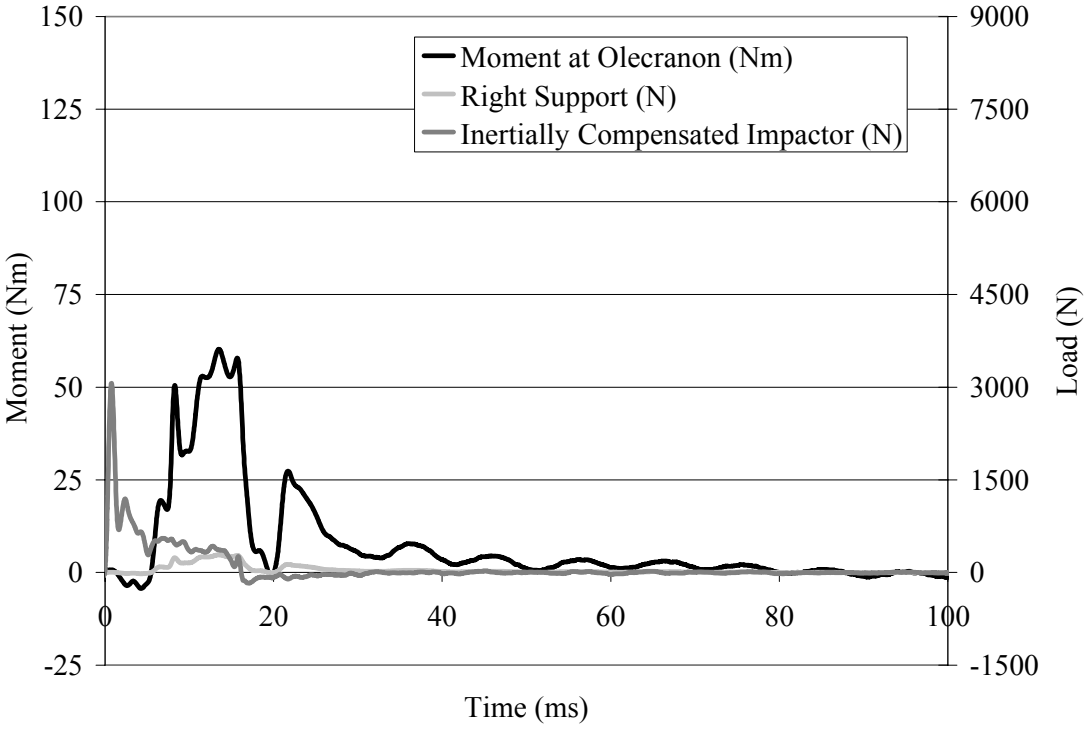

Figure B22: Moment vs. time plot for test 2.22 – low energy.

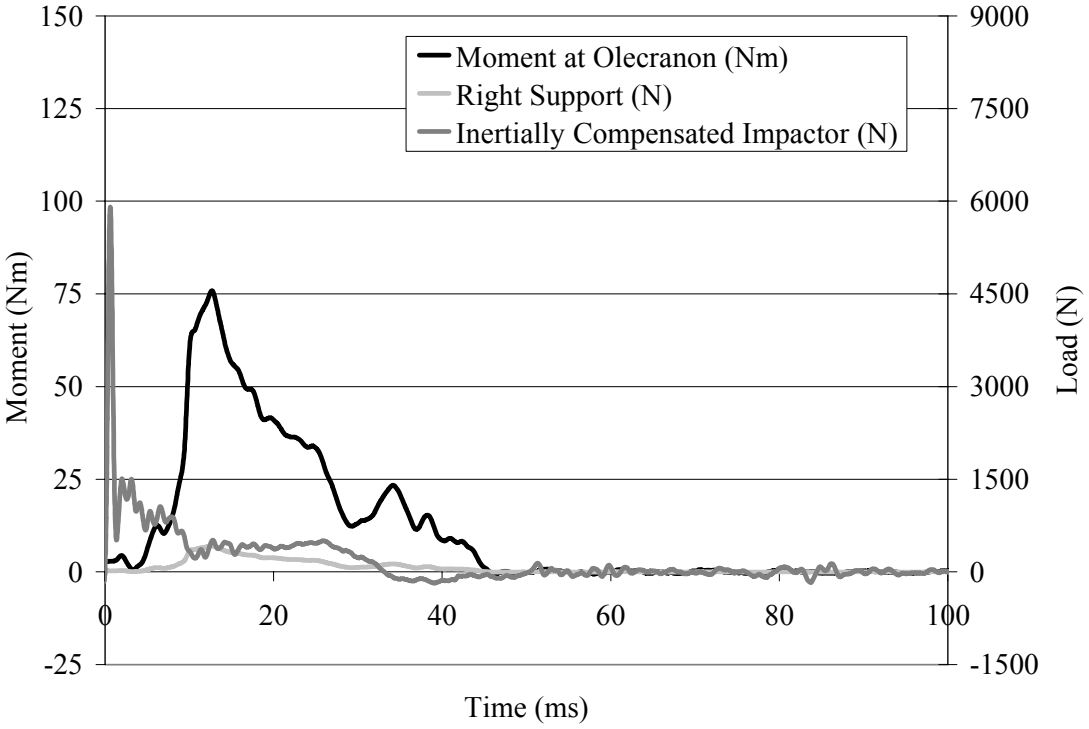

Figure B23: Moment vs. time plot for test 2.23 – high energy.

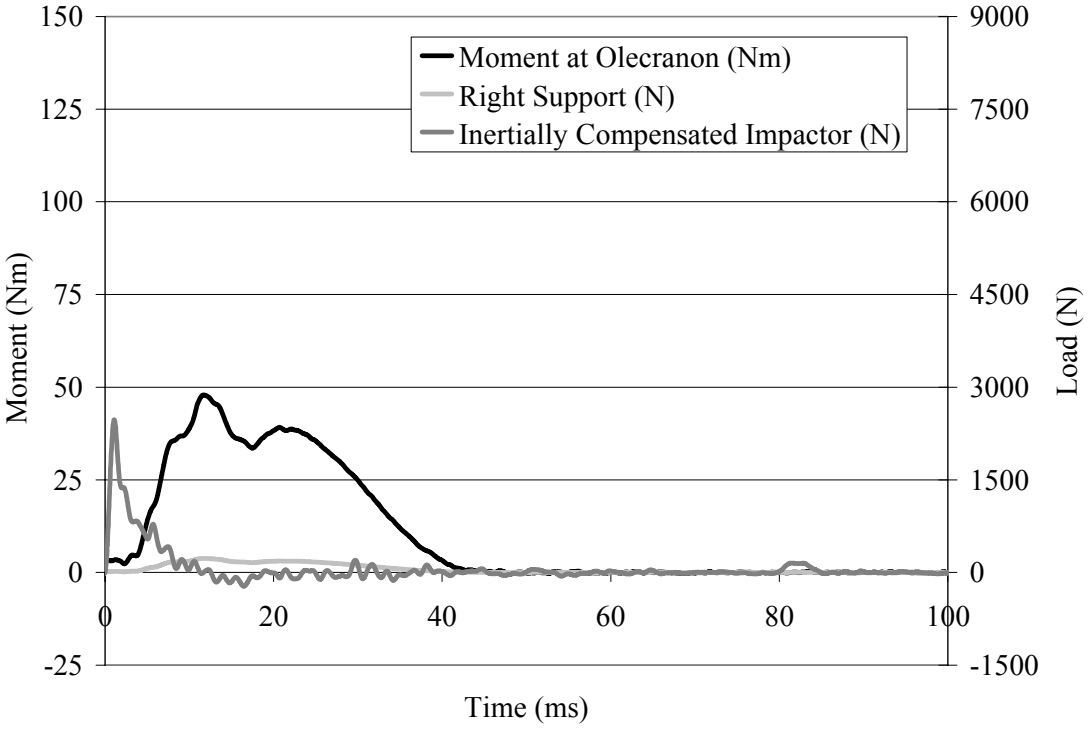

Figure B24: Moment vs. time plot for test 2.24 – low energy.

Appendix C: Cadaver Upper Extremity Injury Chart

Table C1: Elbow injuries of cadaver specimen during the Part II dynamic loading tests.

Test ID	Test Energy	Injuries Observed
2.01	High	• Comminuted transverse fracture of distal humerus at elbow • Chondral fracture of the coronoid
2.02	Low	No injury
2.03	Low	• Avulsion/Osteochondral fracture of the coronoid
2.04	High	• Osteochondral fracture of olecranon • Anterior elbow ligament dislocation
2.05	High	• Extra-articular fracture of distal humerus
2.06	Low	No injury
2.07	Low	• Disruption of the anterior capsule, anterior laterally on radial side of joint
2.08	High	• Condylar fracture to the trochlea • Dislocation of elbow joint
2.09	Low	No injury
2.10	High	• Disruption of the anterior capsule
2.11	Low	• Fracture/fragment of coronoid process • Fracture/fragment of distal trochlear notch • Partial tear to radial head ligamentus
2.12	High	• Extra-articular, supracondylar fracture of distal humerus
2.13	High	• Fracture/fragment of edge of coronoid process • Fracture medial of coronoid process • Anterior dislocation of elbow joint
2.14	Low	No injury
2.15	High	• Comminuted fracture of distal humerus
2.16	Low	No injury
2.17	Low	No injury
2.18	High	• Supracondylar fracture of distal humerus at the trochlea • Chondral lesion to radial head • Chondral fracture of radial head
2.19	Low	No injury
2.20	High	• Dislocation of elbow joint
2.21	High	• Medial/lateral ligaments nearly completely torn • Dislocation of elbow joint
2.22	Low	• Extra-articular, supracondylar fracture of distal humerus
2.23	High	• Fracture/fragment of coronoid process • Ligaments completely torn apart functionally • Anterior dislocation of elbow joint
2.24	Low	No injury

Appendix D: Cadaver Upper Extremity Test and Injury Pictures

Test 2.01 - High Energy

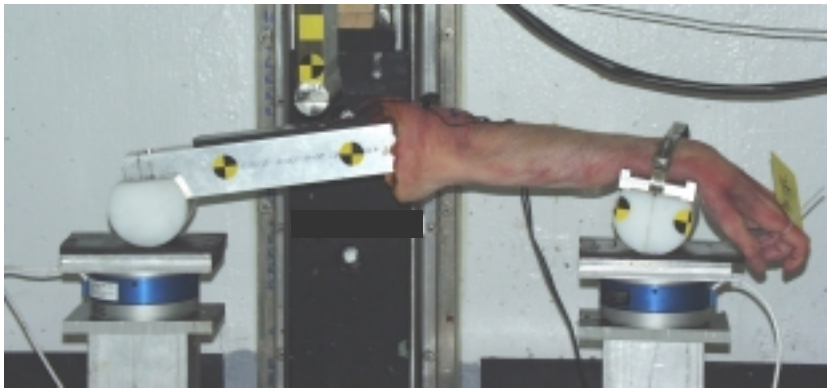

Figure D1: Pre-test set-up.

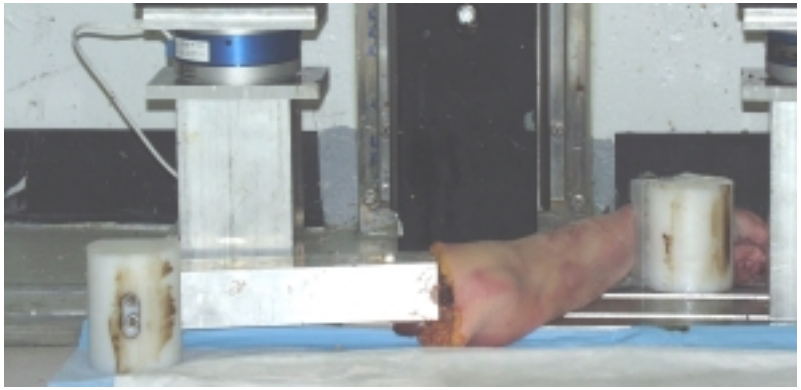

Figure D2: Post-test specimen position.

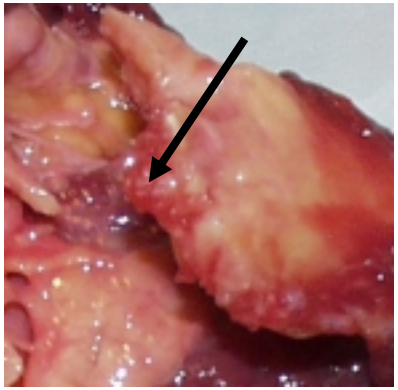

Figure D3: Comminuted transverse fracture of the distal humerus at elbow.

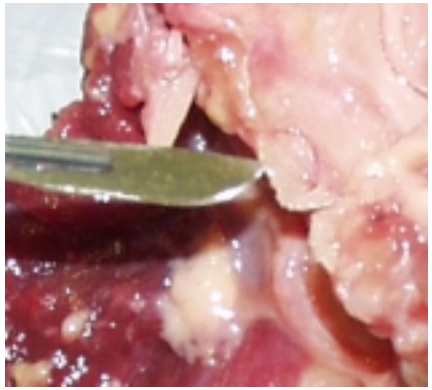

Figure D4: Fracture line through middle of olecranon fossa; olecranon popped into back of humerus causing fracture.

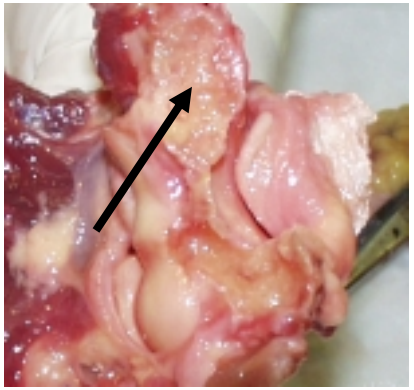

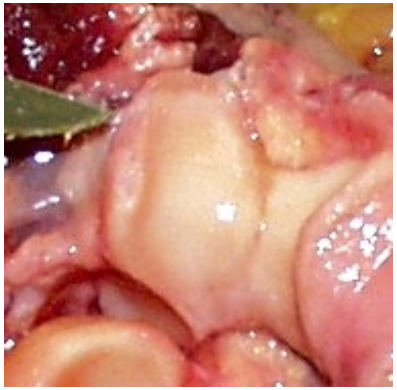

Figure D5: Chondral fracture of the coronoid.

Test 2.02 – Low Energy

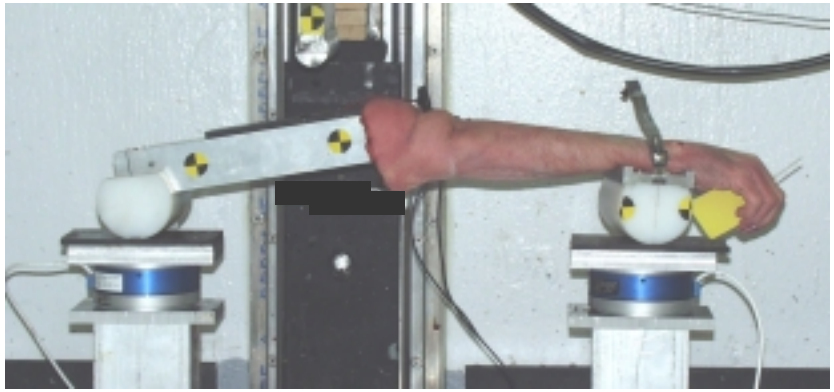

Figure D6: Pre-test set-up.

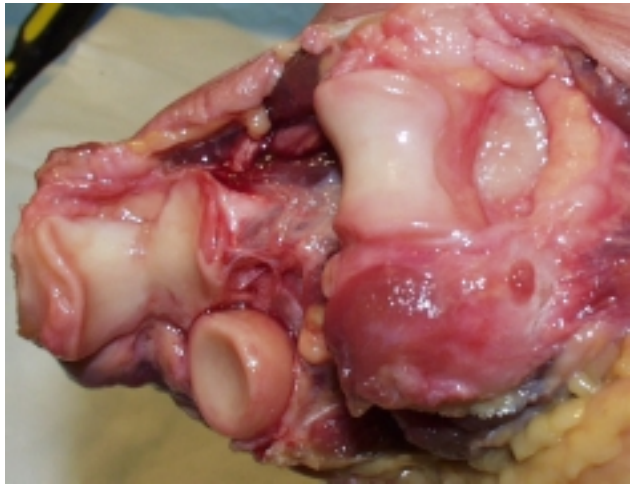

Figure D7: No Injury.

Test 2.03 – Low Energy

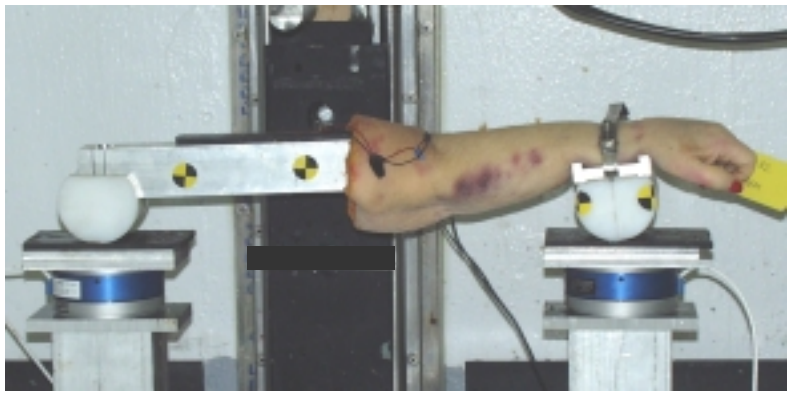

Figure D8: Pre-test set-up.

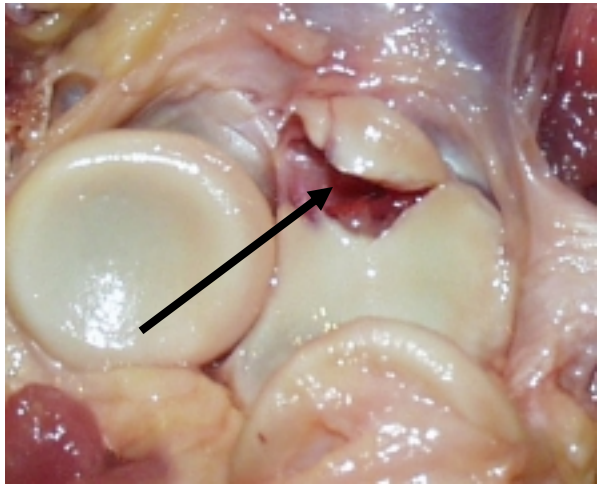

Figure D9: Avulsion/Osteochondral fracture of the coronoid.

Test 2.04 – High Energy

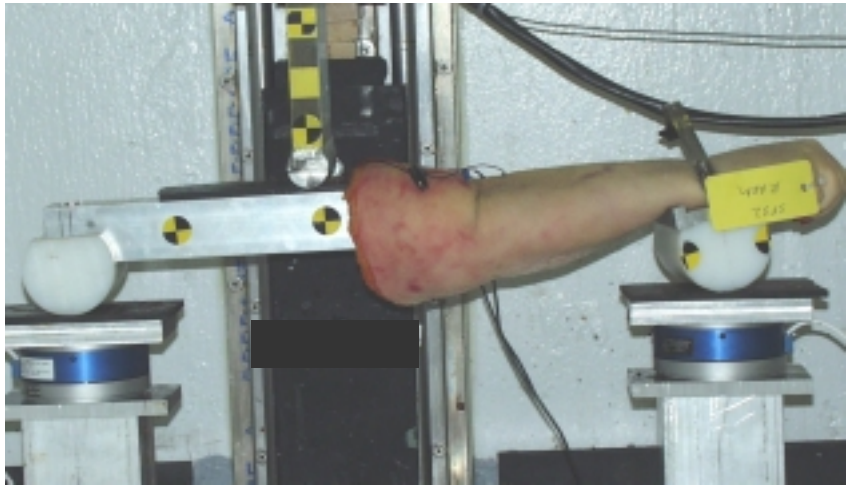

Figure D10: Pre-test set-up.

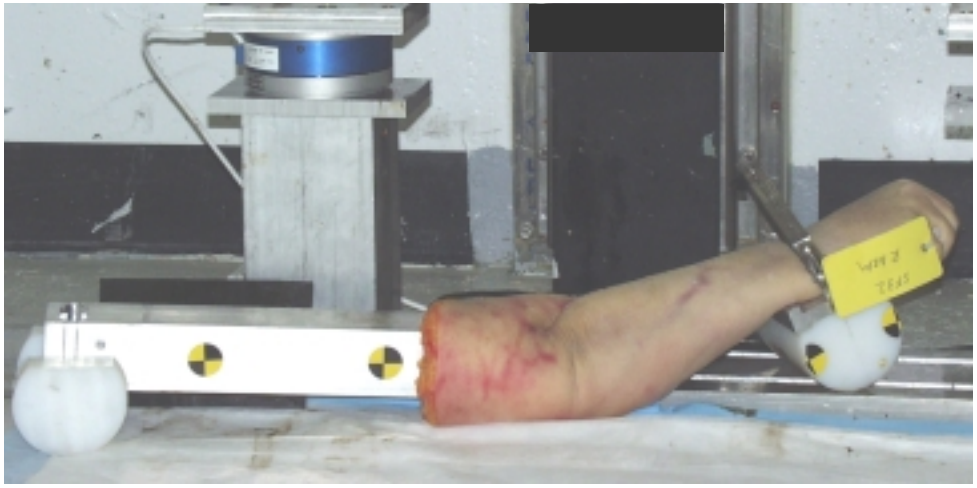

Figure D11: Post-test specimen position.

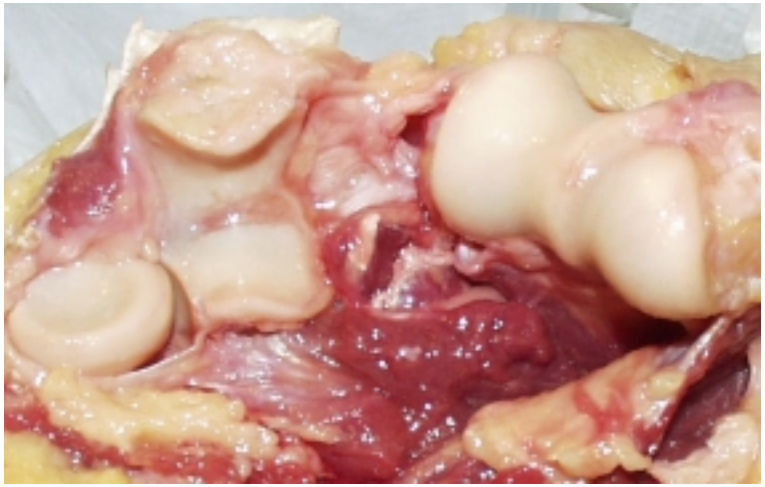

Figure D12: Osteochondral fracture of olecranon.

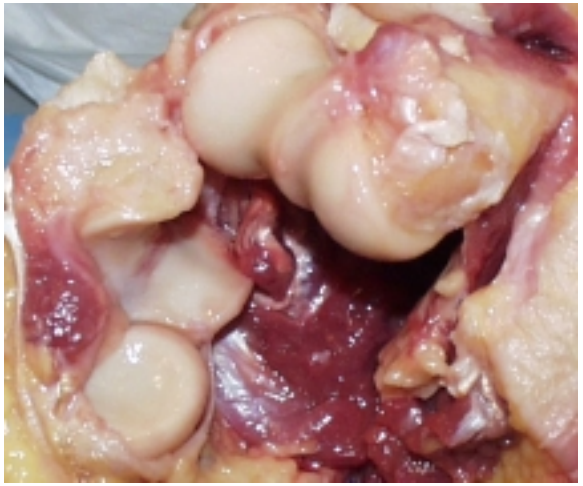

Figure D13: Anterior elbow ligament dislocation.

Test 2.05 – High Energy

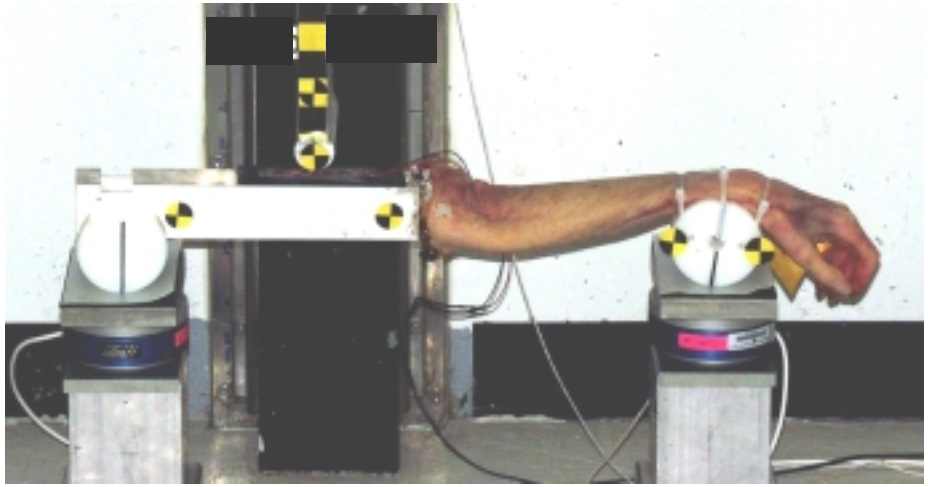

Figure D14: Pre-test set-up.

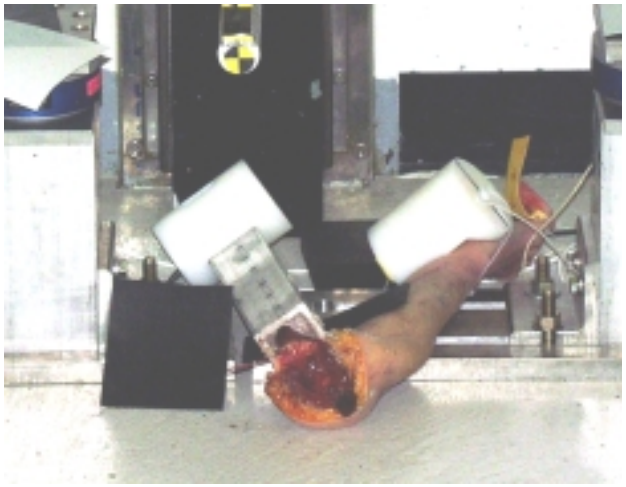

Figure D15: Post-test specimen position.

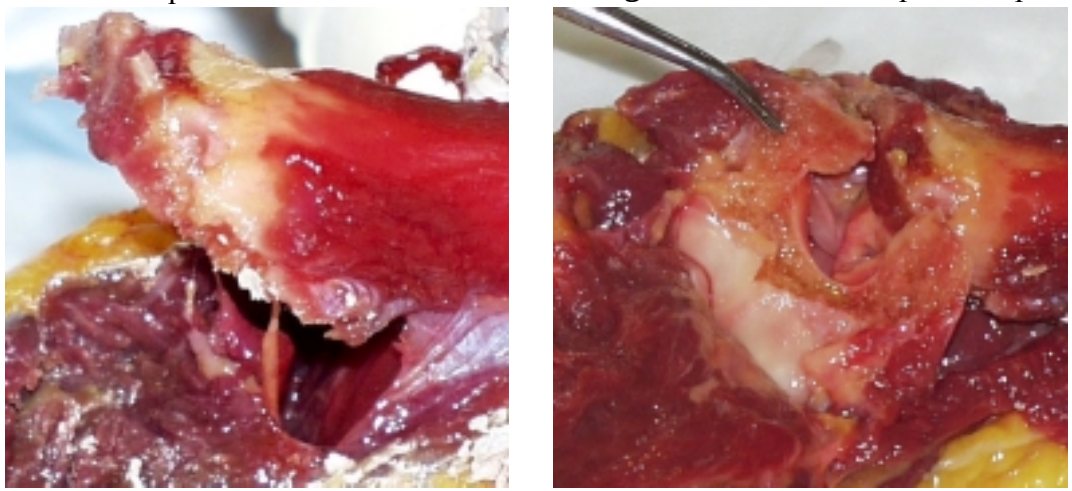

Figure D16: Extra-articular fracture of distal humerus.

Test 2.06 – Low Energy

Figure D17: Pre-test set-up.

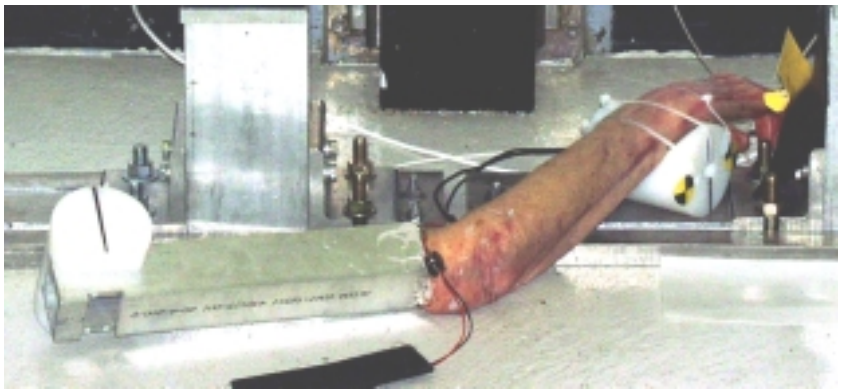

Figure D18: Post-test specimen position.

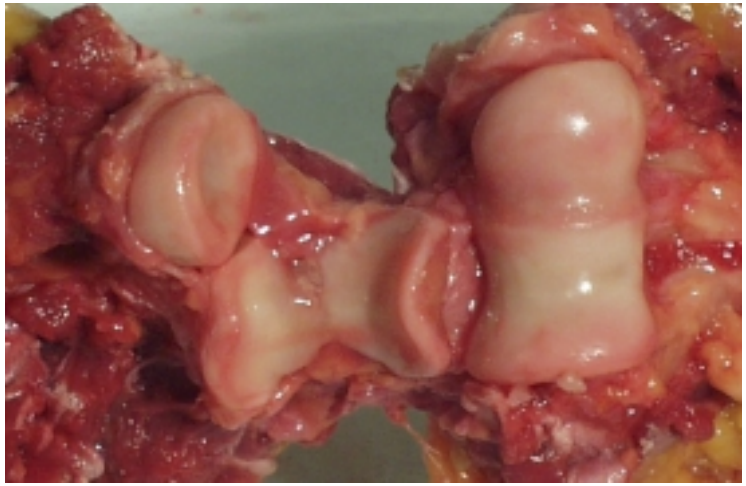

Figure D19: No Injury.

Test 2.07 – Low Energy

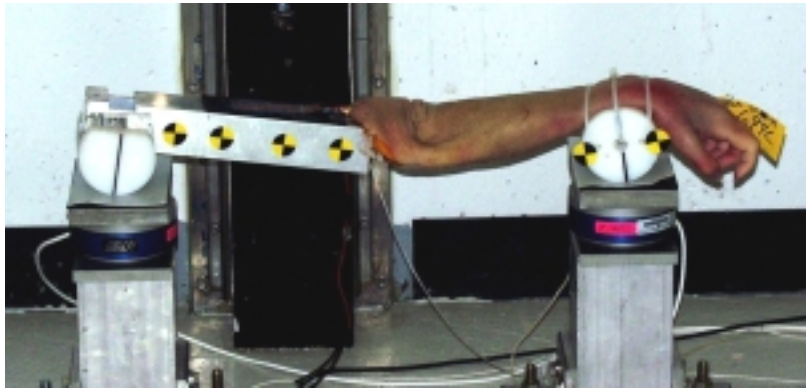

Figure D20: Pre-test set-up.

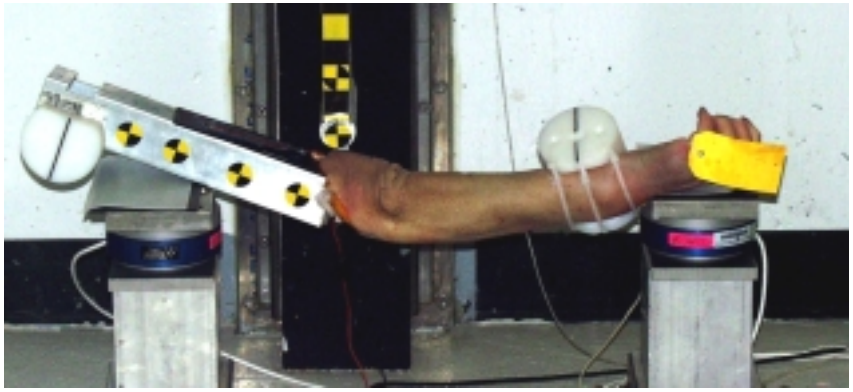

Figure D21: Post-test specimen position.

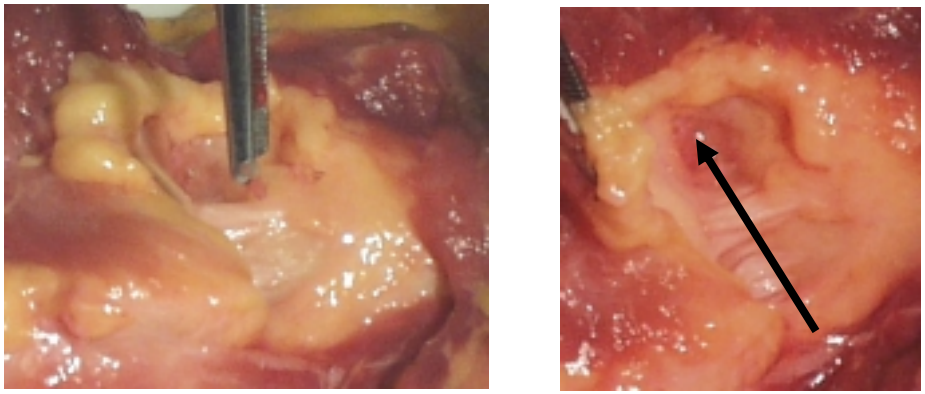

Figure D22: Disruption of the anterior capsule, anterior laterally on radial side of joint.

Test 2.08 – High Energy

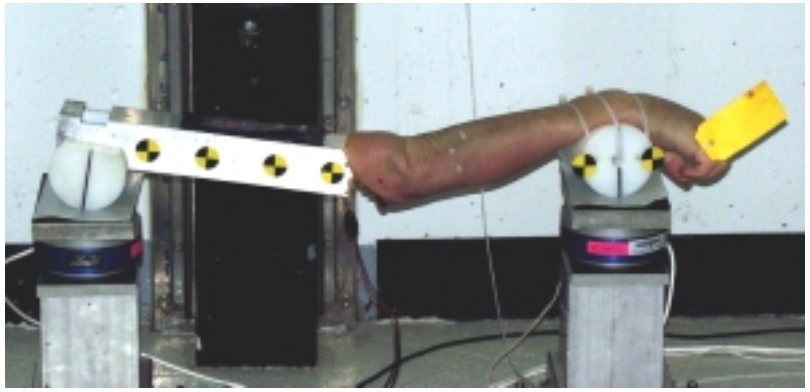

Figure D23: Pre-test set-up.

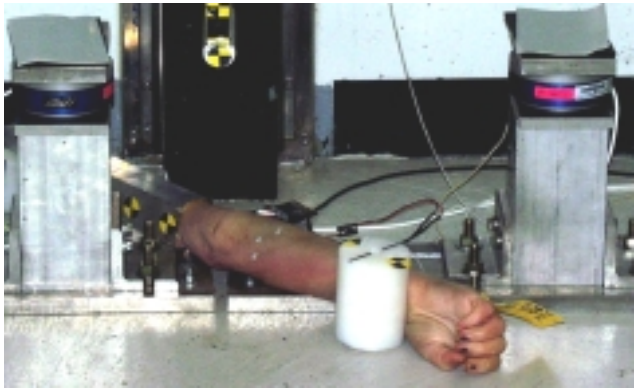

Figure D24: Post-test specimen position.

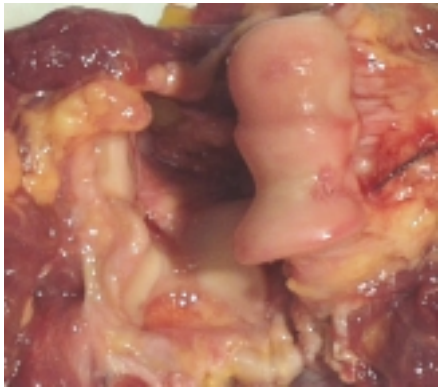

Figure D25: Dislocation of elbow joint; anterior tissue capsule completely torn away.

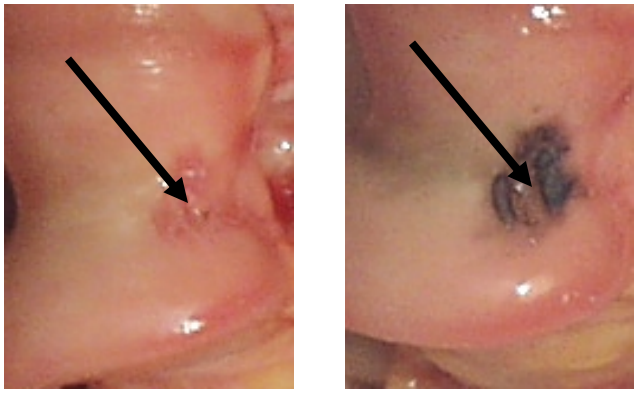

Figure D26: Condylar fracture to the trochlea: a) before ink staining technique; b) after ink staining technique.

Test 2.09 – Low Energy

Figure D27: Pre-test set-up.

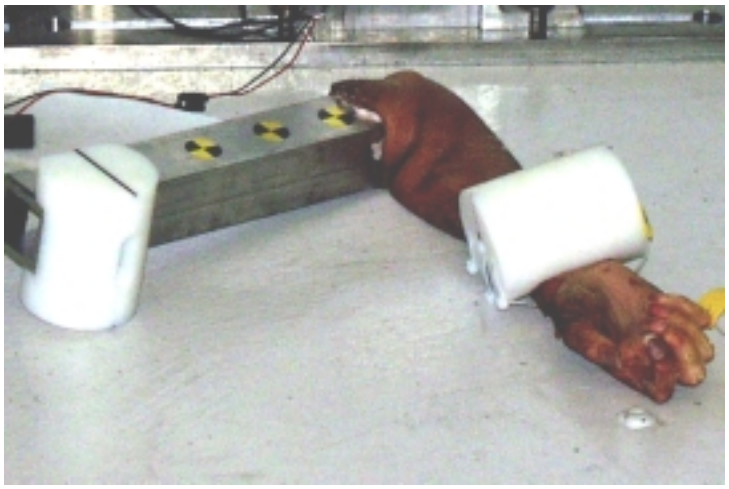

Figure D28: Post-test specimen position.

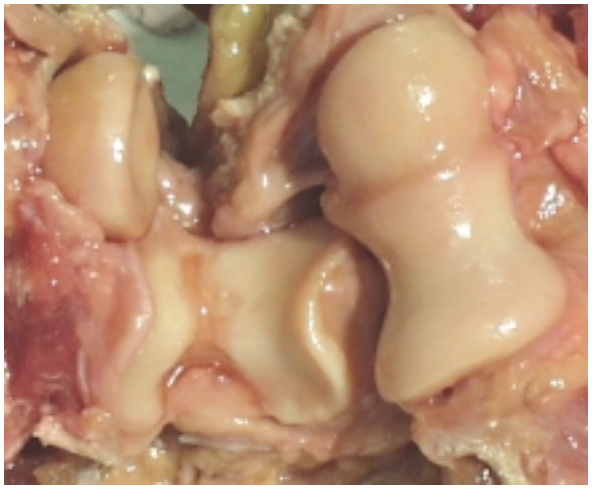

Figure D29: No Injury.

Test 2.10 – High Energy

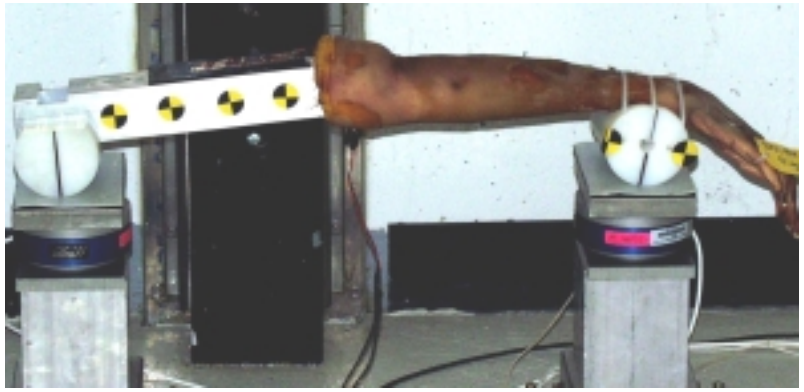

Figure D30: Pre-test set-up.

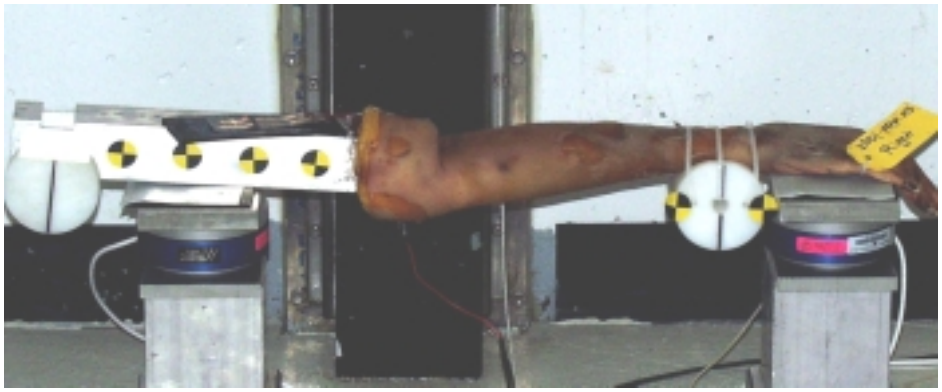

Figure D31: Post-test specimen position.

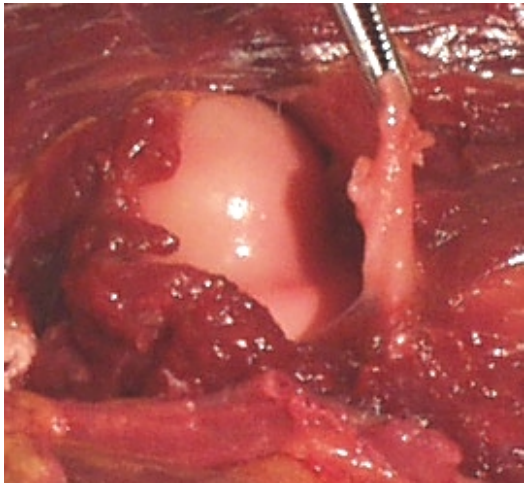

Figure D32: Disruption of the anterior capsule.

Test 2.11 – Low Energy

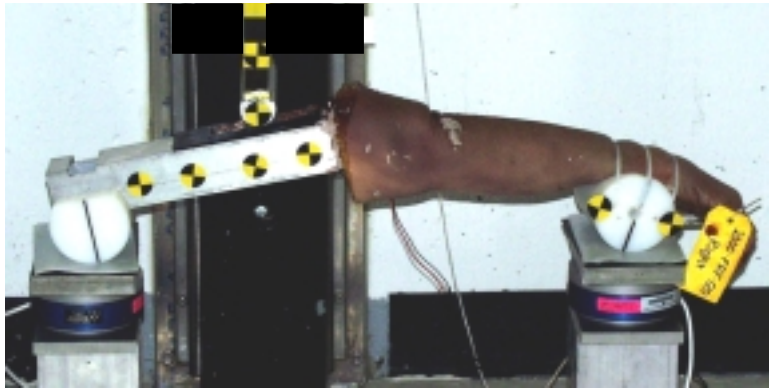

Figure D33: Pre-test set-up.

Figure D34: Post-test specimen position.

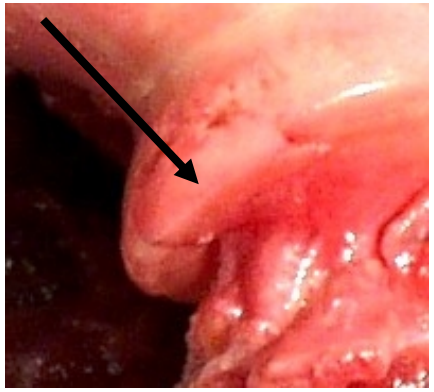

Figure D35: Fracture/fragment of coronoid process.

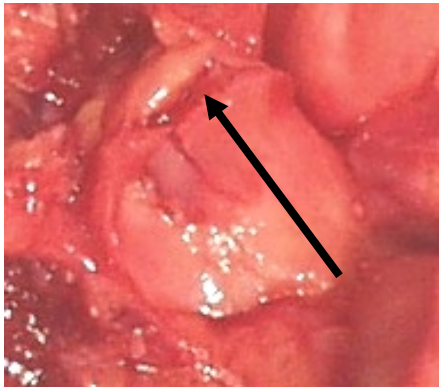

Figure D36: Fracture/fragment of distal trochlear notch.

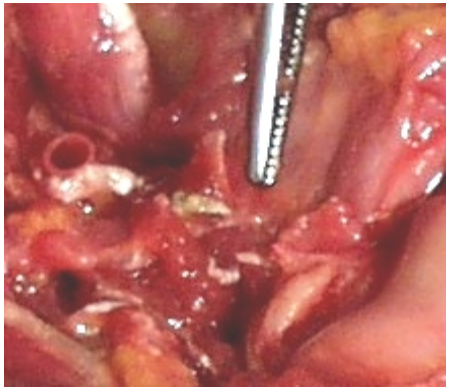

Figure D37: Partial tear to radial head ligamentus.

Test 2.12 – High Energy

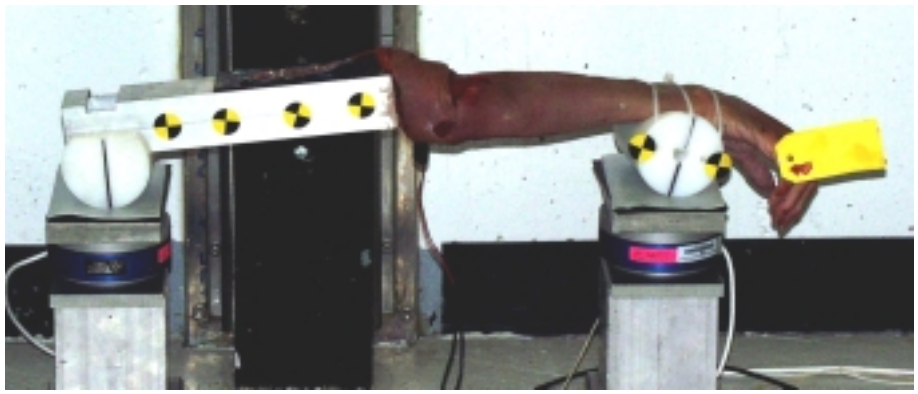

Figure D38: Pre-test set-up.

Figure D39: Post-test specimen position.

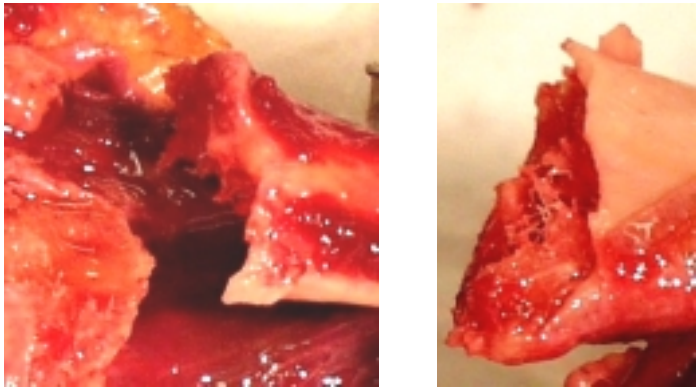

Figure D40: Extra-articular, supracondylar (above condyles) fracture of distal humerus.

Test 2.13 – High Energy

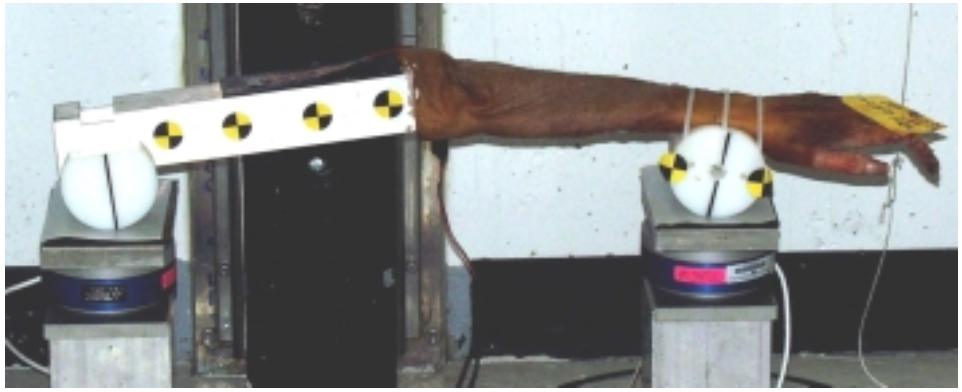

Figure D41: Pre-test set-up.

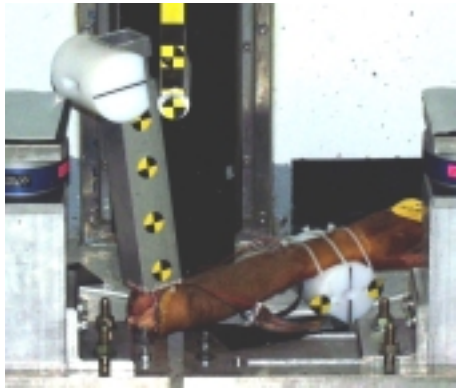

Figure D42: Post-test specimen position.

Figure D43: Fracture/fragment of edge of coronoid process; fracture/fragment medial of coronoid process.

Figure D44: Anterior dislocation of elbow joint; anterior tissue capsule completely torn away.

Test 2.14 – Low Energy

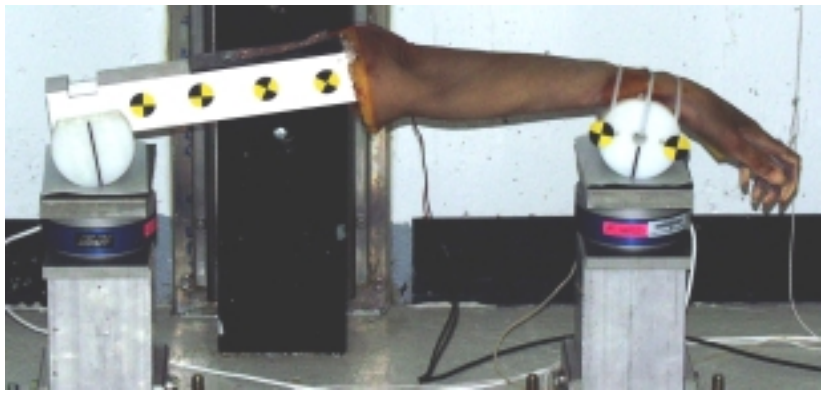

Figure D45: Pre-test set-up.

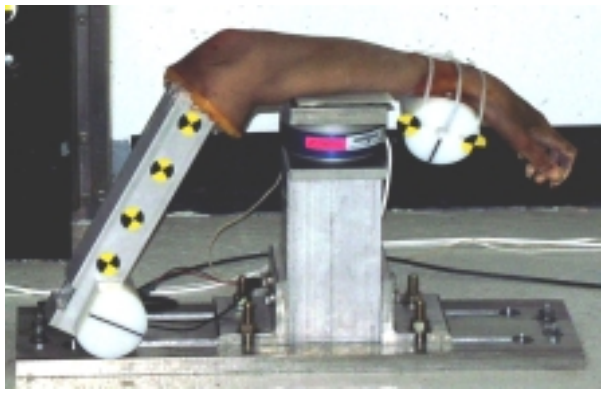

Figure D46: Post-test specimen position.

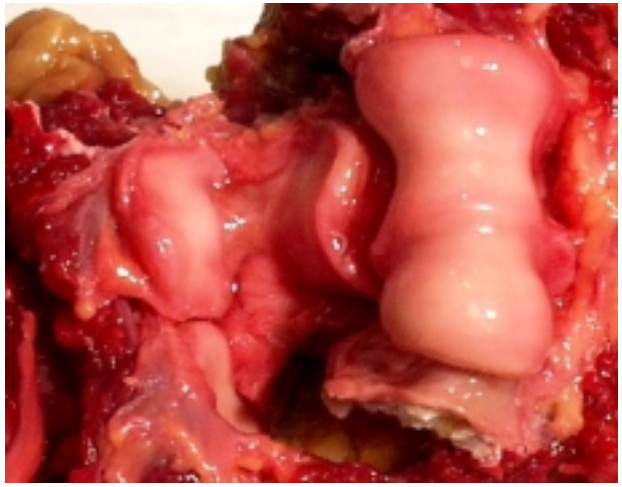

Figure D47: No injury.

Test 2.15 – High Energy

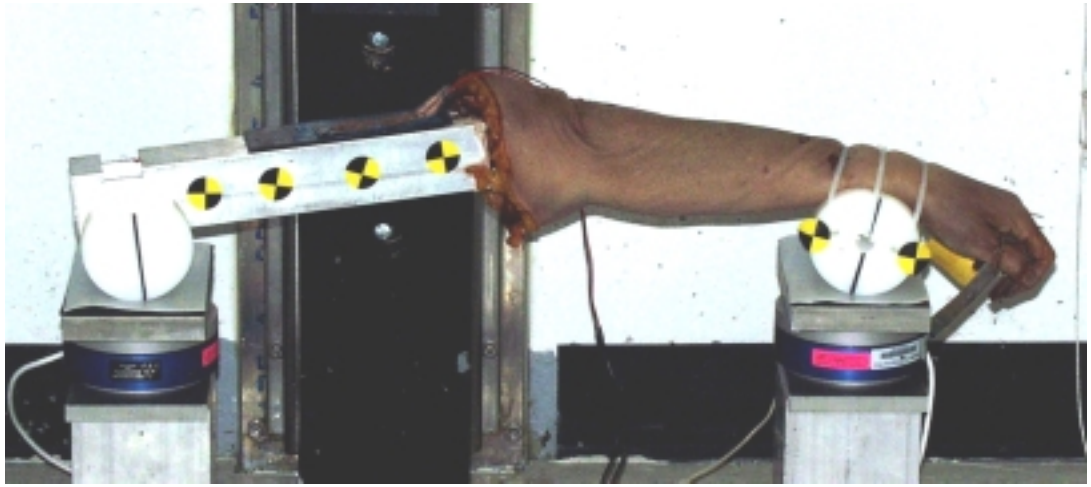

Figure D48: Pre-test set-up.

Figure D49: Post-test specimen position.

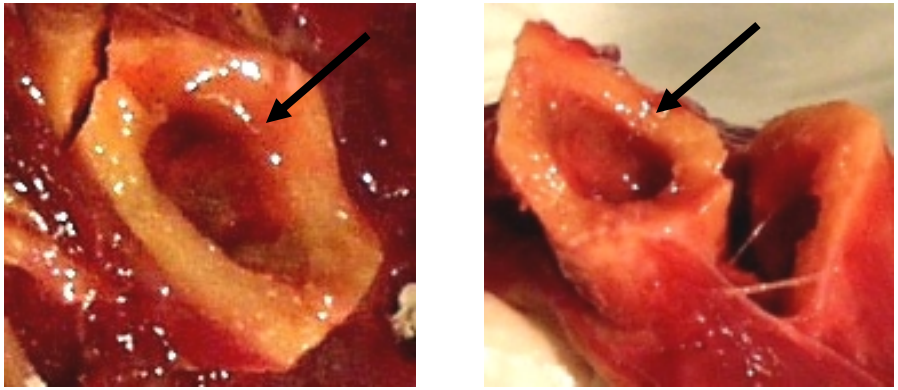

Figure D50: Comminuted fracture of distal humerus just below pot.

Test 2.16 – Low Energy

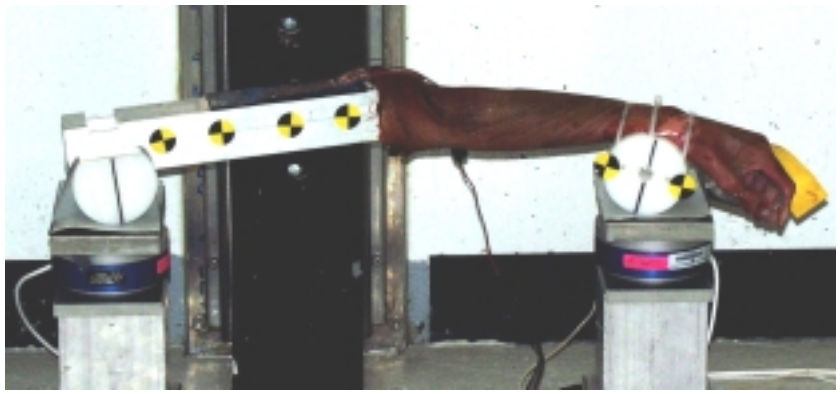

Figure D51: Pre-test set-up.

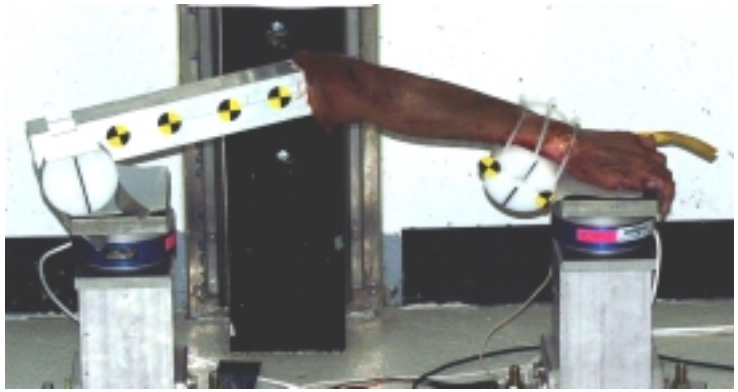

Figure D52: Post-test specimen position.

Figure D53: No injury.

Test 2.17 – Low Energy

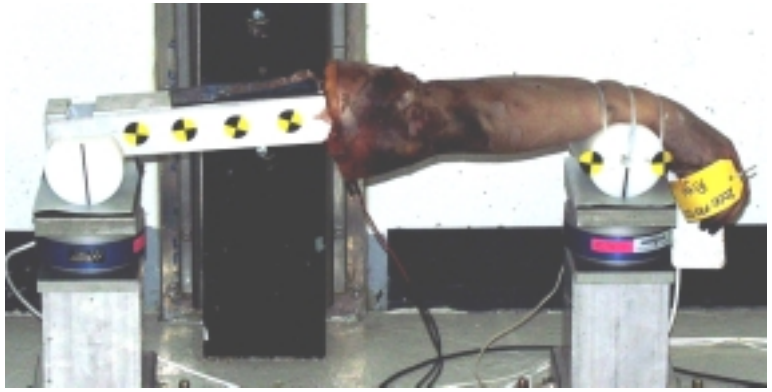

Figure D54: Pre-test set-up.

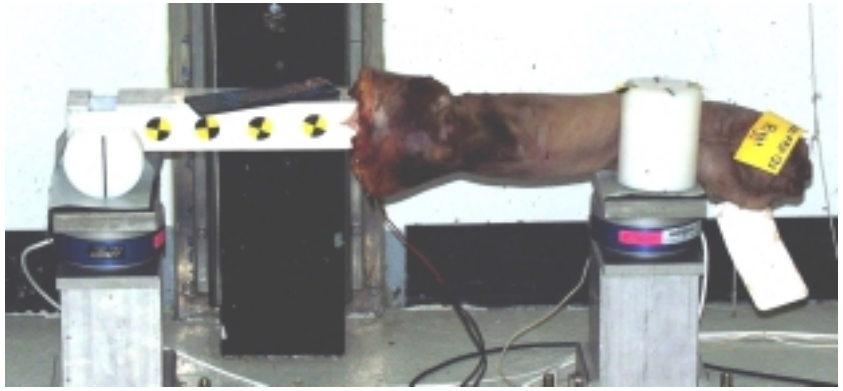

Figure D55: Post-test specimen position.

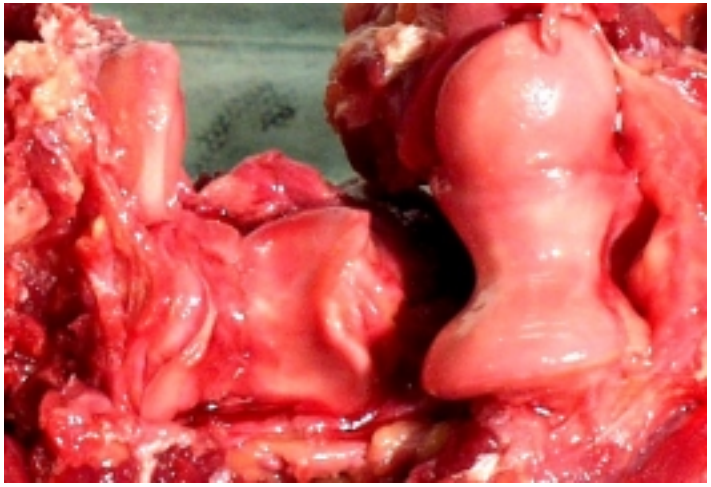

Figure D56: No injury.

Test 2.18 – High Energy

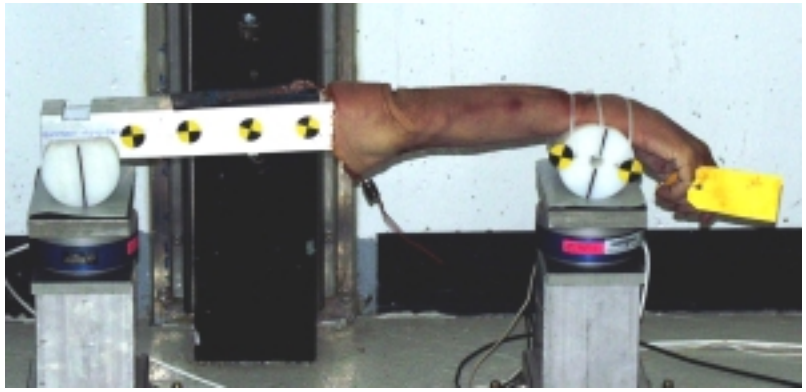

Figure D57: Pre-test set-up.

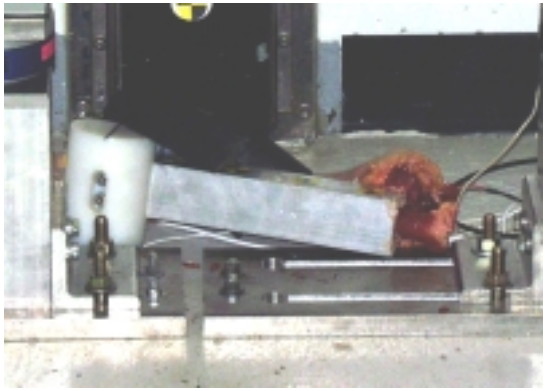

Figure D58: Post-test specimen position.

Figure D59: Supracondylar fracture of distal humerus at trochlea.

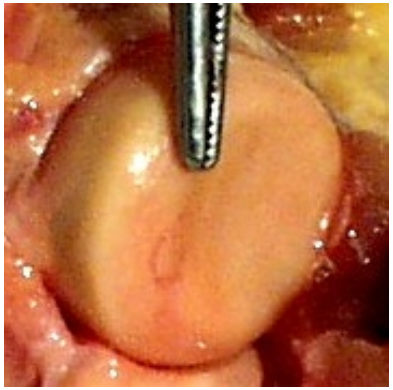

Figure D60: Chondral lesion to radial head.

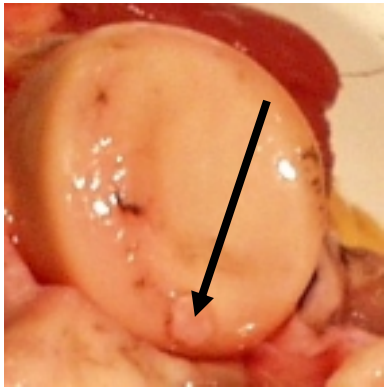

Figure D61: Chondral fracture to radial head.

Test 2.19 – Low Energy

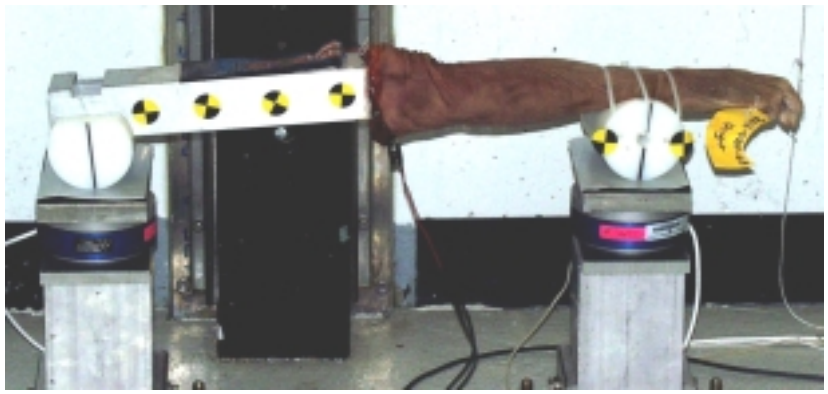

Figure D62: Pre-test set-up.

Figure D63: Post-test specimen position.

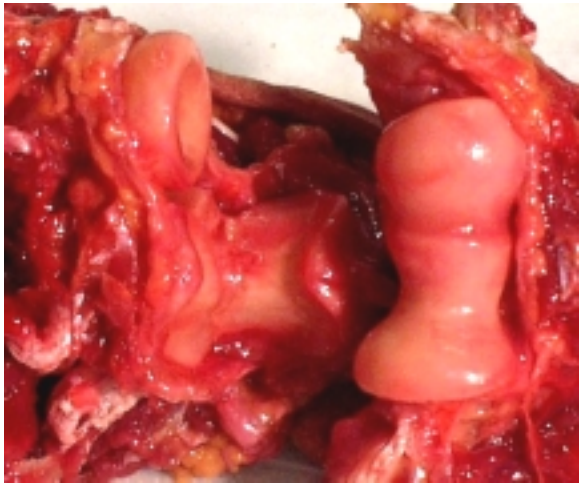

Figure D64: No injury.

Test 2.20 – High Energy

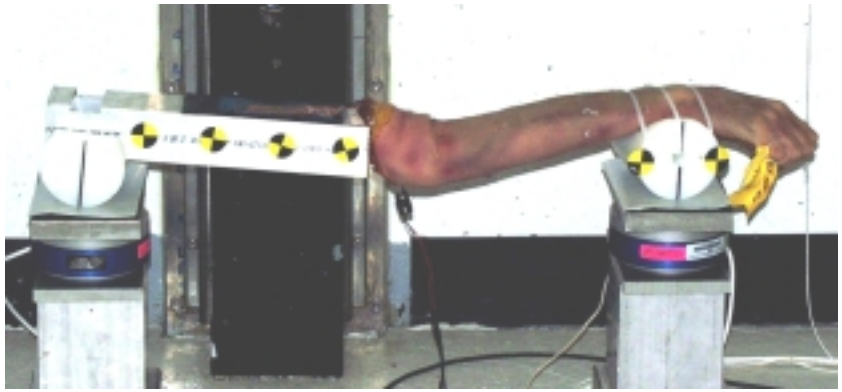

Figure D65: Pre-test set-up.

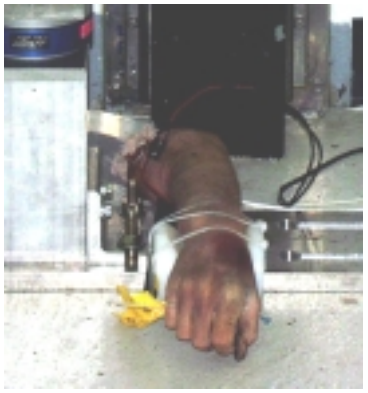

Figure D66: Post-test specimen position.

Figure D67: Elbow joint dislocation; anterior joint tissue capsule torn.

Test 2.21 – Low Energy

Figure D68: Pre-test set-up.

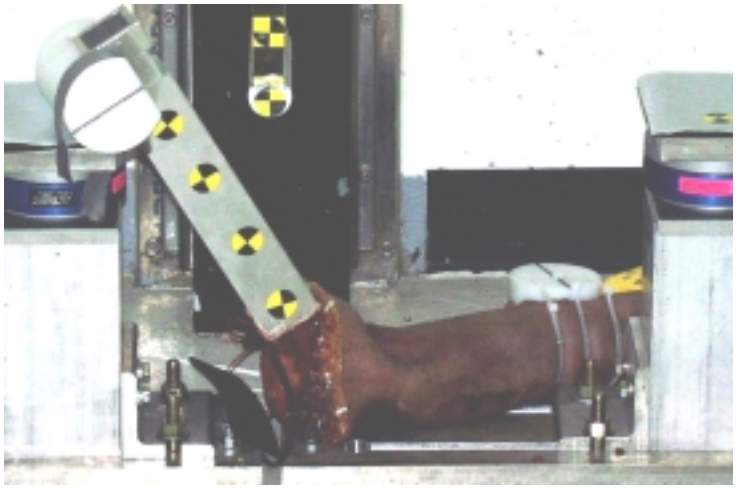

Figure D69: Post-test specimen position.

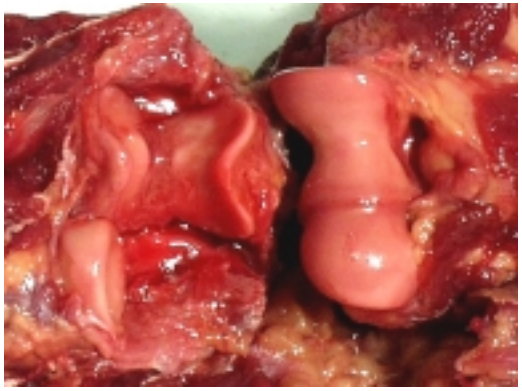

Figure D70: Elbow joint dislocation; anterior tissue capsule torn.

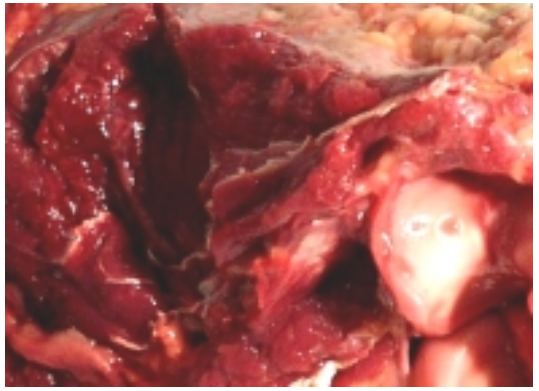

Figure D71: Medial/lateral ligaments almost completely torn.

Test 2.22 – Low Energy

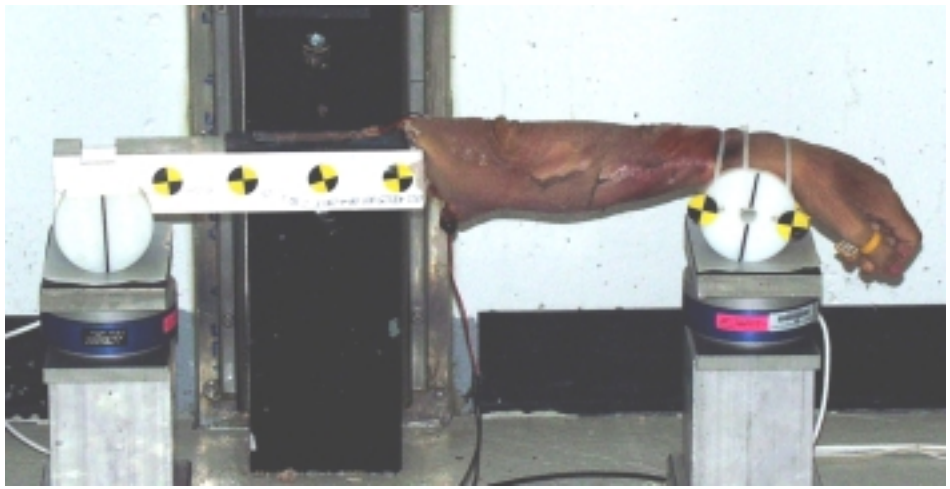

Figure D72: Pre-test set-up.

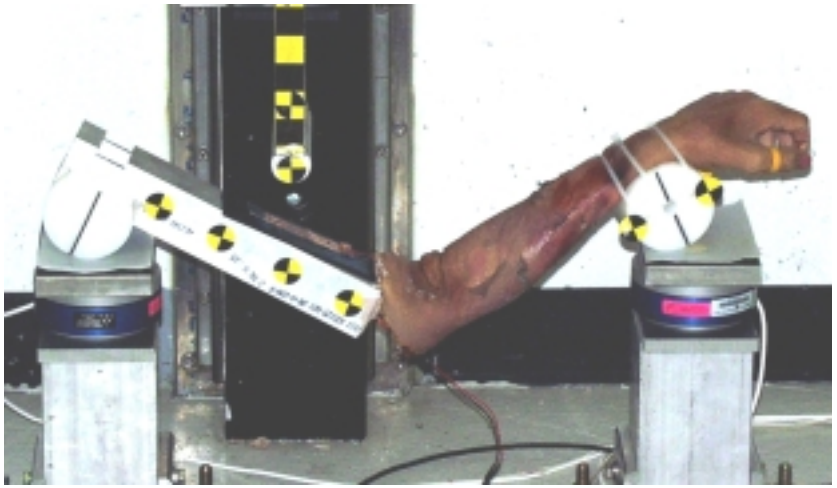

Figure D73: Post-test specimen position.

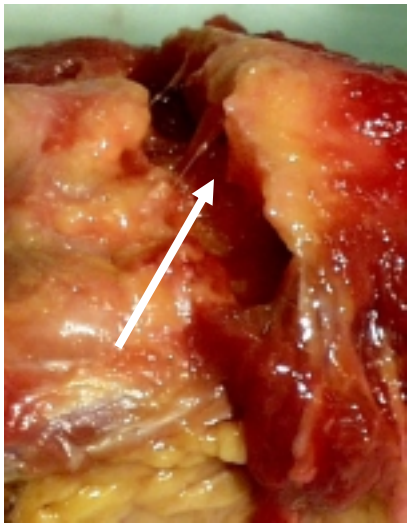

Figure D74: Extra-articular, supracondylar (above condyles) fracture of distal humerus.

Test 2.23 – High Energy

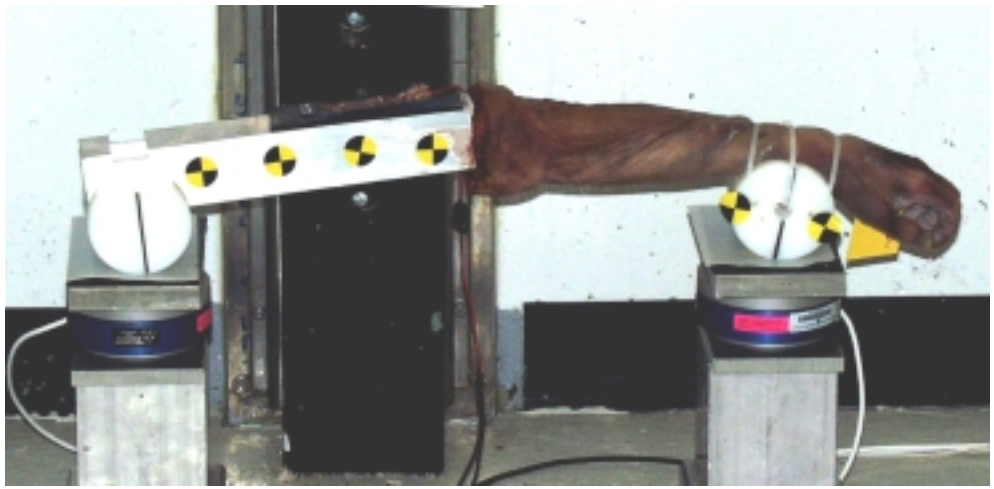

Figure D75: Pre-test set-up.

Figure D76: Post-test specimen position.

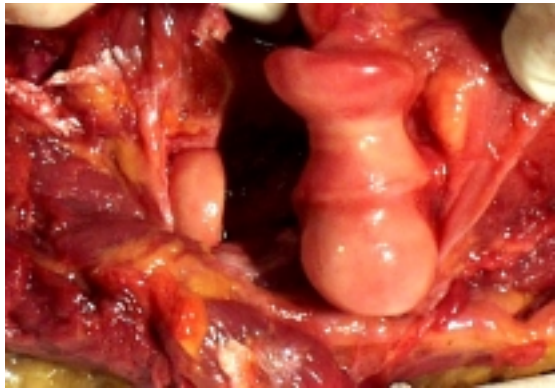

Figure D77: Anterior dislocation of elbow joint; anterior tissue capsule disrupted.

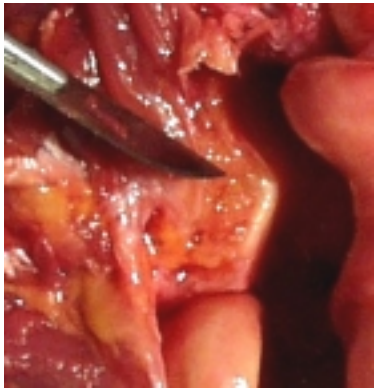

Figure D78: Fracture/fragment of coronoid process.

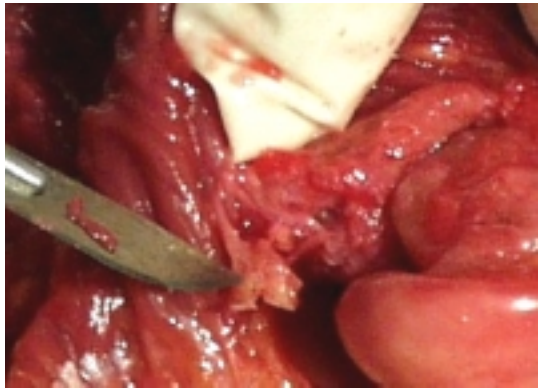

Figure D79: Ligaments completely torn apart functionally.

Test 2.24 – Low Energy

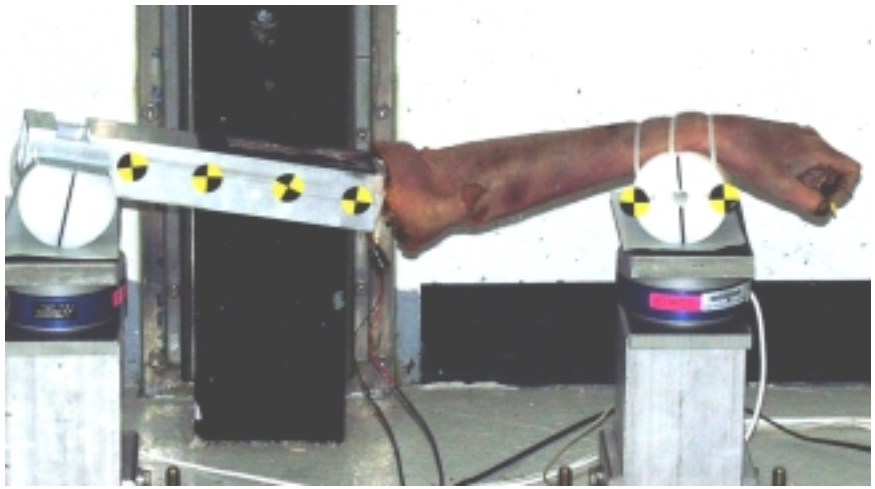

Figure D80: Pre-test set-up.

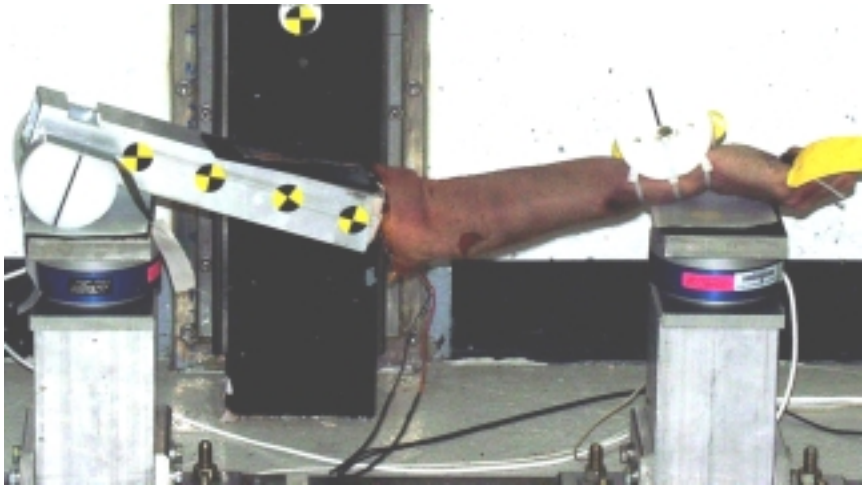

Figure D81: Post-test specimen position.

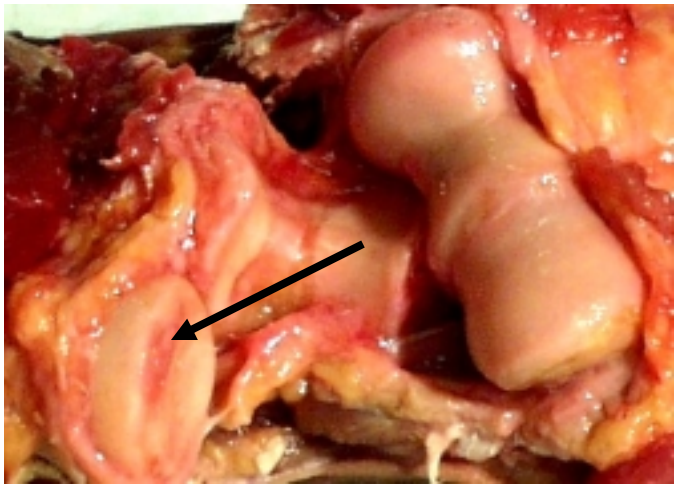

Figure D82: No injury but radial head lesion due to pre-existing condition.

Appendix E: Multivariate Injury Risk Functions

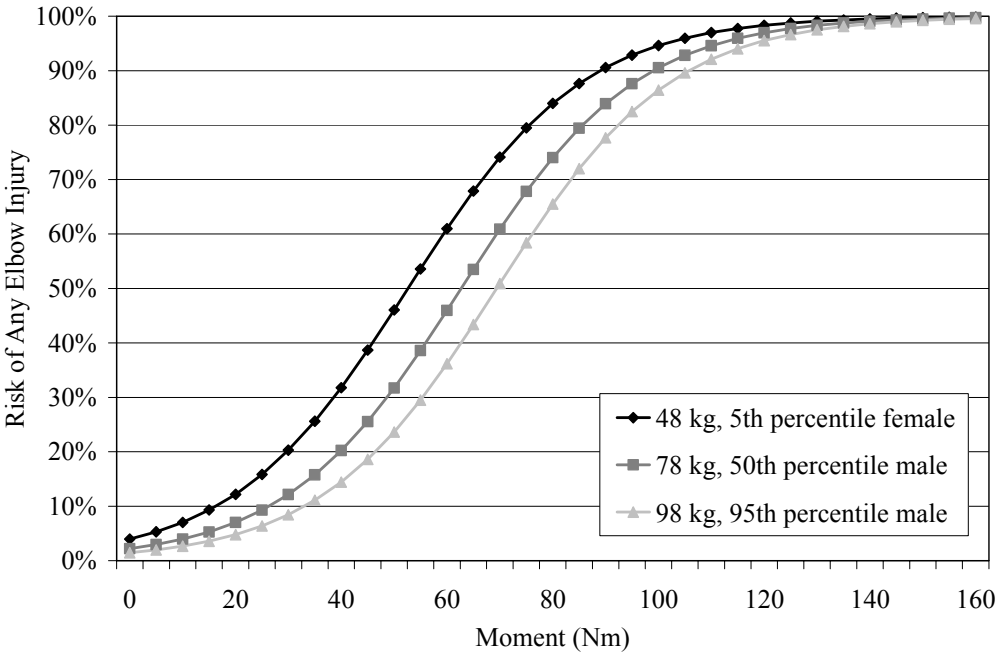

Figure E1: Risk of any elbow injury based upon peak elbow bending moment for three specimen mass values (p=0.061).

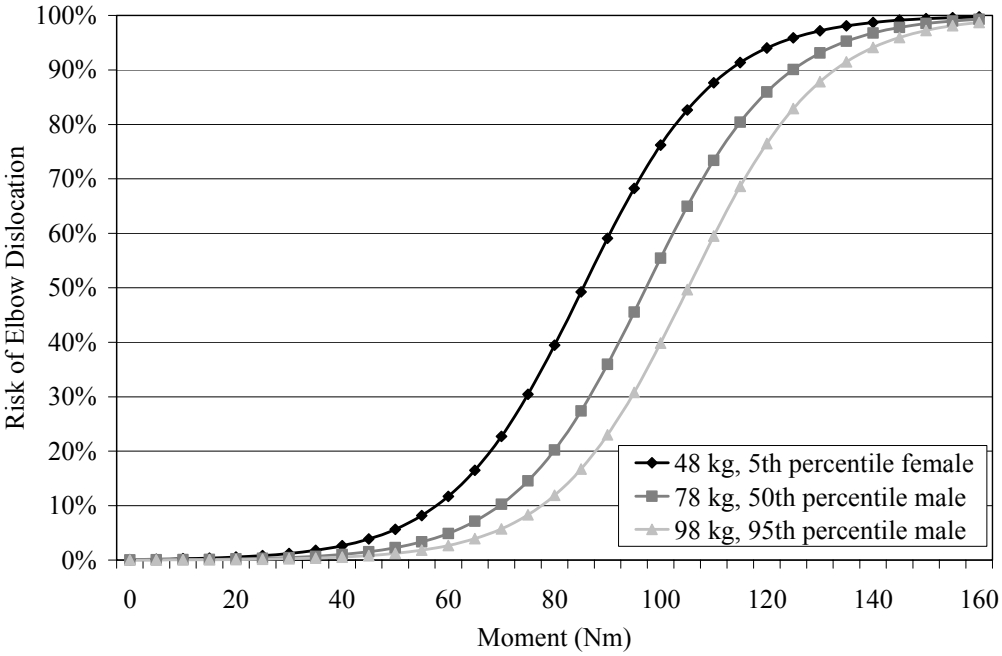

Figure E2: Risk of elbow dislocation based upon peak elbow bending moment for three specimen mass values (p=0.001).

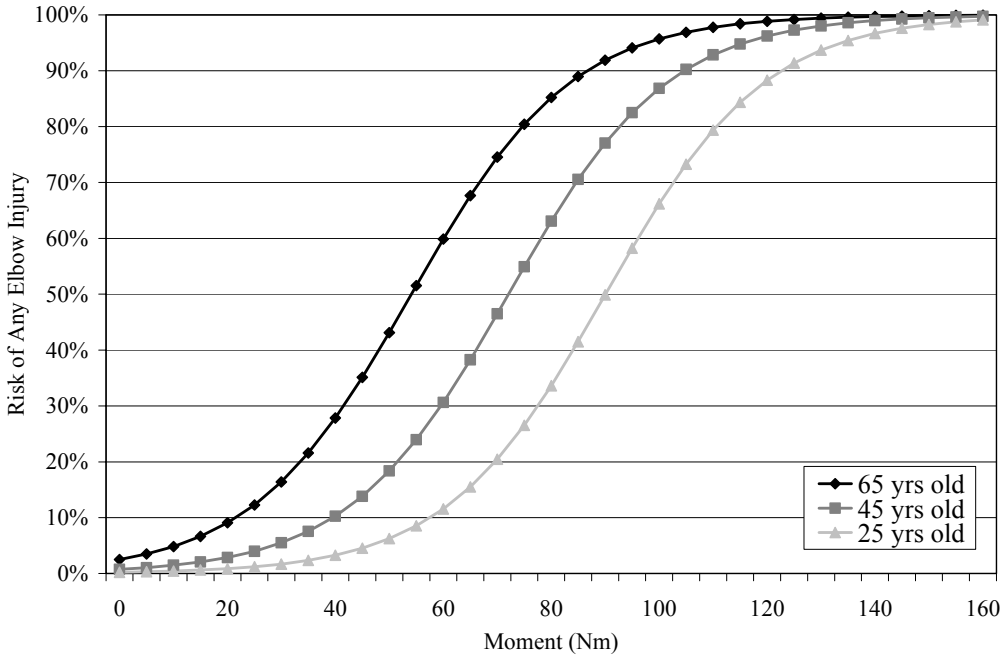

Figure E3: Risk of any elbow injury based upon peak elbow bending moment for three specimen ages (p=0.021).

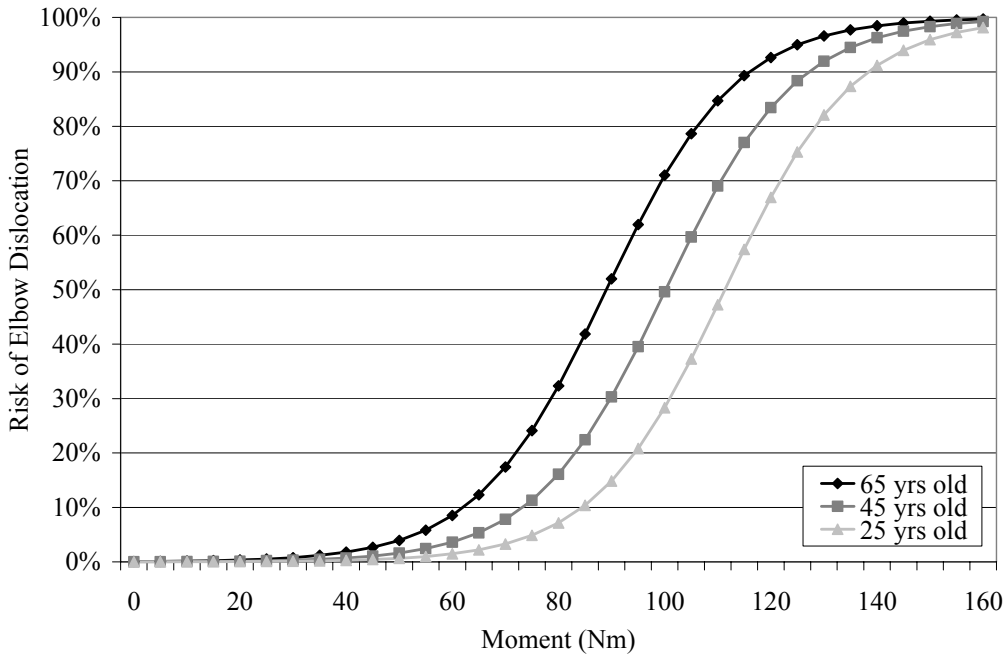

Figure E4: Risk of elbow dislocation based upon peak elbow bending moment for three specimen ages (p=0.001).

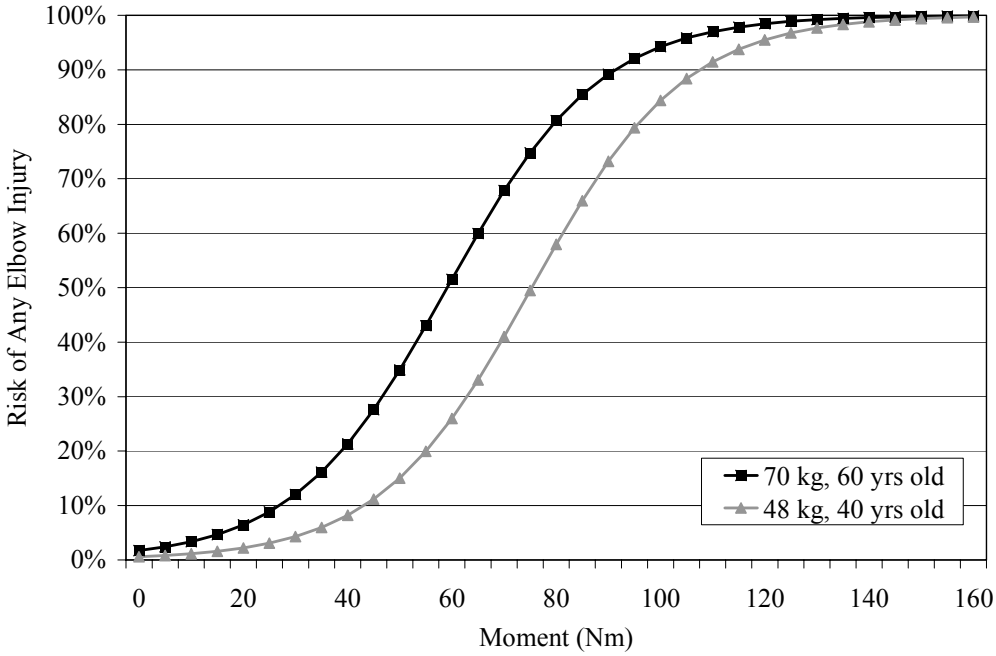

Figure E5: Risk of any elbow injury based upon peak elbow bending moment for two specimen mass and age combinations (p=0.051).

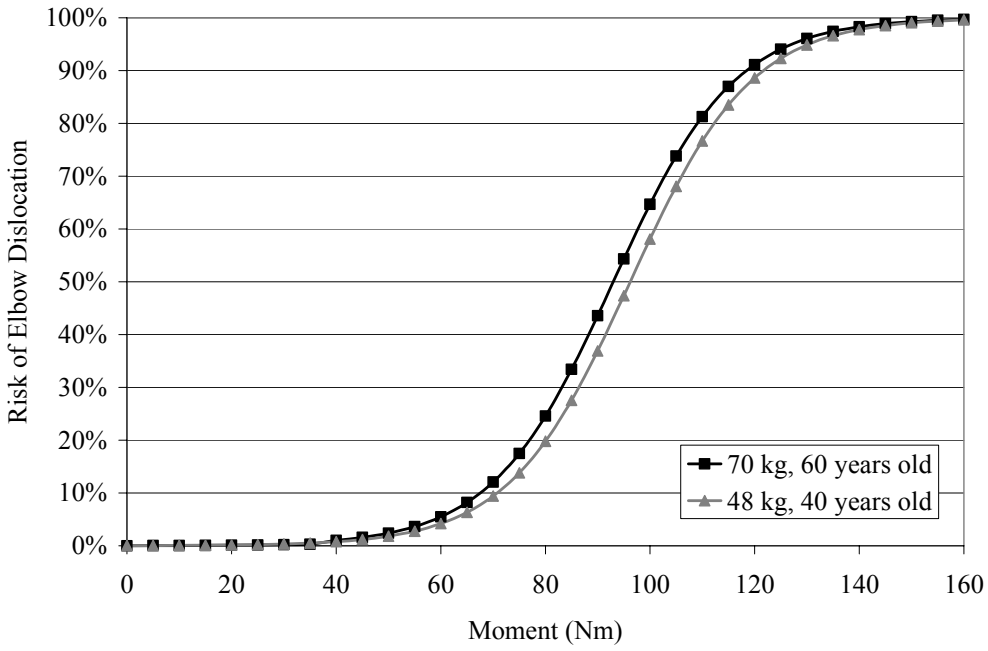

Figure E6: Risk of elbow dislocation based upon peak elbow bending moment for two specimen mass and age combinations (p=0.001).

Appendix F: Relevant Test Pictures

Figure F1: SAE 5th percentile female instrumented upper extremity (Denton ATD, Inc.).

Figure F2: SAE 5th percentile female instrumented upper extremity disassembled (Denton ATD, Inc.).

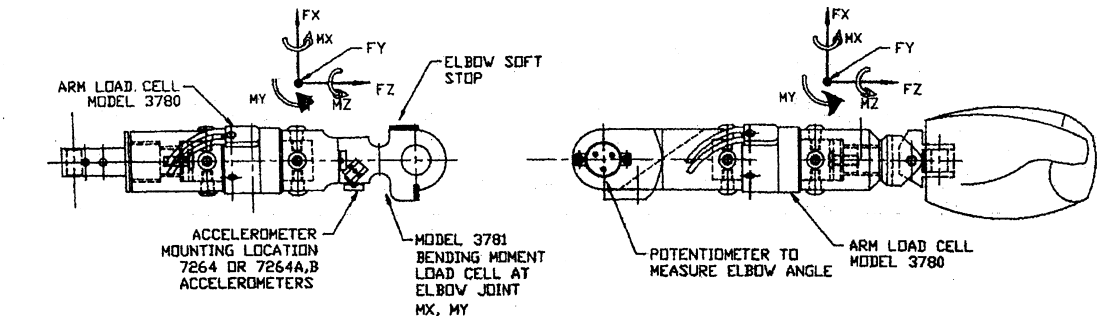

Figure F3: SAE 5th percentile female instrumented upper extremity with associated instrumentation polarities (Denton ATD, Inc.).

Figure F4: UH-60 Black Hawk utility helicopter.

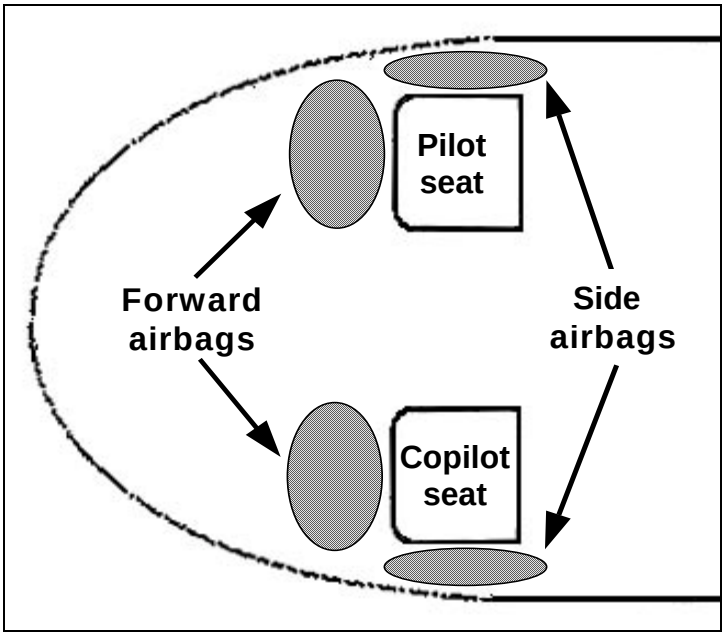

Figure F5: Cockpit Airbag placement in the UH-60 Black Hawk helicopter.

Figure F6: Copilot forward and side airbags under static inflation in a flight simulator.

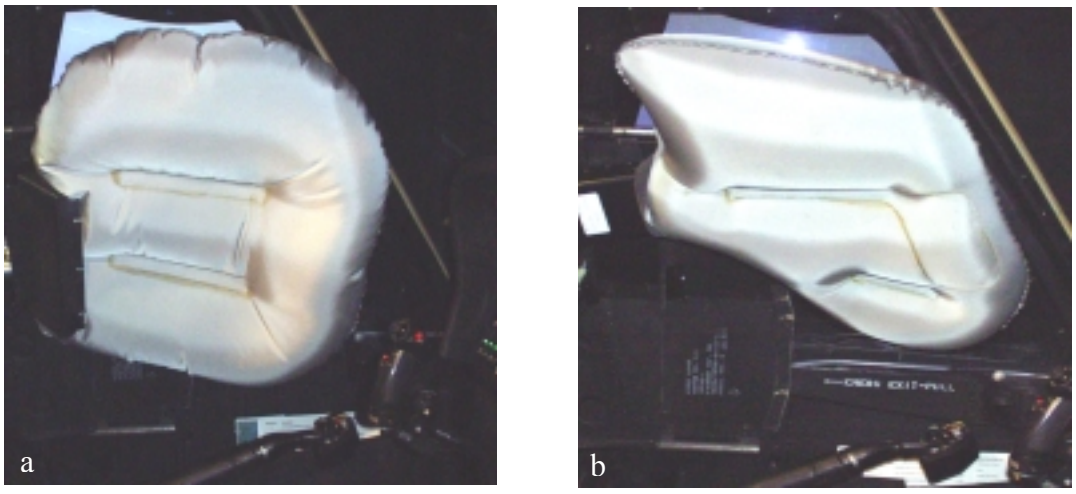

Figure F7: Original (a) and enhanced (b) side airbags under static inflation in a flight simulator.

Figure F8: Enhanced side airbag viewed from the nose of the aircraft.

Figure F9: Test setup with dummy dressed in flight suit and situated in typical aviator position.

Figure F10: Dummy's seat positioned to represent a worst case scenario.

Figure F11: Dummy's seat positioned to represent typical aviator position.

Figure F12: Comparison of dummy worst case position (a) and stature of 2nd percentile female aviator (b).

Figure F13: Comparison of female (a) and male (b) aviator stature positions in relation to airbag deployments.

Figure F14: Lateral view of UH-60 Black Hawk helicopter cockpit.

Vita

Gail Ann Hansen

Gail Ann Hansen was born in Madison, Wisconsin on July 30th, 1980. She attended Edsel Ford High School in Dearborn, Michigan, where she graduated with honors in May of 1998. Gail went on to obtain a Bachelor of Science Degree in Mechanical Engineering from Michigan Technological University in Houghton, Michigan, where she graduated with *Magna Cum Laude* honors in May of 2002. While attending Michigan Tech, Gail was a 4-time varsity letter-winner in Women's Tennis and was consecutively named to the GLIAC Athletic Conference All-Academic Team. Furthermore, she participated in the 2002 NCAA Division II Tournament and was awarded the 2002 ITA Scholar-Athlete Honors. Also while at Michigan Tech, she acquired relevant engineering experience through internships in the automotive industry with Venture Industries and Ford Motor Company. Upon completion of her degree, she was offered full time engineering positions at both Ford Motor Company and Daimler Chrysler. Instead she chose to further her education by pursuing a Master's Degree in Mechanical Engineering at Virginia Tech in Blacksburg, Virginia. As a graduate student and research engineer at the Virginia Tech Center for Injury Biomechanics, her research focused on investigating human tolerance to impact loading by combining experiments using human surrogates with statistical analyses to develop human impact injury criteria; applications included automobile safety and military restraints. She was awarded a Pratt Scholastic Fellowship by the Mechanical Engineering Department along with an Impact Biomechanics Laboratory Scholarship. Gail was given numerous opportunities to present and publish her research at biomechanics conferences and symposiums. She was granted the 2003 Best Student Paper Award by the Association for the Advancement of Automotive Medicine (AAAM) for her conference paper presented in Lisbon, Portugal. Gail was also named a finalist of the Paul E. Torgersen Graduate Student Research Excellence Award by the College of Engineering for her thesis work. Based on her interests and experience, her objective was to acquire a position in automotive safety engineering upon graduation. However, due to the effects of a struggling economy on the industry, few opportunities in this specific field were available to her. She was instead granted an exciting opportunity to work for NASA – United Space Alliance in Mission Control at the Johnson Space Center in Houston, Texas. She will work as a member of the EECOM Thermal Systems and Life Support group on the space shuttle program as of June, 2004.

Further information can be obtained by writing to her permanent address:

3147 Roosevelt St.
Dearborn, MI 48124